ADVANCED ENERGY MATERIALS
www.advenergymat.de

Advances and Challenges in Designing Efficient NiFe-Based Oxygen Electrocatalysts for Rechargeable Zn–Air Batteries

Xiaohong Zou, Mingcong Tang, Qian Lu, Kouer Zhang, Lizhen Wu, Zongping Shao,* and Liang An**

Designing cost-effective bifunctional electrocatalysts with high activity claims essential features for accelerating the practical application process of rechargeable Zn–air batteries. NiFe-based catalytic materials are viable candidates for bifunctional electrocatalysts, benefiting from abundant reserves, low costs, adjustable electron structures, and high catalytic activities. To accelerate the industrialization process of NiFe-based materials in rechargeable Zn–air batteries, it is necessary to systematically explore their design strategies for promoting bifunctional catalytic activities. This review first introduces the working principle, reaction mechanism, and challenges of rechargeable Zn–air batteries, which aim to understand the cathodic catalyst design criteria. Furthermore, the categorization of NiFe-based catalysts is illustrated in detail to introduce the design strategy. Based on the understanding, the design strategy of NiFe-based catalysts, including anionic modification, cation doping, supporting effect, embedding effect, and multi-component construction, is summarized to boost the performance in rechargeable Zn–air batteries with high activity and sustained stability. Finally, some personal insights on developing practical NiFe-based electrocatalysts are proposed. It is believed that this review can offer valuable insights for guiding future research on the advancement of NiFe-based catalysts in rechargeable Zn–air batteries.

1. Introduction

The pursuit of economically viable and environmentally sustainable energy storage and conversion technologies is a promising direction to relieve the environmental crisis caused by CO_2 emissions.[1–5] Among various energy systems, Zn–air batteries are considered promising candidates for next-generation energy devices, considering their benefits of low cost, environmental friendliness, available security, and high theoretical energy density.[6–8] Unfortunately, the practical deployment of Zn–air batteries is impeded by the sluggish reaction kinetics and limited cycling stability of the cathodic oxygen-electrochemistry electrocatalysts.[9,10] Currently, the noble metal composites, such as Pt/C + IrO_2/RuO_2, have been commonly utilized as bifunctional oxygen electrocatalysts to address the slow kinetics of oxygen reduction reaction (ORR) and oxygen evolution reaction

X. Zou, M. Tang, K. Zhang, L. Wu, L. An
Department of Mechanical Engineering
The Hong Kong Polytechnic University
Hung Hom, Kowloon, Hong Kong SAR 999077, P. R. China
E-mail: liang.an@polyu.edu.hk

Q. Lu
Jiangsu Collaborative Innovation Center of Atmospheric Environment and Equipment Technology
Jiangsu Key Laboratory of Atmospheric Environment Monitoring and Pollution Control
School of Environmental Science and Technology
Nanjing University of Information Science and Technology
Nanjing 210044, P. R. China
E-mail: luqian_0104@nuist.edu.cn

The ORCID identification number(s) for the author(s) of this article can be found under https://doi.org/10.1002/aenm.202501496

DOI: 10.1002/aenm.202501496

Q. Lu
Department of Chemistry
The Chinese University of Hong Kong
Ma Lin building, Shatin, Hong Kong SAR 999077, P. R. China

Z. Shao
WA School of Mines: Minerals
Energy and Chemical Engineering (WASM-MECE)
Curtin University
Perth, WA 6102, Australia
E-mail: zongping.shao@curtin.edu.au

L. An
Research Institute for Advanced Manufacturing
The Hong Kong Polytechnic University
Hung Hom, Kowloon, Hong Kong SAR 999077, P. R. China

L. An
Research Institute for Smart Energy
The Hong Kong Polytechnic University
Hung Hom, Kowloon, Hong Kong SAR 999077, P. R. China

L. An
Research Centre for Carbon-Strategic Catalysis
The Hong Kong Polytechnic University
Hung Hom, Kowloon, Hong Kong SAR 999077, P. R. China

(OER) occurring on the air cathode side. However, the substantial expense and restricted stability of noble metal electrocatalysts significantly restrict their widespread application in rechargeable Zn–air batteries.[11–13] Consequently, the development of cost-effective, non-noble metal, and highly efficient bifunctional electrocatalysts has currently become a research highlight in the domain of rechargeable Zn–air batteries.

Accordingly, plenty of efforts are devoted to exploiting cost-effective bifunctional electrocatalysts with high performance for rechargeable Zn–air batteries, including carbon materials, metal oxides/alloys, metal-derived composites, as well as special organic-inorganic compounds.[14–18] Among them, NiFe-based 3d transition metal electrocatalysts have been regarded as a suitable direction to design high-activity and long-stability bifunctionally electrocatalysts, benefiting from the tunable Ni and Fe ratio and various morphology and electronic structures.[19,20] In particular, pristine NiFe catalysts usually perform the electrochemical reconstruction phenomena, which form NiFeOOH active species on the surface of the designed catalyst, thereby possessing remarkable OER activity.[21,22] However, pristine NiFe compounds show low electron conductivity owing to the semiconductor property of NiFeOOH, inferior OER stability arising from the segregation of Fe in the alkaline medium, as well as poor ORR activity.[23,24] To address the requirement for rechargeable Zn–air batteries, it is crucial to explore the NiFe-based catalytic materials that exhibit both highly bifunctional activity and extended durability.

In general, carbon material with high electron conductivity and affordable ORR activity could be applied to combine with NiFe-based catalysts to facilitate electron transport and promote the ORR activity.[25,26] More importantly, carbon materials, such as graphene, carbon nanotubes, and carbon quantum dots, could supply a large surface area for supporting NiFe-based nanocatalysts and regulate the electron structure of NiFe-based catalysts to accelerate the mass/charge transfer for the oxygen redox chemistry.[27–29] In addition, the novel strategy, including oxygen vacancy, heteroatom doping, cation defect, core-shell structure, interfacial engineering, and morphology construction, can be applied to modify NiFe-based catalysts to achieve the bifunctional ORR/OER activity.[30–34] To construct more advanced bifunctional NiFe-based electrocatalysts, conducting a systematic analysis of the design strategy and criteria for the NiFe-based electrocatalysts is necessary.

This review primarily concentrated on summarizing the design strategies and recent advancements in bifunctional NiFe-based electrocatalysts for rechargeable Zn–air batteries, as revealed in **Scheme 1**. Initially, a concise introduction of the air cathode for the Zn–air battery is provided, detailing the cell configuration, reaction mechanism, and current challenge. Then, we provide a brief introduction to the categorization of NiFe-based catalysts to offer a fundamental understanding and direction for improving ORR and OER activities. Moreover, the design strategy of NiFe-based catalysts in rechargeable Zn–air batteries, including anionic modification, cation doping, supporting effect, embedding effect, and multi-component construction, is summarized in detail. Finally, we propose some personal insights on developing practical NiFe-based electrocatalysts. This review aims to inspire the construction of high-performance NiFe-based catalytic materials for bridging the gap between laboratory research and industrial applications for rechargeable Zn–air batteries.

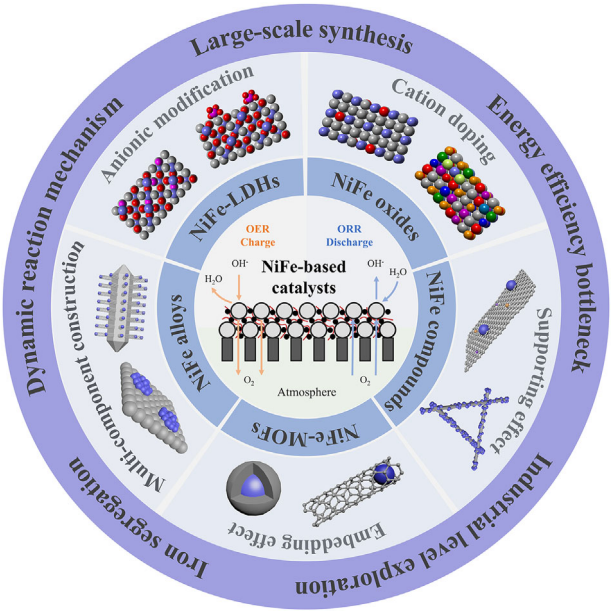

Scheme 1. Summary of the introduction and design strategy of NiFe-based electrocatalysts in Zn–air batteries.

2. Introduction of the Air Cathode

Since the pristine Zn–air battery with aqueous NH_4Cl electrolyte was first reported by Maiche in 1878, an enormous number of researchers have devoted themselves to pursuing high-activity and long-durability Zn–air batteries.[35] Normally, the typical configuration of Zn–air batteries is composed of three main components, including the air cathode, zinc anode, and electrolyte. Typically, the zinc anode is usually a fresh zinc plate or a mixture of zinc powders and polymer binders, which ensures the insertion/extraction of Zn^{2+} cation.[36–39] However, owing to the Zn dendrites corresponding with the parasitic hydrogen evolution reaction, the Zn anode still faces the challenges of the heavily decayed utilization rate of zinc and the reduced lifespan of Zn–air batteries.[40,41] Constructing a surface protective layer on the zinc anode can avoid direct contact between high-concentration alkaline electrolyte and metallic zinc anode, thus alleviating the issue of zinc dendrite.[42,43] The composition of the electrolyte is a 6 M KOH solution mixed with a 0.2 M zinc salt additive, in which the OH^- could promote the ion exchange between the two electrodes to ensure a reversible reaction, and zinc ions can reduce the energy barrier for solvation of metallic zinc during the charge process.[44] Moreover, the polymer electrolyte has been designed to relieve water volatilization and side reactions generated from the high-concentration salt solution, finally achieving stable cyclic performance.[45] For the air cathode, bifunctional electrocatalysts act as the main component to affect the energy efficiency and lifespan of Zn–air batteries.[46] Understanding the configuration of air electrodes, involved reaction mechanisms, and current challenges is crucial for developing efficient bifunctional oxygen electrocatalysts.

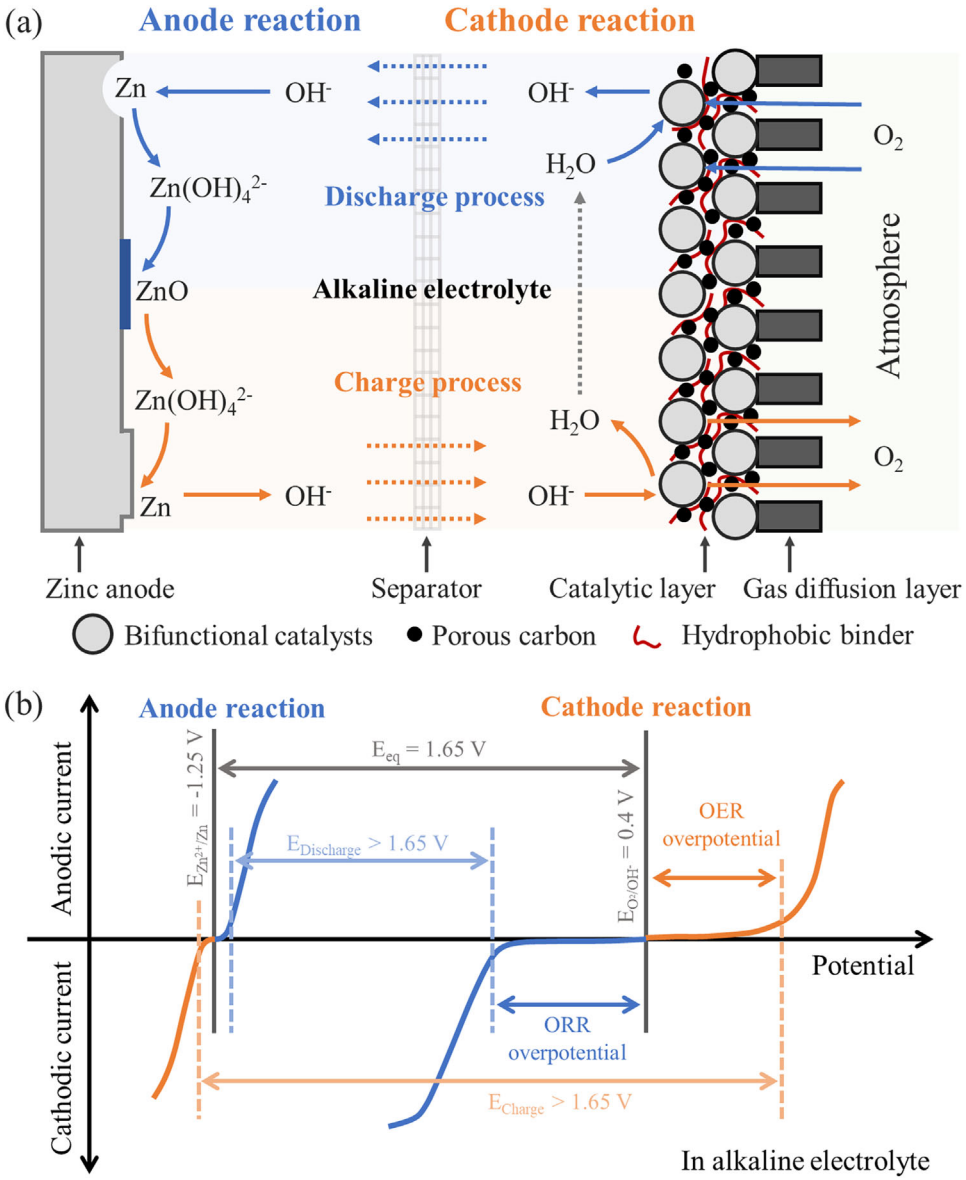

Scheme 2. Scheme illustration of a) the configuration and reaction process of rechargeable Zn–air batteries, and b) corresponding typical polarization curves in zinc anode and air cathode.

2.1. Air Cathode Configuration

Typically, the air cathode is composed of three main components: the current collector, the gas diffusion layer, and the catalytic layer. These main components function together to create a favorable environment for the catalytic reaction at the gas/solid/liquid triple-phase interface[47] The current collector mainly selects material with high electron conductivity, flexibility, and the inhibition of corrosion, such as Ni foam, Ti mesh, and stainless steel, to support the fast electron transfer from catalysts[48] The gas diffusion layer, which is usually composed of a mixture of hydrophobic PTFE (polytetrafluoroethylene) binder and porous carbon with the mass ratio of 7: 3, constructs the channel for oxygen transport and electrolyte penetration on the catalyst surface[49] More importantly, the catalytic layer contains the conductive porous carbon, bifunctional ORR/OER electrocatalyst, and polymer binders, in which the hydrophobic binder, such as Nafion and PTFE, was employed to facilitate oxygen diffusion and avoid the water flooding effect[50] Generally, the current collector is positioned between the catalytic layer and gas diffusion layer, generating a unique sandwich structure[51] In most research, the gas diffusion layer can also be used as the current collector because conductive carbon paper or carbon cloth is used as the gas diffusion layer. In this configuration, the catalytic layer is oriented toward the electrolyte to facilitate the ORR and OER reactions on the gas/solid/liquid triple-phase interface (**Scheme 2a**)[7]

Specifically, the bifunctional ORR/OER electrocatalyst within the catalytic layer is vital for determining the cyclic overpotential and lifespan of Zn–air batteries. To develop an efficient

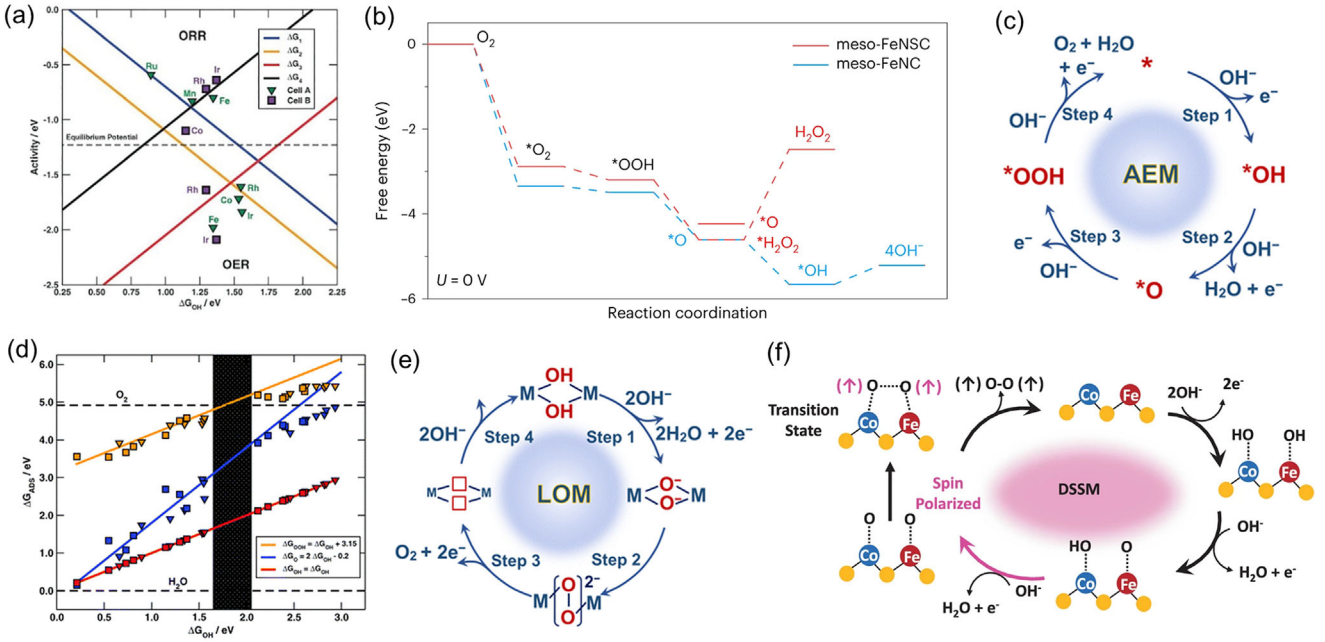

Figure 1. a) Theoretical volcano plots for ORR and OER. Reproduced with permission.[53] Copyright 2011, Royal Society of Chemistry. b) The ORR route based on the four- and two-electron route. Reproduced with permission.[54] Copyright 2024, Springer Nature. c) The AEM pathway. Reproduced with permission.[62] Copyright 2024, Royal Society of Chemistry. d) The scaling relationship between the adsorption energies of intermediate oxygen species. Reproduced with permission.[53] Copyright 2011, Royal Society of Chemistry. e) The LOM pathway. Reproduced with permission.[62] Copyright 2024, Royal Society of Chemistry. f) and The OPM pathway. Reproduced under the terms of 4.0 International License.[65] Copyright 2024, The Authors, published by Springer Nature.

air cathode for rechargeable Zn–air batteries, attentions must be given to several crucial aspects: i) The oxygen electrocatalyst must exhibit high activity for both ORR and OER to minimize the charge/discharge overpotential and improve the energy efficiency of rechargeable Zn–air batteries; ii) The catalytic layer must have the ability to resist corrosion under high-concentration alkaline electrolytes and electrochemical oxidation under high voltage, thus ensuring a long cycle life under repeated testing. iii) The air cathode should deliver a large surface area to offer abundant active sites by constructing an abundant gas–liquid channel; iv) The three-phase interface in air electrodes must balance the transport of oxygen and electrolytes on the catalyst surface by adjusting the hydrophobicity of the catalytic layer to block the liquid electrolyte leakage. Therefore, developing highly active oxygen electrocatalysts while reasonably designing the three-phase interface of the catalytic layer is the research direction for developing advanced air electrodes.

2.2. Reaction Mechanism

For the Zn–air battery in Scheme 2a, oxygen initially diffuses from the air to the gas/solid/liquid triple-phase interface, where it reacts with H_2O to form OH^- on the cathode side during discharge. Meanwhile, the zinc metal at the anode side reacts with OH^- in the alkaline electrolyte to produce the soluble $Zn(OH)_4^{2-}$, which subsequently decomposes spontaneously into ZnO.[52] The charging process involves the opposite reaction to the discharge process, enabling the entire battery system to operate reversibly. The reaction equation is as follows:

$$\text{Aircathodeside}: O_2(g) + 2H_2O(l) + 4e^- \rightarrow 4OH^-(aq)\ E^0 = 0.40\,Vvs.SHE \quad (1)$$

$$\text{Zincanodeside}: Zn + 4OH^- \rightarrow Zn(OH)_4^{2-} + 2e^-, Zn(OH)_4^{2-} \rightarrow ZnO + H_2O + 2OH^-(aq)\ E^0 = -1.26\,Vvs.SHE. \quad (2)$$

Although the theoretical equilibrium voltage is 1.65 V for the Zn–air battery, the actual charging and discharging potentials often deviate significantly from the equilibrium voltage owing to the slow ORR/OER kinetics (Scheme 2b), such as discharge voltages typically below 1.3 V and charge voltages typically above 1.9 V. The significant gap in charge-discharge voltage is primarily influenced by the oxygen electrocatalyst.

We assess the bifunctional catalytic activity of these electrocatalysts by defining the potential difference (ΔE) between OER and ORR. Studies indicate that ORR and OER activities of oxygen electrocatalysts exhibit a volcanic relationship concerning *OH adsorption energy. To construct bifunctional oxygen electrocatalysts with high performance, it is necessary to match the vertices of the ORR and OER volcano plots, as shown in **Figure 1a**.[53] We further illustrate the ORR/OER mechanism for understanding the design concept of the oxygen electrocatalyst.

Regarding the ORR mechanism, two potential reaction pathways have been identified: a four-electron pathway and a peroxide two-electron pathway, which are based on the bidentate and

end-on O_2 adsorption mode on the catalyst's surface (Figure 1b).[54] The two-electron pathway mainly generates the intermediate product H_2O_2, as exhibited in the following equations:

$$O_2\,(g) + H_2O\,(l) + 2e^- \rightarrow HO_2^-\,(aq) + OH^-\,(aq)\; E^0 = -0.07 Vvs.SHE \quad (3)$$

In general, the generation of H_2O_2 during the charging and discharging process may restrict energy efficiency and reduce the cycling life due to irreversible charging-discharging processes. Therefore, we believe that a fully reversible four-electron pathway is necessary during the charging and discharging process.

To further understand the ORR mechanism, the density functional theory (DFT) theoretical calculation could be applied, which theoretically revealed the adsorption free energy for intermediate species. Subsequently, the rate-determining step of ORR could be calculated through the free energy barrier of the four-step elementary reaction, which can deeply guide the improvement of catalyst activity.[55] The four-step elementary reaction for ORR is as follows:

$$O_2\,(g) + * + e^- + H_2O\,(l) \rightarrow OOH* + OH^- \quad (4)$$

$$OOH* + e^- \rightarrow O* + OH^- \quad (5)$$

$$O* + H_2O\,(l) + e^- \rightarrow OH* + OH^- \quad (6)$$

$$OH* + e^- \rightarrow * + OH^- \quad (7)$$

In which the OOH*, O*, and OH* are the adsorbed intermediates, * represents the active sites in oxygen electrocatalysts.

In addition, DFT calculations can identify the real active site by regulating the adsorption model of four intermediates.[56,57,58] The conversion of OH* to O* mainly occurs on the Ni site of Fe-Ni-N_6 catalysts based on the optimized adsorption structure.[59] Interestingly, Li et al. proposed that a two-electron redox chemistry with a two-electron ORR pathway could facilitate energy efficiency in a neutral medium for the rechargeable Zn–air batteries, owing to the fast reaction kinetics. They found that the OOH* protonation is preferred on FeN_2S_2 sites to favor the two-electron reaction through the DFT calculation.[54] This new type of two-electron pathway benefits the reaction kinetics in the gas–liquid–solid three-phase interface, thus reducing the working overpotential of neutral Zn–air batteries. Recently, plenty of operando characterization has been performed to probe the ORR mechanism, such as FTIR (Fourier-transform infrared spectroscopy), Raman, XAS (X-ray absorption spectra), and so on, to support the result of DFT calculations.[60] As an example, Liu et al. observed the superoxide *OOH intermediate emerging on Ni^{4+} sites on the ORR process through the operando synchrotron spectroscopies, which is consistent with the four-electron reaction pathway. The *operando* approach plays an essential role in probing and understanding dynamic changes in the atomic and electronic structures of oxygen electrocatalysts.[61]

The OER process mainly involves four concerted proton-electron transfer (CPET) pathways with the reverse process of ORR when executing the traditional adsorbate evolution mechanism (AEM) pathway (Figure 1c).[62] The OH* and OOH* adsorption energies demonstrate a linear scaling relationship, which leads to the theoretical OER overpotential of 0.37 V based derived by the AEM pathway (Figure 1d).[53] To break the linear relationship of the AEM pathway, researchers found that the participation of oxygen vacancies in the OER process can avoid the formation of OOH*, thus improving the OER activity (Figure 1e).[62] In general, the strong metal-oxygen covalency in high-valence metal oxides facilitates the participation of oxygen vacancies and charge transfer in catalytic reactions. The high valency metal-oxide bond induces a downshift in the metal d-band to improve the overlap with the oxygen p-band, thus activating lattice oxygen, which serves as the active site, to be involved in the water oxidation process through lattice oxygen mechanism (LOM) pathways. Initially, adsorbed *O species attack the lattice oxygen to produce $*O_2^{2-}$ intermediate species. Subsequently, O_2 is released to create the oxygen vacancy, while OH^- ions adsorb into the oxygen vacancy to form *OH species on oxygen sites. Finally, the active oxygen site is regenerated through a coupled proton and electron transfer.

Unlike the conventional AEM pathway, the LOM pathway follows a non-concerted proton-electron transfer route. This arises from the mismatch between the hydroxide affinity at the catalyst/electrolyte interface and electron transfer kinetics, leading to a pronounced pH-dependent OER activity. To characterize the LOM pathway, Hou et al. applied in situ ^{18}O isotope labeling mass spectrometry to detect the $^{34}O/^{36}O$ product using Ir/CoNiB catalysts.[63] In addition, tetramethylammonium cation (TMA^+) can also be applied as a probe to distinguish the stable peroxo-like (O_2^{2-}), serving as the key intermediate in the LOM pathway, and unstable superoxo-like (O^{2-}) species, serving as the key intermediate in the AEM pathway. The decrease in OER catalytic activity indicates the reaction between TMA^+ and O_2^{2-} intermediate species, indicating that the catalysts follow the LOM pathway. In addition, there exist typical dynamic reconstruction behaviors in some transition metal-based catalysts, such as CoFeOOH and NiFeOOH, which need to further explore the active OER sites at the atomic level during the dynamic evolution route. As a proof of concept, the Cu doping can modulate the electronic structure surrounding the CoFeO, which induces the generation of ligand holes with intramolecular electron transfer, thus triggering the lattice oxygen to participate in the subsequent OER process.[64] The complex lattice oxygen pathway makes the exploration of reaction mechanisms extremely difficult, thus requiring more advanced technologies for investigation.

Although following the LOM pathway is advantageous for improving the OER activity, the involvement of lattice oxygen can easily cause lattice collapse, compromising electrochemical stability. The formation of *OOH is the key factor that limits the catalytic efficiency of catalysts operating via the AEM pathway. Thus, preventing *OOH formation during the OER process can disrupt the scaling relationship inherent in the OER process. To simultaneously improve OER activity and stability, researchers have proposed the oxide pathway mechanism (OPM) pathway to avoid the generation of *OOH species and the participation of lattice oxygen (Figure 1f).[65] The *O species formed on two asymmetric metal center sites, coupled with each other to form *OO without forming *OOH species. Therefore, the OPM pathway generally occurs on catalysts with multiple metal components. Similarly, our group also proposed that catalysts, with Mn-O-Ru dual-sites,

following the OPM pathway with breaking the O═O bond, can reduce the energy barrier during the ORR process.[11]

Elucidating the fundamental mechanisms governing OER pathways (e.g., AEM, LOM, OPM, etc.) is critical for rationally designing NiFe-based electrocatalysts with enhanced activity and operational stability. Despite intensified efforts to develop high-performance NiFe catalysts, persistent uncertainties regarding their dynamic structural evolution under operando conditions hinder progress.[66–68] A paradigm shift toward atomistic-level understanding of catalytic mechanisms (e.g., active-site coordination, charge-transfer kinetics) and transient phase transformations is imperative to bridge empirical optimization with theoretical guidance.[69] Central to this challenge is the dynamic reconstruction of NiFe catalysts during OER. Recent studies demonstrate that irreversible structural transformations, such as the formation of Ni/Fe oxyhydroxides (e.g., $Ni_{1-x}Fe_xOOH$), govern the catalytic performance. In situ/operando characterization techniques, including XAS,[70,71] Raman spectroscopy,[72–74] X-ray photoelectron spectroscopy (XPS),[75] and FTIR,[76,77] coupled with computational simulations, enable real-time monitoring of electronic state transitions, lattice oxygen participation, and intermediate adsorption/desorption behaviors during oxygen evolution processes, thereby providing atomic-level insights into structure, activity, and stability relationships. For instance, Wei et al. revealed that Co-doped NiFe layered double hydroxides (LDHs) undergo reconstruction into $Ni(Co)_{1-x}Fe_xOOH$ species during OER, where Co doping lowers Ni oxidation potentials and accelerates active phase formation.[78] Similarly, Yu et al. demonstrated that dealloyed Ni-Fe-B-Si-P amorphous catalysts exhibit optimized surface environments through phosphate/silicate/borate oxo-anions, shortening the $Ni^0 \rightarrow Ni^{4+}$ oxidation pathway and reducing OER energy barriers.[79] The simultaneous activation of metal and lattice oxygen sites to establish a synergistic multi-mechanism catalysis is anticipated to enhance OER by providing abundant active sites and balancing catalytic activity and stability. However, significant challenges persist in achieving this goal. Based on this consideration, Mu et al. demonstrate that anodic activation initiates the redox processes of both metal and lattice oxygen sites, involving the formation and replenishment of oxygen vacancies. Consequently, Fe and S are co-introduced through chemical etching, which induces numerous structural defects and facilitates the complete transformation to R-NiFeOOH@SO_4 active sites during electrochemical activation.[80] Despite these advancements, the specific effect of incorporated Fe heteroatoms remains ambiguous, largely due to a lack of direct understanding of the dynamic interactions between Ni and Fe species under OER conditions. Therefore, real-time monitoring of OER-related behavior in NiFe LDHs, focusing on the evolution of the local coordination environment, is crucial for gaining deeper insights into the catalytic mechanism. Yao et al. employed in-situ electrocatalysis-fit ED-XAFS (energy-dispersive X-ray absorption fine structure), machine learning, and theoretical calculations to conduct a time-resolved study of the deprotonation of NiFe LDH under OER conditions, elucidating the enhancing role of Fe in this process.[70] Through the integration of XAFS fitting and O 1s XPS results, it was found that Fe substitution significantly shifts the Ni d-band center energy from −2.214 eV to −2.511 eV. This downshift results in weaker metal-oxygen binding, particularly for *O, thereby improving OER activity. A comprehensive understanding of the reaction mechanism is vital for designing highly active and stable oxygen catalysts, while the rational design of such catalysts necessitates a profound comprehension of catalyst design strategies.

2.3. Challenges of the Air Cathode

Although the equilibrium voltage is 1.65 V at the Zn–air battery system, the actual discharging and charging voltages are usually much lower and higher than the equilibrium voltage, respectively, finally causing the limited round-trip efficiency of around 55–65%.[81] The complex reaction environment at the gas-liquid-solid interface and the sluggish kinetics at the catalytic layer in the air cathode side have become the biggest impediment to the battery efficiency and power density.[82] Therefore, rationally designing the air cathode with bifunctional electrocatalytic activity can effectively minimize the potential gap between the discharge and charge voltage. More importantly, the highly efficient bifunctional electrocatalyst requires some ideal properties, such as a large surface area, high catalytic activity, sufficient pore structure for mass transfer, robust architecture for mechanical and chemical stability for sustaining durability in strongly alkaline conditions, high electron conductivity, and the uniform distribution of catalytic sites. However, most electrocatalysts are far from acceptable, there still exist many challenges to the air cathode to enable practical Zn–air batteries: i) Efficient bifunctional catalytic activity. In the air cathode, two completely reversible electrochemical reactions make it difficult for a single active site to simultaneously promote efficient ORR and OER activity. The scaling relationship between different oxygen intermediates (*O, *OH, and *OOH) also heavily impeded the simultaneous realization of bifunctional catalytic activity[83]; ii) The durability under high oxidation voltage. Under high oxidation voltage, most catalysts will encounter issues such as the electrochemical decomposition of carbon materials or the oxidative dissolution of metal compounds, resulting in significant structural changes in the catalyst and serious damage to catalytic activity, which is more pronounced under high current densities[84]; iii) The mass transport and charge transfer at solid–liquid–gas three-phase interface. The main reactants, O_2, H_2O, and OH^-, involved in the catalytic layer include the oxygen and liquid electrolyte. Therefore, robust three-phase interfaces need to be designed through hydrophobic treatment to construct efficient gas and liquid transport channels for reactants from different phases.[85] However, during repeated charging-discharging processes, the catalyst is easily infiltrated by the electrolyte, causing gas channels to be blocked, which can lead to a sharp decline in discharge performance. In addition, carbon dioxide in the air may diffuse into the gas diffusion layer to react with OH^- to generate the side product carbonate in the gas channel, which may cause the blockage of gas transport channels, thus decaying the cycling life of Zn–air batteries[86]; iv) Catalyst cost. The cost of catalysts comes from two aspects: material cost and synthesis cost. Noble metal catalysts exhibit superior catalytic activity, such as Pt/Pd and RuO_2/IrO_2 for ORR and OER, respectively. However, the high price and poor durability impede the large-scale application process of noble-metal materials in the Zn–air battery system.[87] At present, the catalytic activity of some oxygen catalysts using low-cost elements has surpassed that of noble

metal catalysts, but the complex preparation process makes the catalyst cost very high, such as graphene and MXene.[88] Developing a simple strategy for synthesizing highly active non-noble metal catalysts still exists as a challenge.

The three-phase interface is essential for determining the cyclic lifespan of Zn–air batteries, prompting the design strategies for enormous advanced air cathode structures to enhance their durability. Additionally, oxygen electrocatalysts greatly influence the performance and cycling stability of rechargeable Zn–air batteries. Consequently, the advancement of highly active and stable bifunctional oxygen electrocatalysts is essential for advancing the practical deployment of rechargeable Zn–air batteries. In this context, NiFe-based materials have surfaced as particularly promising candidates. We will elaborate on the structural classification of NiFe-based electrocatalysts in the next section.

3. Categorization of NiFe-Based Electrocatalysts

According to the volcano plots, Ni-based catalysts exhibited moderate binding energy similar to noble metals, thus expressing a low theoretical OER overpotential. At the early stage, Corrigan et al. revealed that the low concentration Fe atom with the content of 0.01% added into Ni-based oxides could significantly enhance the OER activity.[89] Since then, the variety of NiFe-based OER electrocatalysts has been rapidly developed. However, most NiFe-based electrocatalysts lack ORR activity owing to their intrinsic property, including poor oxygen adsorption energy and surface reconstruction.[90] To apply NiFe-based electrocatalysts into the Zn–air battery system, many strategies are designed for boosting the ORR performance of NiFe-based electrocatalysts, such as doping the metal element (such as Mn and Co) with ORR properties,[91] alloying NiFe-based catalysts,[92] creating pore structure with unique morphology (such as nanowire, nanoparticles, and core–shell structures),[93] surface modification with organic molecules or inorganic species,[94] constructing structural defects,[27] and introducing supports (such as carbon, TiO_2, or TiN).[95,96] These strategies leverage the unique structure and electronic properties of NiFe-based materials to overcome their ORR limitations. Although decreasing the overpotential gap between the ORR and OER is essential for designing bifunctional electrocatalysts, other factors, such as long-term degradation under harsh conditions, large-scale synthesis, cost-effectiveness, industrial current operation, and suitable electrolyte-catalyst interactions, should also be considered in the catalyst design criteria to pursue the commercial application. As shown in **Figure 2**, different NiFe-based catalysts exhibit different characteristics and advantages resulting from the different catalyst structures. For instance, the NiFe-layered double hydroxides (LDH) exploit their tunable interlayer anions to balance ion diffusion and active-site exposure, enabling bifunctional OER activity. NiFe oxides utilize rigid 3D frameworks and mixed-valent metal sites for robust OER stability. NiFe compounds combine metallic conductivity and anion regulation to achieve operation under high current density. NiFe-MOFs achieve ultrahigh porosity and adjustable topology structure, or serve as the precursor for metal/carbon derivatives, enhancing gas-involving reactions like ORR. NiFe alloys exhibit ultra-high electrical conductivity, phase structure-dependent activity, and corrosion resistance, enabling them to achieve bifunctional activity at high currents. In this section, we will continue elaborating on categorizing NiFe-based catalysts to understand the design strategy.

1) NiFe-LDHs: LDHs are composed of positively charged metal hydroxide layers interspersed with charge-balancing anions, following the general formula of $[M^{2+}_{1-x}M^{3+}_{x}(OH)_2]^{x+}\cdot[A^{n-}_{x/n}]^{x-}\cdot mH_2O$, where M^{2+} and M^{3+} denote divalent and trivalent cation, respectively, X represents the molar ratio of the $M^{2+}/(M^{2+} + M^{3+})$ ranging from 0.2 to 0.33, and A^{n-} refers to either organic or inorganic anion, have been extensively studied to enhance the OER performance.[97] Various NiFe-LDH can be synthesized by intercalating different inorganic anions, such as CO_3^{2-}, SO_4^{2-}, Cl^-, and NO_3^-, within the NiFe-LDH layers, as shown in Figure 2a.[98] It has been reported that the LDH could achieve a theoretically specific surface area of approximately 1000 $m^2\ g^{-1}$ due to the delamination and exfoliation process, which produces positively charged nanosheets within a unilamellar thickness of less than 1 nm and an aspect ratio exceeding 100.[99] In particular, the NiFe-LDH with its unique structure has made the rapid diffusion of the products and reactants, as well as a fast proton-coupled electron transfer kinetics during the oxygen evolution process. Wei et al. created a new electrochemical synthesis route to prepare Fe-containing LDH hierarchical nanoarrays (MFe LDH, where M = Ni, Co, Mn), with NiFe LDH demonstrating the most thermodynamically favorable reaction pathway and superior electrochemical performance in OER.[100] Sun et al. investigated the OER route on the NiFe LDH through the first-principle DFT + U calculations, revealing that the Fe in NiFe LDH enhances electron transport and exhibits higher activity than $Ni(OH)_2$.[101] Nonetheless, the catalytic efficiency of NiFe-LDH is heavily restricted by the aggregate, insulating characteristics, and limited durability. Therefore, advanced strategies, such as exploring new preparation methods, inserting the organic or inorganic anion in the LDH layer, combining the NiFe-LDH with carbon conductive (Graphene, carbon dots, or carbon nanotubes), and so on, could be applied to boost the activity and activity of the pristine NiFe-LDH, benefiting from the promoted electron conductivity and enlarged surface area.[27,29,102] Although original NiFe-LDH catalysts exhibit poor ORR activity, the lamellar NiFe-LDH can anchor other metal ions with ORR activity to obtain sufficient bifunctional catalytic activity. Moreover, applying support with ORR activities to load NiFe-LDH catalysts can create reasonably expected ORR activity and enhance the bubble desorption on the NiFe-LDH surface.
2) NiFe Oxides: Compared to NiFe-LDH, NiFe-based oxide exhibits a stable crystal structure to achieve superior long-term durability in an alkaline medium. In NiFe oxides, Ni is usually considered the main active site, while doped Fe can adjust the electronic structure of Ni element corresponding with enhanced Ni-O covalency.[103] Therefore, the Fe content is usually low in NiFe oxides. Fe-doped NiO is an important class of ORR/OER catalysts. The NiO crystal structure is like NaCl, which belongs to the rock-salt structure. Ni atoms and O atoms are located on the lattice points of the face-centered cube, forming a regular octahedral arrangement (Figure 2b).[104] In addition to simple oxides, NiFe-based spinel oxides exhibit superior performance, due to

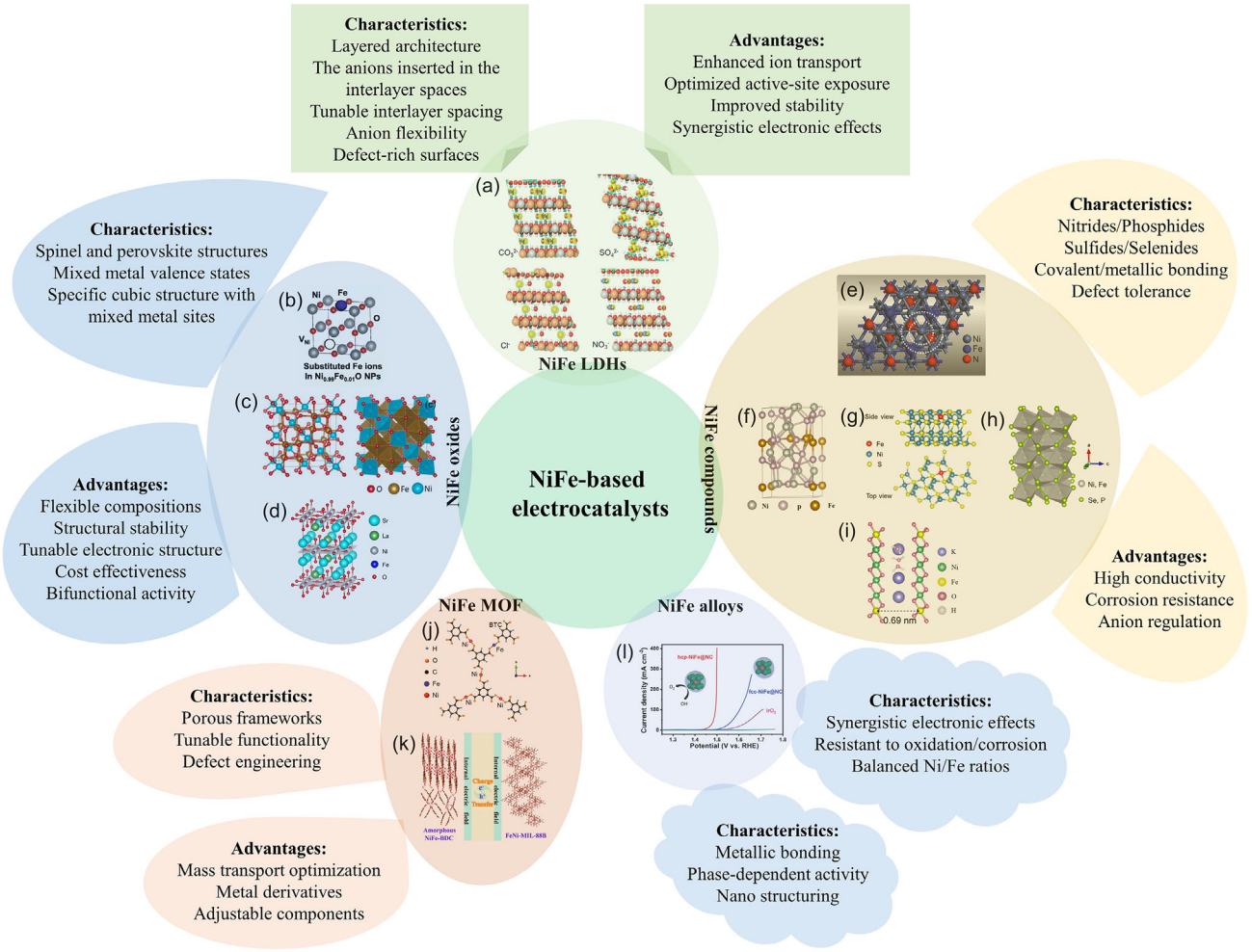

Figure 2. The structure corresponding to the characteristics and advantages resulting from the catalyst structure of a) NiFe-LDH with CO_3^{2-}, SO_4^{2-}, Cl^-, and NO_3^- in interlamination. Reproduced with permission.[98] Copyright 2023, Wiley-VCH. b) Fe-doped NiO. Reproduced with permission.[104] Copyright 2021, Elsevier. c) NiFe-based spinel oxide. Reproduced with permission.[105] Copyright 2024, Elsevier. d) NiFe-based perovskite oxide. Reproduced under the terms of 4.0 International License.[108] Copyright 2018, The Authors, Published by Springer Nature. e) Ni_3FeN. Reproduced with permission.[112] Copyright 2018, Wiley-VCH. f) Fe-doped NiP. Reproduced with permission.[113] Copyright 2022, American Chemical Society. g) Fe-doped Ni_3S_2. Reproduced with permission.[114] Copyright 2021, Springer Nature. h) $Ni_{0.75}Fe_{0.25}Se_2$. Reproduced with permission.[115] Copyright 2021, Elsevier. i) Ni_3FeOOH. Reproduced with permission.[118] Copyright 2025, Elsevier. j) NiFe-MOF. Reproduced with permission.[120] Copyright 2021, Wiley-VCH. k) Crystalline/amorphous-NiFe-MOF. Reproduced with permission.[121] Copyright 2022, Royal Society of Chemistry. l) Face-centered cubic (fcc) and hexagonal close-packed (hcp) structures for NiFe alloys. Reproduced with permission.[122] Copyright 2019, Wiley-VCH.

their unique electronic and chemical features. As for $NiFe_2O_4$ spinel oxides, the divalent cation Ni^{2+} occupies the tetrahedral sites, while the trivalent cation Fe^{3+} is located in the octahedral sites, as illustrated in Figure 2c.[105] In particular, the $NiFe_2O_4$ spinel oxides feature multivalent redox couples, especially the Ni^{2+}/Ni^{3+} and Fe^{3+}/Fe^{4+}, which provide essential surface redox-active metal centers for the activation and adsorption and oxygen electrochemistry-based reaction intermediates, finally boosting the oxygen redox chemistry. For instance, Fortunelli et al. extensively investigated the OER reaction mechanism for the $NiFe_2O_4$ through the DFT method, revealing that the spinel structure favors a partially dissociated water coverage (*OH + *H, $*H_2O$) on metal sites as the resting state, with Fe serving as the assistant sites and the Ni as the active site.[106] However, the p-type semiconductor properties of pristine $NiFe_2O_4$ greatly limited the electron transfer of the catalyst, resulting in low conductivity, insufficient utilization of active sites, as well as inferior OER performance. To mitigate these issues, the $NiFe_2O_4$ spinel oxides are usually combined with carbonaceous materials to promote electronic conductivity or inserted with ORR activity elements such as Co or Mn to boost bifunctional activities. NiFe-based perovskite oxide is another important oxygen catalyst.[103,107] The typical perovskite oxide structure comprises rare earth or alkaline earth metal cations with 12-fold coordination in the A-site and transition metal cations (such as Ni and Fe) with 6-fold coordination in the B-site (Figure 2d).[108] As a result, doping the various transition metal ions into the B-site can

effectively modulate the ORR and OER activity for NiFe-based perovskite oxides.

3) NiFe Compounds: Usually, NiFe oxides/hydroxides exhibit poor conductivity, while doping anions can enhance the intrinsic conductivity of NiFe compounds. In addition, the adsorption state and electronic structure of the reaction intermediates for NiFe compounds can also be regulated by the anions, owing to anionic heteroatoms that can interact with cations and act as electron donors.[109] Particularly, NiFe compound catalysts with different anionic atoms (N, P, S, Se, B, etc.), all demonstrated superior catalytic activity and stability, benefiting from that the heteroatom dopants can optimize the local coordination environment of NiFe sites with reduced binding energies.[110,111] So far, NiFe compounds with different anions, such as Ni_3FeN (Figure 2e),[112] Fe-doped NiP (Figure 2f),[113] Fe-doped Ni_3S_2 (Figure 2g),[114] and $Ni_{0.75}Fe_{0.25}Se_2$ (Figure 2h),[115] have been prepared to adjust the ORR and OER activities. As reported by Gao et al., the electron-deficient boron could enhance the formation of high-oxidation-state Ni by inducing a cathodic shift in the $Ni^{2+}(OH)_2 \rightarrow Ni^{3+\delta}OOH$ transition potential and reducing energy barriers for the reaction. This modification ultimately resulted in outstanding catalytic activity and exceptional long-term durability for OER in an alkaline medium.[116] More importantly, it is essential to design catalysts with superior abundant active sites and high conductivity, which could heavily reduce the effect of the large charge resistance between catalysts and electrolytes. Xiong et al. reported a NiFeP catalyst with metallic bonds, high macroscopic conductivity, and large surface active sites for OER. The thin layer NiFeOOH on conductive NiFeP catalysts obtained through surface reconstruction serves as the true active site, while the bulk NiFeP enables the fast electron transfer.[117] Generally, for NiFe compounds, the NiFeOOH formed by surface reconstruction provides the main active sites for OER, as shown in Figure 2i, while the anion could effectively regulate the electronic structure and induce proper distorted structures in NiFeOOH to boost catalytic activities.[118]

4) NiFe-MOFs: Metal–organic framework (MOF) with metal ions and organic ligands has aroused great attention for the oxygen redox chemistry system, benefiting from the large surface area corresponding with abundant active sites, unique pore structure for fast mass transfer, tunable compositions and structures, as well as the crystalline topologies and changeable porosities.[119] Currently, the NiFe-based MOF catalysts have been successfully applied to OER and ORR processes, owing to their stable skeleton structure and high electrochemical activity in alkaline media. The Ni and Fe atoms coordinate with oxygen sites in organic ligands to generate a cage-type structure (Figure 2j). To better understand the reaction mechanism of the bimetallic NiFe-MOF, Zhao et al. systematically illustrate the crucial structural parameters for OER performance via the in-depth characterizations combined with theoretical calculation, in which the OER activity has been affected by the hierarchy properties, while the charge transfer efficiency can be influenced through accessible sites.[120] Notably, the surface area of accessible MOF has been promoted from 89 to 437 $m^2\ g^{-1}$ due to the substitutive Fe cations on Ni sites, finally facilitating the desorption of water. In addition, Wang et al. induced the carboxylated carbon quantum dots into the two-dimensional NiFe-MOF to efficiently boost the Zn–air flow battery, mainly owing to the offset valence state of metal ions. Different organic ligands could be applied to prepare different types of NiFe-MOF catalysts. Han et al. developed the crystalline/amorphous NiFe-based MOF catalysts, which contained the amorphous NiFe-BDC and crystalline FeNi-MIL (Figure 2k).[121] After assembling the design catalysts into a typical three-electrode system, the OER performance claimed super-high activity with a low OER overpotential of only 236 mV at 10 mA cm^{-2}. Although the NiFe-based MOF catalyst could promote the Zn–air battery performance, the wastage of raw materials in the construction of MOF material, limited morphologies/sizes, and poor electronic conductivity all remained as challenges for efficiently utilizing the MOF structures. Therefore, the MOF has been widely used as the sacrificial template or precursor to fabricate metal derivatives to enhance electrical conductivity, catalytic activity, and durability via pyrolysis strategies.

5) NiFe Alloys: According to the different arrangements of Fe and Ni atoms, the NiFe alloys can be distinguished into different structures, including face-centered cubic (fcc), face-centered tetragonal (fct), hexagonal close-packed (hcp), as well as body-centered cubic (bcc) types. For the different Ni and Fe stacking modes in NiFe alloys, the electronic properties would be affected to regulate the intrinsic activity. Wang et al. report that hcp-NiFe catalysts achieve superior OER activity than conventional fcc-NiFe catalysts (Figure 2l).[122] Therefore, NiFe alloys with stable crystal structure and high electron conductivity can be applied as a suitable matrix to construct bifunctional ORR/OER catalysts through various modification strategies.[123,124] Moreover, many techniques are used to create NiFe alloys combined with other components and tailor their compositions. As an example, Wang et al. synthesized the NiFe alloy with the N-doped carbon (hcp-NiFe@NC) to boost the catalytic performance. Benefiting from its controlled crystal structure and composition, the hcp-NiFe@NC exhibited exceptional OER performance characterized by a low overpotential.[122] Additionally, the NC coating on the NiFe surface contributed to prolonged stability by preventing Fe segregation. In addition, Xu et al. demonstrated that constructing the core@shell nanostructure for NiFe alloy can facilitate the bifunctional electrocatalytic activity of the designed catalysts because the NiFe alloy provides abundant valence states and regulates the electronic structure of Fe_3NiN.[125] Particularly, there exist some disadvantages for NiFe alloys, and they need further improvement to design bifunctional catalysts, such as insufficient stability in the high concentration of alkaline medium and high charge voltage, and unstable catalytic sites owing to nanoparticles aggregating under the electrochemical process. Therefore, more efficient approaches and advanced techniques need to be developed to optimize the OER and ORR activities of NiFe alloys with long durability and high activity.

4. Evaluation of NiFe-Based Electrocatalysts

The assessment of NiFe-based electrocatalysts for Zn–air batteries requires a comprehensive technique that integrates material

characterization, electrochemical performance assessment, actual catalytic site exploration, and system-level validation. The exploration processes for evaluating their structure–activity relationship can be conducted below.

i. Synthesis Methods and Catalyst Properties: The formation and structure of electrocatalysts will influence the activity and lifespan performance, while the synthesis method is also decided based on the laboratory conditions. In the process of exploiting the NiFe-based catalysts, many synthetic methods can be screened for designing the NiFe-based catalysts with tuned crystal particle size, microstructures, and special physical/electrochemical proprieties, such as coprecipitation of metal precursors methods, electrodeposition techniques, microwave combustion method, hydrothermal method, and metal corrosion on the metal matrix.[126,127] For instance, Huang et al. have successfully constructed well-designed NiFe-based catalysts through a simple hydrothermal treatment by adding extra Fe^{3+} resource,[128] demonstrating excellent scalability potential. The confirmation of morphology and structural properties for the NiFe-based catalysts is conducted after preparing the NiFe-based catalyst to explore the physical characteristics. The scanning electron microscope (SEM), transmission electron microscopy (TEM), and nitrogen adsorption-desorption isotherm can be used to evaluate particle aggregation, surface reconstruction, and specific surface area.[128] Moreover, the X-ray diffraction (XRD), XPS, XAS, Raman, and FTIR have been employed to detect the phase transformations, analyze surface composition changes, resolve dynamic coordination changes, as well as identify the surface functional group.[129,130]

ii. Bifunctional Activity and Stability Assessment: ORR and OER activities are conducted in a three-electrode system using a rotating disk electrode (RDE) to obtain linear sweep voltammetry (LSV) polarization curves. To evaluate the ORR and OER activities with the uniform criteria and construct the comprehensive electrochemical system, the higher ORR half-potential ($E_{1/2}$) (vs RHE) indicates excellent ORR activity, while the lower OER potential value at the current density of 10 mA cm^{-2} ($E_{OER@10}$) signifies the higher OER activity. More importantly, the bifunctional activity of the NiFe-based catalyst can be evaluated through the ΔE value ($\Delta E = E_{OER@10} - E_{1/2}$), in which a smaller ΔE (below 0.6 V for the current best catalyst) reflects higher bifunctional OER/ORR activity. Calculating the Tafel slopes from LSV curves can evaluate reaction kinetics, while the lower slopes (e.g., below 60 mV dec^{-1} for OER and ORR) suggest favorable charge-transfer kinetics, especially under high current conditions. In addition, the rotating ring-disk electrode (RRDE) measurements can determine the electron transfer number (n, ideally ≈4 for a $4e^-$ ORR and OER pathway) and H_2O_2 selectivity (below 5%), coupling well with the catalytic efficiency.[.][131] For the accelerated degradation tests, the continuous cyclic voltammetry cycling tests can be performed within the OER/ORR potential window to detect the activity retention, while the long-term chronopotentiometry and chronoamperometry can be exhibited at constant current densities (10–100 mA cm^{-2}) and potential (potential corresponding to limited current density) to assess the stability and Faradaic efficiency for OER and ORR, respectively.[132,133] As an example, inspired by the structural advantages of NiFe-LDH/Fe_1-N-C heterostructure hollow nanorods, Xu et al. evaluated their bifunctional ORR/OER performance. The NiFe-LDH/Fe1-N-C catalyst exhibits a remarkable bifunctional activity with the highest $E_{1/2}$ of 0.90 V (**Figure 3a**) and an excellent OER activity of 1.55 V at 10 mA cm^{-2} (Figure 3b), corresponding with the low ΔE of around 0.65 V (Figure 3c), and also demonstrate better stability than noble metal catalysts at constant potential (Figure 3d).[134]

iii. Active Catalytic Site Recognition: NiFe catalysts are prone to structural reconstruction phenomena during the OER process, which can affect their subsequent stability and ORR performance. To comprehensively investigate the structural evolution of NiFe-based electrocatalysts in alkaline media, a multi-modal approach combining electrochemical experiments, in situ/operando characterization, and computational modeling is essential.[135,136] To explore the dynamic evolution of NiFe-LDH/Ni_4Mo, Hou et al. employed the in-situ Raman (Figure 3e) and operando FT-IR (Figure 3f) techniques, in which NiFe-LDH/Ni_4Mo undergoes a phase transition from $Ni(OH)_2$ to γ-NiOOH during OER, with reduced onset potentials (1.40 V vs. RHE), indicating enhanced transformation kinetics due to Ni_4Mo incorporation. The intensified and upshifted νOH bands in FTIR spectra further demonstrate stronger *OH adsorption on NiFe-LDH/Ni_4Mo, attributed to optimized lattice oxygen interactions facilitated by the Ni_4Mo interface.[137] As a powerful characterization, operando XAFS tests can track dynamic changes in Ni/Fe oxidation states and local coordination during OER/ORR. For instance, Chen et al. took the operando XAFS measurements reveal that Ni in Ni-SAs@GNM evolves from a mixed 0/+2 oxidation state to Ni^{3+} (resembling NiOOH) during activation in Fe-containing KOH, driven by OH^- adsorption and Fe incorporation. Concurrently, the coordination geometry transitions from square-planar to centrosymmetric octahedral, evidenced by diminishing $1s\rightarrow 3d/4p_z$ transitions and intensified $1s\rightarrow 4p_{x,y}$ peaks in Ni K-edge XANES spectra (Figure 3g-h).[138] Besides, the in-situ XPS can be adopted to analyze surface composition and adsorbed species (e.g., OH^-, OOH^-) after controlled potential holds, while in-situ XRD can be conducted to monitor bulk structural changes (e.g., amorphous-to-crystalline transitions) under operando conditions.[139] Moreover, NiFe composite catalysts consist of multiple components, and understanding the roles of individual components within the composite catalyst is crucial for the rational design of such catalysts. Theoretical calculations can be employed to investigate the energy barriers of elementary reaction steps involving intermediate species (*O, *OOH, *OH) at specific sites within composite catalysts, thereby enabling the exploration of optimal reactive sites.[140,141] As seen in Figure 3i, DFT calculations reveal that the adsorption of BDC ligands on Ni sites in Ni_3Fe-LDH optimizes intermediate (OH*/O*/OOH*) binding via electronic modulation, reducing the OER overpotential from 0.79 V to 0.76 V by shifting the rate-determining step (Figure 3j,k). This mechanistic insight inspires the design of bifunctional electrocatalysts by integrating Ni_3Fe-based MOFs (with inherent BDC ligands) and ORR-active components.[30] In

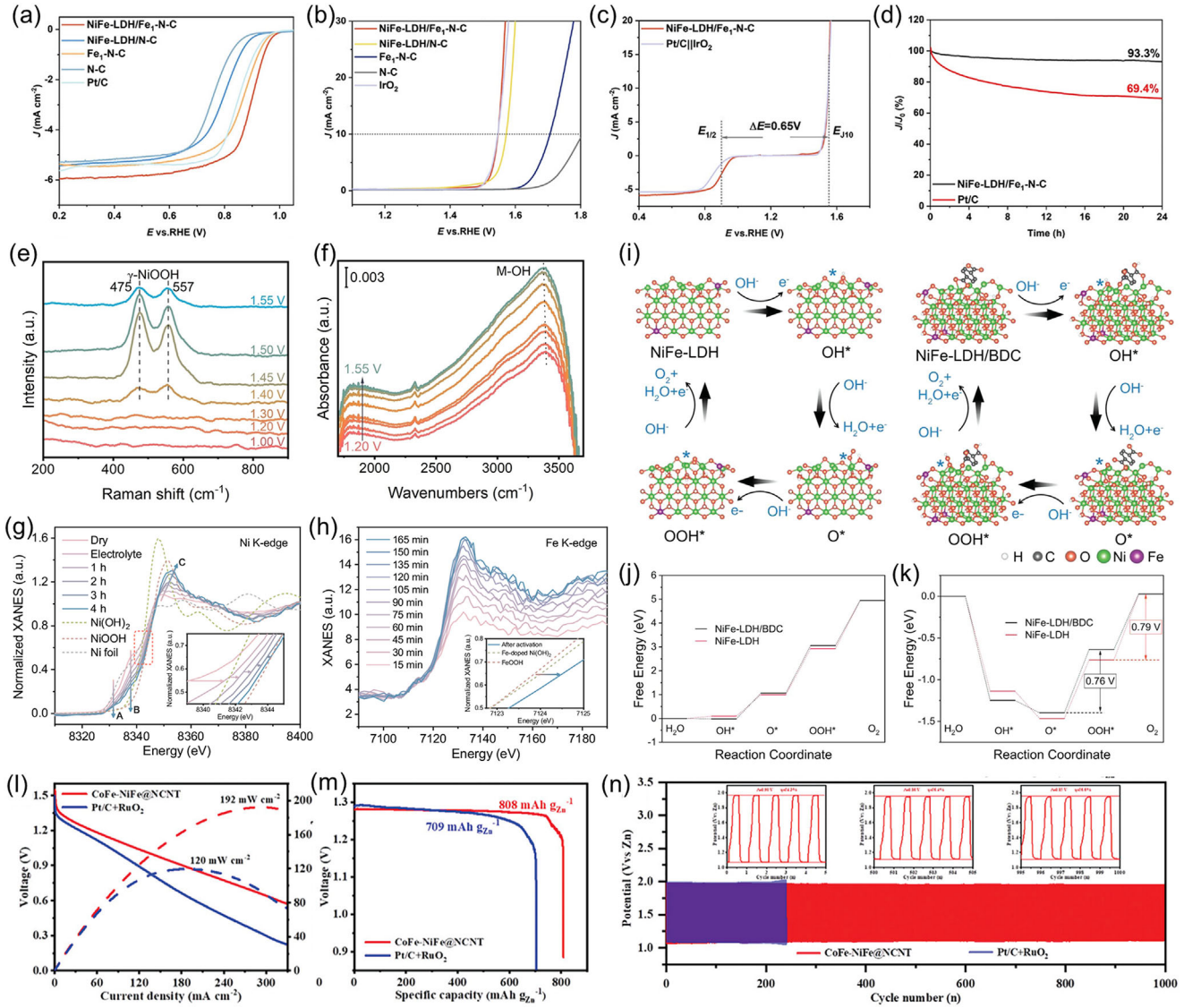

Figure 3. a) ORR activity, b) OER activity, c) bifunctional ORR/OER activity, and d) chronoamperometry test of NiFe-LDH/Fe_1-N-C. Reproduced with permission.[134] Copyright 2023, Wiley-VCH. e) In situ Raman spectra and f) Operando FTIR spectra for NiFe-LDH/Ni_4Mo. Reproduced with permission.[137] Copyright 2025, Wiley-VCH. g,h) Operando XAFS measurements of Ni and Fe K-edge under OER conditions. Reproduced under the terms of 4.0 International License.[138] Copyright 2025, The Authors, Published by Springer Nature. i–k) DFT Theoretical calculation results for NiFe-LDH/BDC. Reproduced with permission.[30] Copyright 2023, Wiley-VCH. l) The polarization curve, m) galvanostatic discharge curve, and n) galvanostatic charge/discharge performance of Zn–air batteries assembled with CoFe-NiFe@NCNT catalysts. Reproduced with permission.[130] Copyright 2025, Wiley-VCH.

addition to obtaining the reaction energy barrier, theoretical calculations can also help understand the electronic interactions between different active sites in composite catalysts. For instance, Cho et al. took the DFT calculations to reveal that Ir doping at Ni octahedral sites in $NiFe_2O_4$ (Ir-NFO) enhances oxygen adsorption energy via charge redistribution and d-band center upshifting, stabilizing the Ni-O-Fe motif as the active center.[142]

iv. The Zn–Air Battery Performance: Recently, the Zn–air battery performance in the laboratory was tested with homemade devices, which were conducted in practical configurations (e.g., coin cells, pouch cells) under ambient air. For Zn–air batteries, the cycle life can be investigated through the electrochemical working station with the constant current density, in which the durability (usually around 100 – 500 h at >10 mA cm^{-2}), the discharge capacity (usually around 700–800 mAh g^{-1} at >10 mA cm^{-2}), power density (usually around 100–250 mW cm^{-2}), and the energy efficiency (usually around 55–65% at >10 mA cm^{-2}), are all the essential parameters. As shown in Figure 3l, the CoFe-NiFe@NCNT catalyst exhibits exceptional bifunctional oxygen electrocatalytic activity, evidenced by a low potential gap (ΔE = 0.68 V) and a peak power density of 192 mW cm^{-2} in Zn–air batteries. Demonstrating robust stability, the Zn–air battery

maintains consistent discharge voltages (1.13–1.36 V) across current densities up to 50 mA cm^{-2} and achieves a high specific capacity of 808 mAh g_{Zn}^{-1} at 10 mA cm^{-2} (Figure 3m), with minimal capacity decay over 1000 cycles with 54.3–56.6% round-trip efficiency (Figure 3n).[130]

Through comprehensive characterization of the catalyst's structure and performance, the structure-activity relationship can be elucidated, thereby establishing design principles for NiFe-based catalysts. Subsequent evaluation of their practical charge-discharge performance in actual battery devices, particularly under industrial-grade current, is essential. A techno-economic analysis should then be conducted, incorporating material costs, equipment operating expenses, and the economic value of system operation, to assess the industrial applicability potential of this material design strategy.

5. Catalyst Design

Among low-cost OER catalysts, NiFe-based electrocatalysts have been proposed owing to their dual-active sites, long stability, tunable compositions, facile fabrication, and being environmentally friendly. In particular, the incorporation of Ni and Fe has been claimed to contribute greatly to the enhancement of the OER electrocatalytic properties, including the abundant defects and enormous active sites, fast electron transfer derived from the interatomic bonding, and suitable intermediate adsorption and desorption energy on Ni^{+} and Fe^{3+} sites.[143,144] To design suitable NiFe-based electrocatalysts for Zn–air batteries, the existing serious fundamental factors need to be involved: i) While NiFe-based catalysts demonstrate enhanced OER activity through regulated Ni-O covalent interactions, their ORR performance is limited by unfavorable oxygen adsorption energetics. Therefore, combining the NiFe catalyst with ORR active phase to create dual active sites and introducing the edge defects or oxygen vacancies to boost the ORR active site are effective strategies to construct the bifunctional NiFe-based electrocatalysts. ii) The Fe^{3+} in the crystal lattice of NiFe catalysts will dissolve in alkaline electrolytes during OER cycles, thus degrading the stability of the catalyst. For boosting the structural stability and alleviating the Fe leaching, encapsulating the NiFe catalysts in N-doped carbon shells or conductive polymers is a suitable strategy to suppress Fe leaching. In addition, the stable intercalants (anions or cations) can be inserted into the NiFe structure to anchor Fe and prevent layer collapse. iii) The insulated NiFe complex usually exhibited poor electrical conductivity with limited electron transfer kinetics. Therefore, the conductive substrates can be integrated with NiFe-based catalysts to regulate the electronic structure and electron conductivity. iv) There exists surface reconstruction for NiFe catalysts during the cycling process, which may generate irreversible phase transitions to block the active sites. Tuning lattice strain or constructing the crystalline-amorphous interfaces in NiFe-based materials can stabilize surface structures and impede the reconstruction effects. v) Complex synthesis procedure hinders mass production and large-scale application. As a result, the establishment of scalable manufacturing protocols enabling high-throughput synthesis of cost-efficient catalysts constitutes a critical pathway toward bridging the laboratory-to-industry gap in energy conversion technologies.

Based on the above consideration, it is expected to obtain the bifunctional catalytic activity for NiFe-based catalysts, thus enhancing the activity and durability of Zn–air batteries. To improve the bifunctional activity and stability of NiFe-based catalysts in alkaline media, various concepts have been proposed, such as introducing anions or cations, compositing second phases, and introducing ORR and OER active components into the catalytic layer. Therefore, we can divide the design strategies of NiFe-based catalysts based on these proposed concepts as follows: anionic modification, cation doping, supporting effect, embedding effect, and multi-component construction. The detailed design concept and advantages will be discussed in the sections below.

5.1. Anionic Modification

As reported, NiFe-based compounds have received enormous attention, benefiting from the high OER performance. Generally, the electrochemical reconstruction phenomena in NiFe-based compounds are primarily responsible for the high OER activity by the generation of high-valence metal oxy-hydroxide (MOOH) active species. Consequently, it is essential to develop electro-oxidation metal species within these compounds to improve the OER performance.[145] One of the main strategies to facilitate the reconstruction by electro-oxidization is the anionic modification strategy, which could obtain high-valence metal sites for OER. For the anionic modification strategy for the NiFe-based electrocatalysts, the chalcogenides (Sulfur, Selenium, Tellurium)-based anions are a vital part, benefiting from the excellent electronic conductivity, tunable electronic structures, and superior OER/ORR performance with long stability.[146,147,148] Chalcogenides (S/Se/Te) function as electron-donating species, modulating the electronic states of transition metal cations (e.g., Ni/Fe) through orbital hybridization and charge redistribution. Their distinct electronic configurations and polarizability critically govern the coordination geometry and catalytic reactivity of active metal centers by regulating the covalent-ionic equilibrium in metal-chalcogen bonding. Crucially, the polarizing capacity of chalcogenides tailors the d-band electronic structure of catalytic sites, which directly influences intermediate adsorption energetics (e.g., *OOH, *OH) by balancing charge transfer dynamics and lattice stabilization effects.[149,150] For example, S-doped NiFe compounds have triggered great interest in improving the electrochemical activity. Based on this, the benefit of co-doping the S and N atom on the graphene integrated with NiFe compounds has been analyzed systematically via Wang's groups.[151] The theoretical calculation results have revealed that the S decoration significantly enhances the generation of OOH* intermediates and substantially reduces the Gibbs free energy across the four fundamental OER steps. To augment the oxygen-based catalytic activity of NiFe (oxy)hydroxide, Pan et al. developed a sulfate ion (SO_4^{2-}) modulation strategy for modifying the pristine NiFe catalysts, benefiting from the electro-oxidation reconstruction of the pre-catalyst as well as the stable OER intermediate (OOH*) (**Figure 4a,b**).[152] This approach derived the NF-S0.15 catalyst, which exhibited exceptional OER activity, characterized by a low overpotential of 234 mV at 50 mA cm^{-2}, sustained lifespan exceeding 100 h, and rapid OER kinetics with a Tafel slope of 27.7 mV

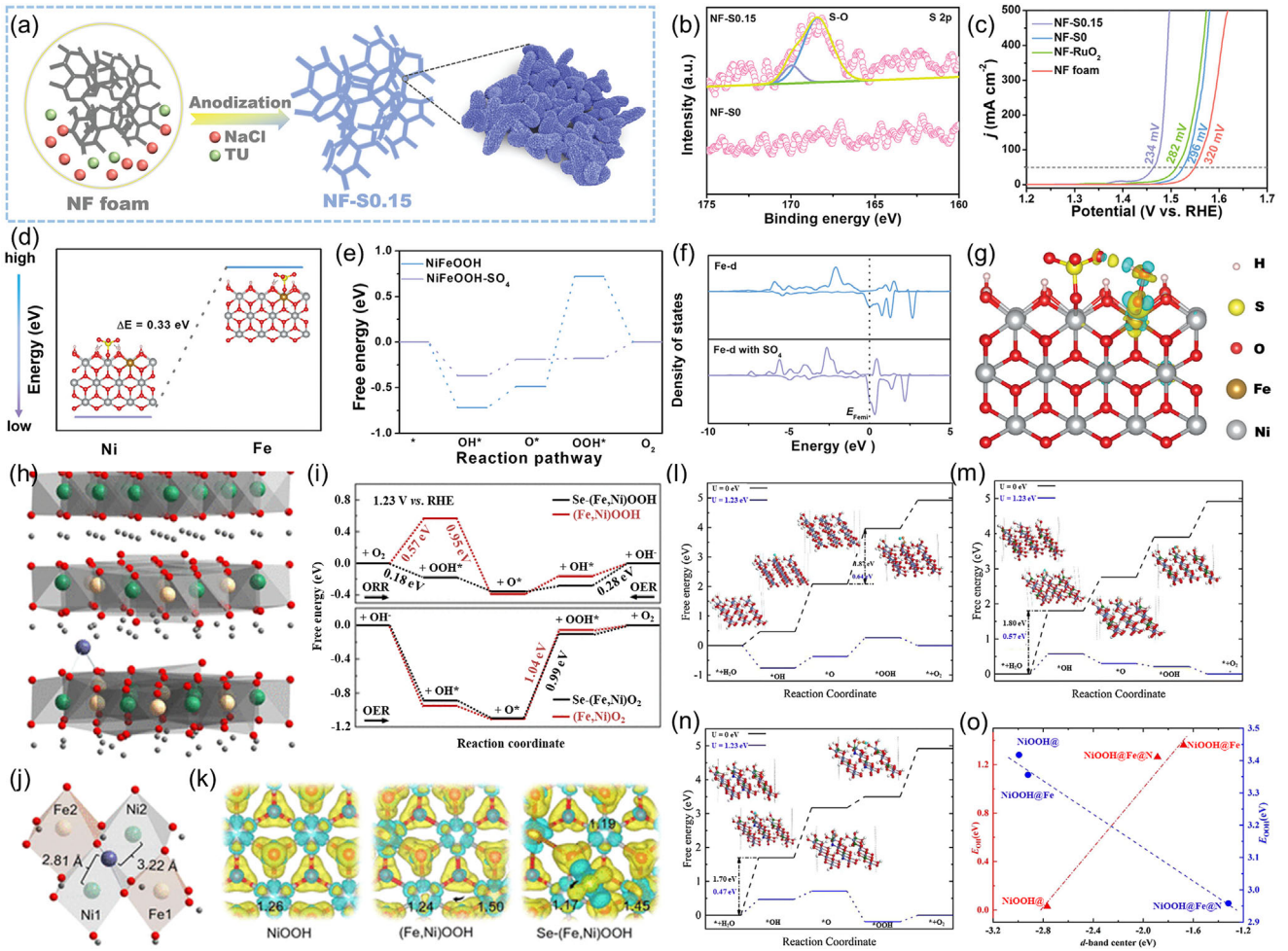

Figure 4. a) The preparation illustration for NF-S0.15. b) XPS characterization of NF-S0.15 and NF for S 2p high resolution. c) OER activity curves of NF-S0.15 with its comparison sample. Theoretical investigations of d) energy of SO_4^{2-} adsorbed on Fe and Ni sites, e) Gibbs free energy diagrams of the OER intermediates, f) DOS spectra, and g) charge density variations in NiFeOOH-SO_4 when OOH* is adsorbed on the Fe site. Reproduced with permission.[152] Copyright 2023, Wiley-VCH. Theoretical predictions explore Se effect: h) calculated models for NiOOH, (Fe, Ni)OOH, and Se-(Fe, Ni)OOH, i) free energies calculations for electrocatalytic intermediate steps with the PDS energies, j) Se-related configuration with metal octahedral, and k) charge density differences among the three models. Reproduced with permission.[154] Copyright 2023, American Chemical Society. Free-energy diagram for OER on (0 1 –1 2) surfaces of l) NiOOH, m) NiFeOOH, and n) N-NiFeOOH, respectively. o) d-band center of the Fe and Ni with formation energy of adsorbed OH (OOH). Reproduced with permission.[155] Copyright 2020, Elsevier.

dec^{-1} (Figure 4c). Theoretical calculation depicted in Figure 4d-g suggests that SO_4^{2-} interacts with the adsorbed OOH* on the Fe active site, thereby stabilizing intermediates (OOH*), altering the rate-determining step, and optimizing Gibbs free energies of the OER intermediate. Both experimental and theoretical studies affirm the dual role of SO_4^{2-} in enhancing OER performances.

The ORR activity constitutes the bottleneck of NiFe-based electrocatalysts. To overcome the existing bottleneck, Zhang's group introduced a 3D integrated and anion-regulated structure for NiFe hydroxysulfide nanosheets, which enhances both the ORR and OER activity in alkaline electrolyte. This improvement is attributed to the monolith's abundant active site and distinctive porous structure.[153] When employed directly as the air electrode, the $Ni_{1.9}FeS_{1.09}(OH)_{4.6}$ monolith enabled an aqueous Zn–air battery to achieve a high peak power density of 248 mW cm^{-2}. Notably, these catalysts can also be encased into the solid-state Zn–air battery with gel polymer electrolyte, maintaining stable discharge-charge voltages even under varying bending angles. This study highlights that the innovative design and effective synthesis of anion-regulated self-supporting hydroxysulfide monoliths significantly enhance Zn–air battery performance. Despite these advancements, the reconstruction mechanism of 3d-metal selenides and the role of anions in Zn–air batteries remain largely unexplored. In response, Chen et al. conducted a comprehensive study into the anionic effects on the dynamic reconstruction of 3d-metal selenides. As illustrated in Figure 4h-k, the potential impact of selenium on the pristine NiFe composite was analyzed using DFT calculations. Particularly, this model focuses on the Se Pourbaix diagram corresponding with strong alkaline conditions in the Zn–air battery system, where form O-sharing bonded selenides motifs through the high-valent cationic state by selenides contribution, thereby facilitating charge redistribu-

tion of the active sites. The Fe/Ni−(O)−Se unique configuration promotes electron localization at active metal sites and lowers the energy barriers for both the ORR and OER potential-determining steps. Finally, the Zn–air battery encased with (Fe, Ni)Se_2 materials demonstrated stable operation exceeding 350 h, retaining a voltage gap of 0.83 V and an energy efficiency of 57.7%.[154]

Besides the chalcogenides regulation, introducing heteroatom N element into NiFe-based compounds could also provide more accessible active centers, in which the DFT calculation has revealed that the dopant of N element could reduce the d-bond center of active metals while facilitating the adsorption ability of OER reaction intermediates (OH^* and OOH^*) on NiFeOOH surface, finally lowering the overpotential of the OER (Figure 4l–o).[155] As an example, Qiao et al. successfully synthesized the N-doped NiFe double layer hydroxide (N-NiFe LDH) in situ on the three-dimensional nickel foam to improve OER activity. The mechanism investigations revealed that unique structures, such as the 3D conductive structure, N–NiFe LDH nanolayer with ultra-thickness (≈0.8 nm), as well as abundant N-doping content (≈17.8%), significantly contributed to effective OER activity and Zn–air batteries performance. Consequently, the catalyst delivered remarkable OER activity, characterized by an ultralow overpotential of 230 mV at 10 mA cm^{-2} corresponding with stable durability exceeding 60 h, and high Zn–air battery performance under alkaline electrolyte.[95] In addition, Goodenough et al. reported that the mesoporous nickel-iron nitride (Ni_3FeN) serves as an effective bifunctional electrocatalyst. This is attributed to its metallic state, ordered face-centered cubic (fcc) structure, high electrical conductivity, and unique hierarchically porous architecture with ample interparticle void space and high surface area. These properties confer Ni_3FeN with outstanding ORR and OER electrocatalytic activities, evidenced by a more positive half-wave potential of 0.78 V and a significantly higher current density of 12.7 mA cm^{-2} at a potential of 1.60 V. Furthermore, the catalyst achieved a lower discharge–charge potential gap and prolonged lifespan exceeding 100 h in Zn–air batteries.[156]

NiFe materials incorporating targeted anion modification strategies have emerged as a cornerstone for designing bifunctional electrocatalysts in Zn–air batteries due to their tailorable interlayer electronic configurations and adaptive structural architectures. Doping anions into NiFe-based compounds could promote the performance of rechargeable Zn–air batteries with OER/ORR activity and durability, mainly focusing on facilitating the oxygen reaction charge transfer and improving the electronic conductivity. However, NiFe-based compounds with anions typically undergo electrochemical reconstruction during the OER process, making the actual catalytic active sites inconsistent with the original catalyst surface. The leaching of anions during electrochemical reconstruction is an uncontrollable process that affects the precise construction of valuable active sites in NiFe-based compounds. Specific anions can enhance the durability of NiFe-based materials by stabilizing metal sites through coordination interactions; however, their strong surface binding affinity may concurrently reduce the accessibility of active sites. Conversely, anions acting as proton acceptors/donors can accelerate the kinetics of surface proton-coupled electron transfer processes, yet typically exhibit compromised structural stability due to surface reconstruction. To date, the atomistic mechanisms governing anion-regulated modulation of Ni/Fe redox couples remain unresolved. Therefore, the rational utilization of electrochemical reconstruction phenomena to optimize the activity performance of NiFe-based catalysts with long durability through anionic modification is also a major focus at present.

5.2. Cation Doping

Cation doping has emerged as a strategic approach to enhance the catalytic performance of NiFe-based materials in oxygen-redox electrochemical processes.[157] This methodology involves substituting or introducing cations, such as Co, Cr, Zn, Mo, or other transition metal cations into the NiFe host lattice, which systematically modulates three critical aspects: i) Electronic structure modulation. Cation dopants fine-tune the d-band center of Ni/Fe through ligand and strain effects, optimizing the adsorption energy for key intermediates (e.g., *OOH, *O).[158] As an example, ternary NiFeM (M: La, Mo) catalysts are engineered with distinct M-NiFe coordination units to achieve targeted electronic structure modulation. The incorporation of La dopants induces ligand-field redistribution and compressive lattice strain, which collectively upshift the d-band center of Ni/Fe and strengthen hybridization between metal d-orbitals and oxygen 2p-orbitals. This synergistic electronic restructuring optimizes adsorption energies for oxygen intermediates and reduces the energy barrier of the rate-determining step, as evidenced by operando XAS and microkinetic modeling, thereby significantly enhancing OER activity.[132] ii) Crystal field symmetry and strain effects. Dopants induce lattice strain (compressive or tensile), distorting metal-oxygen bonds and generating undercoordinated active sites, especially generated the defect site.[159] For example, the substitution of Cr into the $NiFe_xCr_{2-x}O_4$ lattice induces lattice strain and coordination distortion, destabilizing the crystal field symmetry and promoting preferential Cr leaching during CV (cyclic voltammetry) conditioning. This strain-driven process generates cation vacancies and oxygen defects (O_{vac}), which facilitate the transformation of the anhydrous spinel into a hydrous NiFe oxyhydroxide (MOOH) shell, while compressive strain stabilizes the core–shell interface against structural collapse. The interaction between strain-modulated redox activity and crystal field distortion optimizes the d-band center of Ni, enabling higher valence states ($Ni^{3+/4+}$) and enhanced intermediate adsorption, thus achieving tunable surface reconstruction for superior OER performance.[160] iii) Charge transfer optimization. Dopants with higher electronegativity withdraw electrons from Ni/Fe, enhancing oxidative stability and interfacial charge transfer kinetics.[161] For instance, Zn doping in NiFe-LDH introduces an electron transfer effect from Zn to Ni, which elevates the electron density of Ni sites and suppresses their over-oxidation to unstable high-valence states (Ni^{4+}), thereby preserving the highly active β-NiOOH phase. This electronic modulation reduces the electrochemical reconstruction potential (1.52 V for NiFeZn-LDH vs 1.57 V for NiFe-LDH) and stabilizes the lattice against Ni dissolution, as confirmed by operando Raman spectroscopy and EIS. Coupled with S coordination, the synergistic (Ni, Fe)-S-Zn structure further enhances OER kinetics by optimizing *OOH adsorption while maintaining structural integrity, achieving a dual enhancement of activity and stability.[162] These synergistic effects, electronic tailoring, strain engineer-

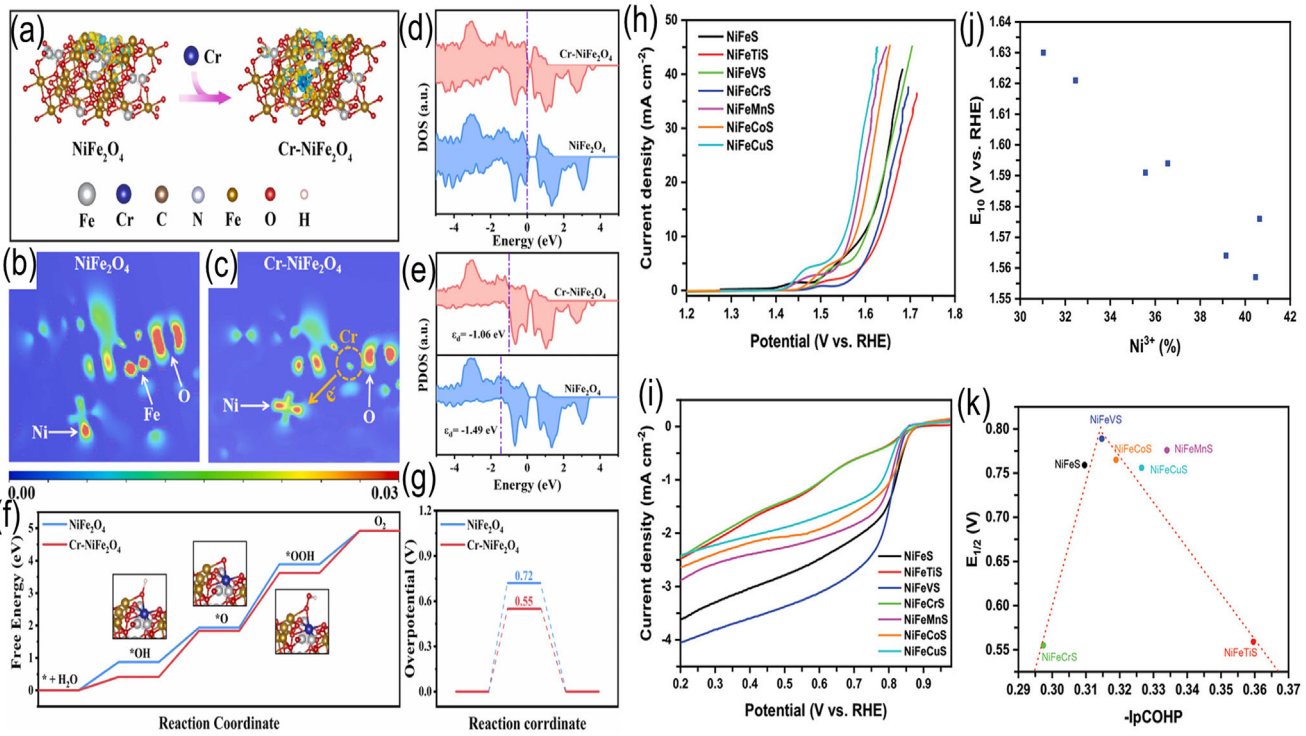

Figure 5. a) The difference between the $NiFe_2O_4$ and Cr-$NiFe_2O_4$ through charge density properties. The extracted 2D data plot for b) the $NiFe_2O_4$ and c) Cr-$NiFe_2O_4$. d) DOS and e) PDOS for $NiFe_2O_4$ and Cr-$NiFe_2O_4$. f) Free energy diagram and g) overpotential calculation value of $NiFe_2O_4$ and Cr-$NiFe_2O_4$. Reproduced with permission.[164] Copyright 2024, Elsevier. h) OER and i) ORR activity curves of NiFeS doping with different metal dopants. j) OER potential value at the current density of 10 mA cm^{-2} as a function of Ni^{3+} concentration. k) ORR value obtained from the Half-wave potential as a function of pCOHP. Reproduced with permission.[165] Copyright 2024, Wiley-VCH.

ing, and charge redistribution, position cation doping as a versatile strategy to break activity-stability trade-offs in NiFe-based electrocatalysts.

Particularly, the unique cations can adjust the electronic structure of Ni or Fe sites to optimize the adsorbed energy of reaction products or intermediates. For instance, Li et al. doped the Fe element into the $FeNi_3$ intermetallic nanoparticle via a facile plasma engineering, in which the excess Fe-ions caused high lattice distortion corresponding with abundant oxygen-active sites, finally achieving ultrahigh performance for the Zn–air batteries.[163] In addition, Hu et al. doped Cr elements into the ferrite $NiFe_2O_4$ to apply as oxygen electrocatalysts (**Figure 5a**). After assembling as the air cathode for Zn–air battery, the designed catalysts achieve a high specific capacity of 740 mAh g^{-1} and a high-power density of 61.1 mA cm^{-2}.[164] In addition, the Cr^{3+} was effectively incorporated into octahedral sites, altering the electronic state surrounding the active site of $NiFe_2O_4$. The Cr dopant acts as the electron donor, modulating the electronic state of Ni^{2+} sites (Figure 5b,c) and reducing the bandgap of $NiFe_2O_4$, thereby improving its conductivity (Figure 5d). Furthermore, the electronic state of Cr-doped $NiFe_2O_4$ is positioned approaching to the Fermi level compared with pristine $NiFe_2O_4$ (Figure 5e), which enhances the adsorption/desorption behaviors of oxygen intermediates (Figure 5f). This adjustment in electronic structure due to Cr doping results in a decrease in the OER overpotential of the Cr-doped $NiFe_2O_4$ catalyst from 0.72 V to 0.55 V (Figure 5g). However, the selection criteria of metal dopants and the reaction mechanism of NiFe-based catalysts are still unclear. To deeply understand the relationship between metal dopants in NiFe-based compounds and catalytic activities, Ting's group investigated several transition metals (Ti, V, Cr, Mn, Co, and Cu) with varying t_{2g} and e_g occupancy for incorporation into NiFeS lattice. They explored the effects on electronic conductivity, electronic state of the active sites, and thermodynamic barrier through theoretical calculations and experiments, correlating these properties with ORR/OER activity (Figure 5h,i).[165] Consequently, the introduction of metal dopants into NiFe sulfide enhanced the OER/ORR bifunctionality, with increased Ni^{3+} content boosting the OER activity (Figure 5j). The projected crystal orbital Hamilton population (pCOHP) method was utilized for assessing the Ni–O bond strength. As depicted in Figure 5k, the ORR activity exhibits a volcanic trend relative to pCOHP, indicating that an optimal Ni–O bond strength is valuable for ORR activity. Additionally, the conductivity of NiFeS was improved by doping Mn, Co, and Cu elements. The d-band center (ε_d) of the Ni active site was elevated through the addition of Ti, V, Mn, Co, and Cu dopants, with the V dopant achieving optimal binding energy for intermediate species and adsorption energy for *O species. The optimal NiFeVS encased into Zn–air battery can present a high specific capacity of 698 mAh g^{-1}, a substantial power density of 190 mW cm^{-2}, and long-term durability over 2400 cycles (400 h).

Single-metal doping on the NiFe system is typically limited, making it challenging to simultaneously enhance ORR/OER activity, given the opposing nature of these processes. To

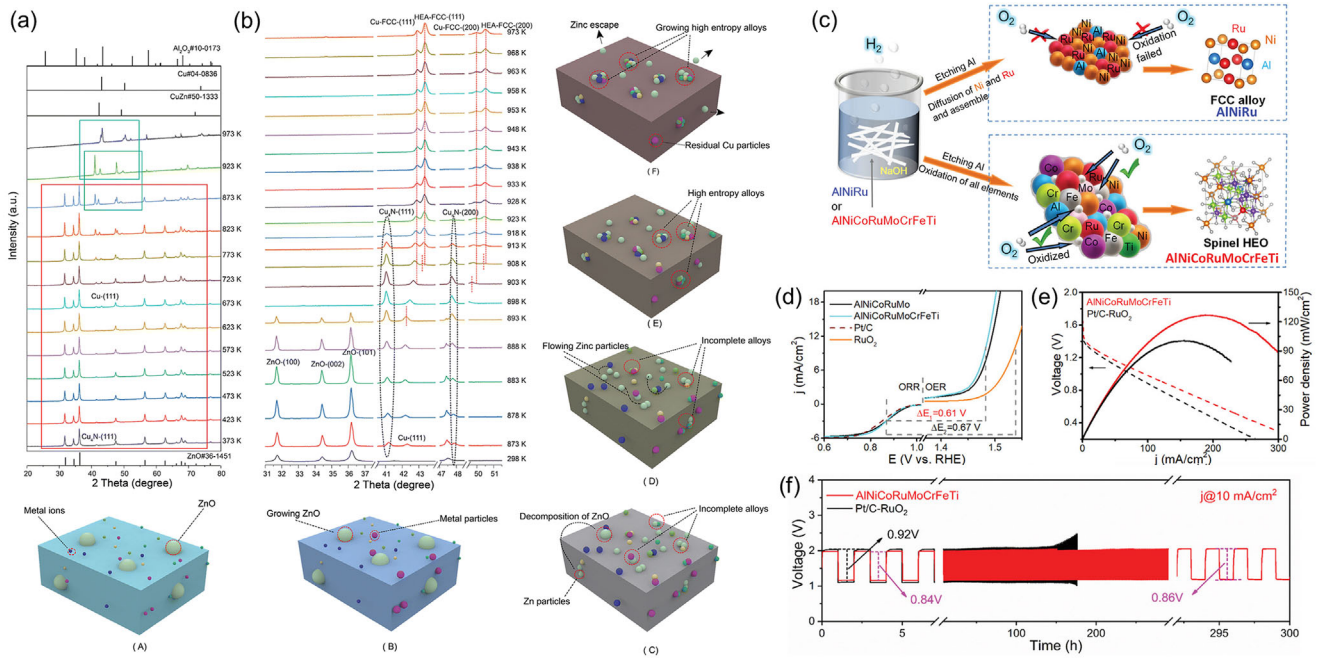

Figure 6. a,b) The in-situ XRD results of HEA nanoparticles. Reproduced with permission.[169] Copyright 2023, Royal Society of Chemistry. c) The schematic illustration of FCC alloy and spinel oxides with low crystallinity. d) The LSV curves for ORR/OER of the quinary high-entropy AlNiCoRuMoCrFeTi catalyst. e) Voltage variations at current densities and f) long-term cyclic performance of the Zn–air battery with AlNiCoRuMoCrFeTi air cathode. Reproduced with permission.[173] Copyright 2022, Wiley-VCH.

leverage the advantages of multiple elements, transition metal high-entropy alloys (HEAs) and their corresponding high-entropy oxides (HEOs), composed of five or more metal elements, have garnered significant interest for effective ORR/OER activity.[166] The multi-compositional nature of the HEAs results in diverse atomic arrangements on their surfaces, modulates the d-band center site of various transition metals, and introduces the lattice distortion effect due to different metallic radii, thereby optimizing the binding energy of reaction intermediates and accelerating the intrinsic activity kinetics.[167] However, synthesizing nanostructured HEAs is challenging due to the varying properties of each metal element, such as ionic radius, which can impede the formation of the single-phase HEAs. Fortunately, HEAs with multiple metal components can be successfully synthesized using the confinement effect of carbon, achieving high activity and long stability due to the altered local electronic structures, well-dispersed metal nanoparticles, increased active sites, and improved interfacial mass/charge transfer.[168] For instance, Zhang et al. synthesized the HEAs (FeCoNiMnCu-1000) nanoparticles encapsulated in the N-doped graphitized hollow carbon tubes via a solid-state thermal reaction strategy, which demonstrated an ORR half-wave potential of 0.78 V vs RHE and maintained stability for over 200 h for Zn–air batteries.[169] As exhibited in **Figure 6**a,b, in situ XRD characterization was conducted to gain insights into the phase transformation process of HEAs during calcination. At high temperatures, stable HEA combined with amorphous carbon can generate a unique hollow configuration, with HEA nanoparticles enveloped by an external carbon layer to prevent aggregation, and ordered graphite-structured carbon at the interface is formed by the neighboring traditional metal catalysis. Despite the excellent catalytic activity achieved, the carbon and HEA cluster exhibited relatively weak interfacial binding strength due to the oxidized carbon corrosion, leading to HEA nanoparticles agglomeration and loss of activity during repeated cycling.[170] Based on this consideration, Qiu et al. fabricate HEAs without noble metals combined with naturally oxidized and multi-component HEOs as bifunctional materials for Zn–air batteries via the top-down dealloying method. Consequently, the battery with np-AlFeCoNiCr exhibited a high open-circuit potential of 1.55 V, a high specific capacity of approximately 800 mAh g^{-1}, and a long-term lifespan of over 60 h.[171] DFT calculation reveals that the favorable bifunctional activity is generated from Cr incorporation, which modifies the electronic state of NiFe-based spinel oxides. The inclusion of Ru as a noble metal in the HEA served as an active component for both OER and ORR, while the construction of HEAs effectively reduced the utilization of noble Ru.[172] Subsequently, Qiu et al. utilized the chemical dealloying method to fabricate optimal eight-component HEOs (Al-Ni-Co-Ru-Mo-Cr-Fe-Ti) and advance the generation of low-crystallinity oxides (Figure 6c). Notably, the AlNiCoRuMoCrFeTi HEO catalyst exhibited a low ORR (half-wave potential) and OER (at the current density of 10 mA cm^{-2}) overpotential gap of 0.61 V (Figure 6d), and enabled a Zn–air battery with a high power density of 123.5 mW cm^{-2} (Figure 6e) and long durability over 300 h at 10 mA cm^{-2} (Figure 6f).[173] These high-performance bifunctional electrocatalysts with dual metal (Cr and Fe) synergistic functions on adjusting the electronic model of active Ni/Ru/Co sites have enhanced the ORR and OER kinetics. The multi-metal component significantly reduced Ru utilization, thereby lowering catalyst costs.

As one of the widely reported strategies in altering the electronic structures of the electrocatalysts, the cation doping strat-

egy is essential for oxygen-related chemistry, benefiting from the wide cation selectivity and the regulation of electronic states. Cation doping has emerged as a pivotal strategy to tailor the electronic, structural, and catalytic properties of NiFe-based electrocatalysts for Zn–air batteries. By introducing cations into the NiFe matrix, researchers aim to optimize bifunctional activity, enhance stability, and address intrinsic limitations of NiFe catalysts. However, for Zn–air batteries with NiFe-based compounds, the single cation-doped strategies seem to need further exploration, owing to the poor ORR activity, failed long lifespan, and unclear reaction mechanism. The concentrations of the cation dopants face unified reference standards between different doping types, while doping a single cation faces the unbalanced ORR and OER activities. For the HEAs and HEOs materials, the methods to achieve uniform dopant distribution and the contribution to catalytic activity of each metal site both need further exploration. In the future, developing in situ doping techniques where dopants migrate to active sites during the electrochemical process can make a more uniform distribution of the metal cation on the NiFe-based matrix, as well as construct more exposed active sites on the surface of the catalyst. Combining the theoretical calculation and the operando characterization technique to screen the dopants with optimal adsorption energetics and track the evolution of valence states of dopants during catalysis.

5.3. Supporting Effect

The intrinsic low electrical conductivity and limited active sites of NiFe oxide/hydroxide significantly hinder their effectiveness as bifunctional electrocatalysts in Zn–air battery. A promising approach to overcome these limitations involves integrating NiFe oxide/hydroxide with materials that possess high electrical conductivity and large surface areas, thereby advancing both the activity and stability of the catalysts in oxygen-related reactions.[174] Carbon materials, characterized by their high electron conductivity of $>10^3$ S cm^{-1} and extensive surface area of >200 m^2 g^{-1}, have been identified as effective supports for developing ORR and OER catalysts in rechargeable Zn–air batteries.[175] More importantly, the incorporation of carbon materials as supports for NiFe oxide/hydroxide can effectively mitigate the agglomeration of NiFe nanoparticles, thereby improving the stability and adding the number of exposed active sites.[176] Ni and Fe ions process empty d-orbits and d-orbit electrons, which could achieve rapid electron transfer between adsorbed oxygen intermediate species and Ni/Fe sites. More importantly, supports with electron donating or electron accepting properties can adjust d-orbital electrons of Ni/Fe sites, thus optimizing the adsorption energy for oxygen intermediate species. Based on this theory, N-doped carbon materials with different types of N species, such as pyridine-N, pyrrole-N, graphite-N, could donate or accept electrons when anchoring NiFe compound nanoparticles, thereby accelerating the ORR and OER kinetics.[177–179] Generally, the ORR activity primarily depends on the adsorption and dissociation steps of O_2, whereas the OER activity is restricted by the generation of OOH^* and O^* intermediates, in the NiFe compounds. Consequently, a single type of active site in NiFe compounds struggles to effectively catalyze both OER and ORR processes.[180–182] In particular, constructing asymmetric dual-sites liking NiFe-N-C structures is highly effective in introducing the bifunctional ORR and OER activity.[183,184] Combining NiFe compound nanoparticles with N-doped carbon supports to build NiFe-N-C structures claim several advantages: i) N-doped CNTs could enhance electrical conductivity of NiFe compounds; ii) The size of NiFe compounds is limited by the carbon support, arousing in plenty of active sites exposures; iii) The N atom could effectively alter the electronic states of Ni or Fe active sites in carbon supports to optimize ORR/OER activity; iv) N-doped carbon is a good ORR material that can compensate for the poor ORR of NiFe compounds.[185–188] For instance, the emerging materials metal-organic framework with diverse metals and special network structure.[189,190] and N-containing organic polymers could directly form NiFe-N-C structure.[175] through high-temperature sintering, which have been employed for Zn–air batteries served as bifunctional electrocatalysts, enhancing both the ORR and OER activities of NiFe compounds and boosting the catalytic durability. Additionally, N-doped carbon nanotubes, N-doped graphene, and self-supporting N-doped carbon skeleton served as effective supports for NiFe compounds, facilitating the creation of advanced bifunctional catalysts for rechargeable Zn–air batteries with reduced charge/discharge potential gaps and extended lifespans. Dong et al. synthesized hierarchical composite (Co-NC@LDH) with dual-active site by depositing the NiFe-LDH nanosheets with OER activity on ZIF (zeolitic imidazolate framework) with ORR activity, generated with carbon-based framework. The synergistic interaction between the Co–N–C and the NiFe-LDH structures allows Co, N-doped CNTs to protect active metal sites and accelerate the mass transfer of reactants. In addition, the carbon framework can provide high electrical conductivity, which can accelerate electron transfer kinetics from the NiFe-LDH during catalysis. As a result, the Co-NC@LDH exhibits a lower overpotential of 819 mV around the ORR (half-wave potential) and OER potential (10 mA cm^{-2}) in alkaline solution, along with outstanding durability exceeding 300 h in Zn–air battery.[191] More interestingly, Zhang's group achieved a significant advancement in ampere-hour-scale zinc-air batteries, achieving a record-breaking $\Delta E = 0.57$ V with the NiFeCe LDH catalysts, where the NiFeCe LDH anchoring with uniform Fe-N-C sites are integrated into a composite.[192] Specifically, practical zinc-air batteries with ampere-hour scale constructed with NiFeCe LDH/Fe-N-C catalysts delivered a capacity of 6.4 Ah and sustained cycling under 1.0 A and 1.0 Ah current condition. This exploration presents the groundbreaking bifunctional ORR and OER electrocatalyst for aqueous zinc-air batteries, promising for next-generation applications.

One-dimensional carbon nanotubes (CNT) are usually adopted as supports for transition metal compounds benefiting from the fast electron transport path, short mass diffusion pathway, and unique structure stability, and even allow the anchored nanoparticle with high dispersity.[193] Du et al. enhanced the OER activity and stability of Fe-Ni bimetal hydroxide nano-sheets by supporting them on the multiwalled carbon nanotubes ($Fe_3NiO_xH_y$/MWCNTs). Additionally, the incorporation of heteroatom B into the $Fe_3NiO_xH_y$/MWCNTs catalyst (B-$Fe_3NiO_xH_y$/MWCNTs) further improved OER activity by modulating local electron density and surface charge states. Thereafter, this design resulted in an amorphous crystalline structure and nano-sheet morphology, reducing the OER overpotential, facilitating reaction kinetics, and enlarging durability.

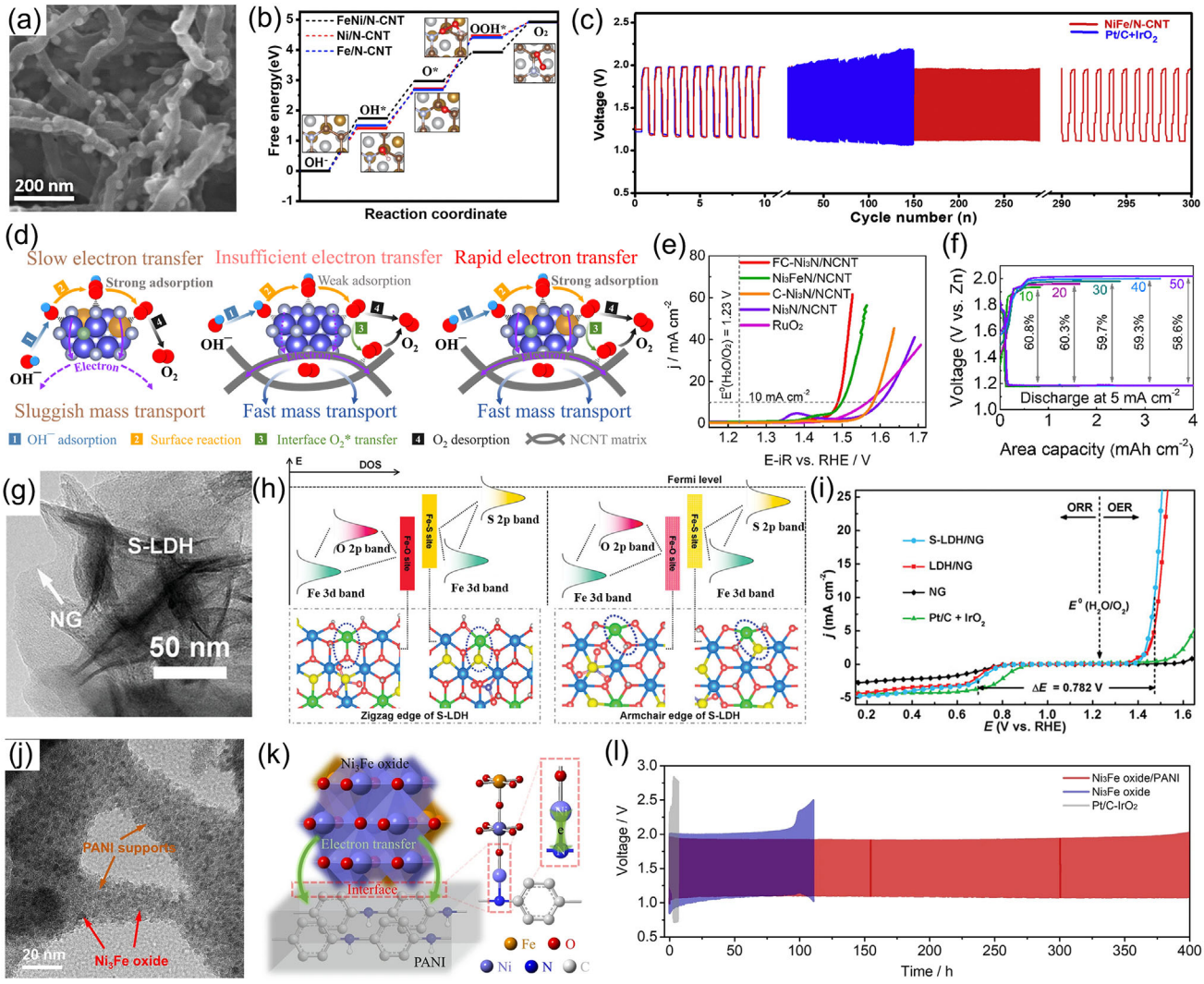

Figure 7. a) TEM image of NiFe/N-CNT; b) Free energy diagram of NiFe/N-CNT catalysts and its comparison; c) The cyclic performance of Zn–air batteries using NiFe/N-CNT catalysts. Reproduced with permission.[198] Copyright 2020, Elsevier. d) Diagram of electron and mass transport in FC-Ni_3N/NCNTs. e) OER polarization curves of FC-Ni_3N/NCNTs catalysts and its comparison. f) Galvanostatic charge-discharge test of FC-Ni_3N/NCNTs at different current densities. Reproduced with permission.[199] Copyright 2021, Elsevier. g) The morphology characterization for S-LDH/NG; h) Schematic of the DOS calculation results for S-LDH/NG; i) Overall OER/ORR polarization curves of S-LDH/NG and its comparison. Reproduced with permission.[206] Copyright 2023, Wiley-VCH. j) HRTEM images of Ni_3Fe oxide/PANI catalysts. k) The interaction between PANI supports and Ni_3Fe oxide. l) The cycling performance for Zn–air batteries utilizing the Ni_3Fe oxide/PANI catalysts at 10 mA cm^{-2}. Reproduced under the terms of 4.0 International License.[209] Copyright 2025, The Authors, Published by Springer Nature.

The assembled Zn–air battery achieved a peak power density of 343.7 mW cm^{-2} and demonstrated long-term stability exceeding 200 h.[194] The N element, with higher electronegativity than C, is also widely doped into CNT supports to adjust the chemisorption energy of oxygen by rearranging the electron distribution of adjacent C atoms.[195–197] For instance, Mai et al. developed NiFe nanoparticles supported on N-doped CNT (NiFe/N-CNT) as bifunctional electrocatalysts for flexible Zn–air battery, with the NiFe nanoparticle uniformly anchored on CNT without significant agglomeration (**Figure 7a**). The NiFe/N-CNT exhibited valuable bifunctional catalytic performance both for ORR and OER, with the minimized ΔE (0.77 V) among all samples in an alkaline solution under a three-electrode system. More importantly, the theoretical calculation, in-situ Raman, and oxygen adsorption studies confirmed that NiFe/N-CNT enhances the OH^- and oxygen absorption process, thereby boosting the ORR and OER activity (Figure 7b). Finally, the Zn–air battery with NiFe/N-CNT catalyst achieved a high peak power density of ≈105.4 mW cm^{-2}, a high open-circuit voltage of 1.41 V, and long cycling stability (Figure 7c).[198] Beyond regulating the adsorption of intermediate oxygen species, carbon nanotubes also enhance electron and species transport in NiFe compounds during OER processes, promoting the charge-discharge rate (Figure 7d). Based on this concept, our group designed a high-performance OER catalyst by loading NiFe nitride onto N-doped CNTs (FC-Ni_3N/NCNTs), which exhibited an ultra-low overpotential of

260 mV at 10 mA cm^{-2} (Figure 7e). The interlaced CNTs network facilitates rapid O_2 desorption and electron transfer for NiFe nitride across the air cathode, delivering an ultra-low charge potential of 2.02 V and high round-trip efficiency of 58.6% at 50 mA cm^{-2} (Figure 7f).[199] The Zn–air battery with FC-Ni_3N/NCNTs provided a long cycling life of 700 cycles and a low charge voltage of 1.96 V at 20 mA cm^{-2}. Therefore, introducing conductive supports into NiFe compounds is thus an efficient strategy for achieving high performance in Zn–air batteries at high current densities. In addition to modifying carbon supports, functionally modified NiFe compounds can optimize the catalytic activity of supported catalysts. Defects, particularly oxygen vacancies in NiFe compound catalysts, can modify the catalyst structure to facilitate the charge exchange between electrolyte and catalyst interface. For example, Arjona et al. constructed the oxygen vacancies in the NiFe LDH/N-doped CNTs, promoting ORR and OER activity with a ΔE of 720 mV and notable rechargeable performance of the Zn–air batteries.[200] The experiment and density of states analyses indicated that the oxygen vacancies and the N-doped carbonaceous substrate enhanced catalyst activity owing to the low charge transfer resistances. Furthermore, Hu et al. grew NiFe-LDH nanosheets in-situ on Co-N-C triangular plates integrated with interwoven carbon nanotubes (Co@NC-CNTs@NiFe-LDH) using a structural engineering strategy to increase sufficient exposure of the active sites, promote the electron conductivity, and facilitate the transport of OH^- corresponded with its intermediates. Moreover, the DFT calculations revealed that the Co@NC-CNTs@NiFe-LDH evaluated the ORR and OER activities due to the synergetic interaction function between the NiFe LDH and Co@NC-CNTs. Interestingly, aqueous Zn–air batteries utilizing Co@NC-CNTs@NiFe-LDH as the air electrodes performed a specific capacity of 786 mAh g_{Zn}^{-1}, a peak power density of 194 mW cm^{-2}, and durability of 760 h at 10 mA cm^{-2}.[201] This work opens the new eyes for achieving high-performance Zn–air batteries by designing bifunctional electrocatalysts with unique structures.

Except for the carbon nanotubes, various carbon materials with different dimensionalities can also serve as support for NiFe compound catalysts. Carbon quantum dots (CQDs) are cost-effective candidates for decorating NiFe-based catalysts, as they can function as structure regulators and active sites. For instance, 2D NiFe-MOF NSs, enhanced by electron-withdrawing carboxylated CQDs, demonstrated excellent OER activity and long-term durability, making them a suitable air cathode for Zn–air batteries.[202] Additionally, graphene quantum dots (GQDs) have been shown to improve ORR activities due to their increased active surface area and modified electron structures. Pan et al. reported that anchoring GQDs can adjust the surface electronic states of NiFe LDH, meaningfully enhancing the OER activity with an ultralow overpotential of 189 mV at 10 mA cm^{-2} and achieving superior performance in Zn–air batteries with a round-trip efficiency exceeding 65%. The XPS combined with theoretical calculations indicated that the improved OER performance resulted from the strong interaction function between GQDs and NiFe LDH, which led to charge accumulation at active Ni sites and regulated charge distribution around these sites.[203] As reported, graphene, with its perfect graphitized structure, offers high electrical conductivity, addressing the conductivity limitations of NiFe-based catalysts. Moreover, combining NiFe nanoparticles with graphene nanosheets, which have a large surface area, can reduce the NiFe nanoparticles' aggregation.[190,204,205] Therefore, Park et al. developed atomic-level sulfur-incorporated NiFe–LDHs on N-doped graphene (S-LDH/NG) as bifunctional catalysts for Zn–air batteries. As shown in Figure 7g, S-LDH/NG catalysts exhibited a flower-like nanosheet morphology, with S-NiFe-LDHs uniformly anchored on the graphene surface. More importantly, theoretical calculations and experiments demonstrated that S anion substitution caused an upward shift in both the spin-up and spin-down Fe d-band centers, enhancing electrochemical activity by facilitating the adsorption of oxygen intermediates (Figure 7h). Consequently, the S–LDH/NG catalyst exhibited a small potential gap of 0.782 V between ORR and OER (Figure 7i), while the Zn–air battery with S–LDH/NG catalysts accomplished a high power density of 165 mW cm^{-2}, a large specific capacity of 665 mAh g_{Zn}^{-1}, and long-term stability of ≈120 h.[206] The graphene with N species and a large surface area can also confine the growth of NiFe compound nanoparticles, creating abundant catalytic sites. For instance, Xue et al. deposited $Ni_{0.5}Fe_{0.5}$ nanoparticles on N-doped graphene, achieving uniform Ni, Fe, N, and C elements dispersion, with an average particle size of 9.5 nm.[207] To date, constructing carbon defects and vacancies on the N-doped graphene with surface-exposed C basal plane edges is an effective way to promote ORR activities, create adsorption sites, and regulate the electron properties of the carbon skeleton. Luo et al. decorated dual isolated metallic atoms (Ni/Fe) on DG support through O/N linkers to achieve feasible ORR activity with a half-wave potential of 0.86 V and OER activity with a low overpotential of 358 mV at 10 mA cm^{-2}. Establishing pyridinic sites by reconstructing nanocarbon support into five-member rings of C atoms and bridging the isolated metallic Ni/Fe with N atoms can result in electron density rearrangement, ultimately enhancing both the ORR and OER activity.[208] Besides carbon supports, other conductive polymers, such as polyaniline and polypyrrole, with rich N content, can also act as supports to regulate the catalytic activity of NiFe compounds. Focused on this, our group deposited Ni_3Fe oxide, with an average size of 3.5 ± 1.5 nm, on polyaniline supports (Figure 7j). The electronic interaction between Ni_3Fe oxides and polyaniline supports improved Ni-O covalency through the formation of interfacial Ni-N bonds (Figure 7k). The polyaniline support also facilitated charge and mass transfer rates on the Ni_3Fe oxide surface. This rational design enabled the Zn–air battery to achieve a long cycling life of 400 h at 10 mA cm^{-2} (Figure 7l) and a low charge voltage of 1.95 V.[209] Therefore, the strategic design of supports is crucial for optimizing the catalytic performance of NiFe compounds.

Although the carbon-based matrix has been widely explored to support the NiFe-based catalysts with excellent electron conductivity, there still exist many limitations that hinder the large-scale application of carbon material in rechargeable Zn–air batteries, such as carbon corrosion under oxidation potential, weak metal-carbon support interaction, limited tolerance to mechanical stress, and undesirable side reactions. Therefore, excepting the carbon materials-based matrix, some multiple metal compounds, such as transition metal oxides, transition metal nitrides or carbides, pyrochlore, and perovskite oxides, could adopted as support materials for NiFe compounds to improve catalytic performance, because of the modified electronic structure and

promoted charge transfer pathway.[210–212] As an example, Bhattacharyya et al. decorated the NiFe-LDH on the perovskite oxides ($Ba_{0.6}Sr_{0.4}Co_{0.79}Fe_{0.21}O_{2.67}$) through the polyethyleneimine linkage, which provides leeway for electron mobility and renders modulation of surface charges on the integrated BSCF/NiFe-25 catalysts.[212] BSCF/NiFe-25 air cathode enables the rechargeable Zn–air battery to deliver a high energy density of 776.3 mWh g_{Zn}^{-1}, as well as maintain long-term durability over 100 h with reduced discharge and charge voltage gap of 1.16 V at 10 mA cm^{-2}. Additionally, the spinel oxides featuring with the unique AB_2O_4 formula (A and B always utilization of the transition metals) exhibit the advantages of tailored electrons between the A and B ions for mass transport, facile adjustment of electrochemically active area for the abundant active sites, high corrosion resistance, rich valence states, and excellent chemical stability.[213] Notably, combining the spinel oxides, such as $NiCo_2O_4$, $CuCo_2O_4$, and $NiFe_2O_4$, with the OER-active NiFe-based complexes with heterostructure or other special structures is a wise method based on the moderate adsorption capability for the reaction intermediate species during the ORR and OER processes, to enhance the catalysis function for NiFe-based complexes.[214–217] Research has shown that unique heterostructures and the presence of oxygen vacancies or defects can synergistically enhance catalytic processes, significantly boosting catalytic performance. Cai et al. constructed an integrated heterostructure of biphasic nanoalloys (CoFe-NiFe/NC) with three obvious parts (carbon layer, NiFe, and CoFe) via ion adsorption/exchange and carbonization strategies, which delivered more exposed active sites, facile ion diffusion/electrolyte penetration, and rapid charge transfer (**Figure 8**a,b).[218] The CoFe alloys and NiFe alloys integrated on an N-doped carbon matrix delivered improved catalytic kinetics, in which the CoFe hydroxides uniformly decorating the NiFe nanoparticles, benefiting from the oriented and interconnected nanoflake heterostructure, sufficient multi-metal catalytic centers, and shortened transport channels on the reaction interfaces. Accordingly, the DFT results revealed that the CoFe-NiFe/NC mainly dominated the $4e^-$ catalytic path during the oxygen-based electrochemical reaction process, thus maximizing the intrinsic functional activities (Figure 8c). Finally, the CoFe-NiFe/NC cathode, for instance, enabled a high-performance Zn–air battery with a power density of 155 mW cm^{-2}, excellent cycling stability over 400 h at 10 mA cm^{-2}, and a stable round-trip efficiency of ≈56% at 20 mA cm^{-2} (Figure 8d–f). More importantly, the hollow structure of the spinel oxides is particularly beneficial for the electrocatalysts, as it provides an extended specific surface area that creates numerous active sites for electrochemical reactions and offers abundant channels for efficient mass diffusion. Building on this concept, Lee et al. developed $Fe_2NiO_4/FeNiS_2$ nanosheets using a three-step process consisting of hydrothermal synthesis, oxidation, and sulfidation to advance the ORR/OER activity and Zn–air battery performance. The heterointerface between the Fe_2NiO_4 and $FeNiS_2$ was found to tailor the electronic structure, while the hollow structure reduced the charge and mass transfer resistance (Figure 8g-j).[219] In particular, the simulation results indicated that Ni1 dominated as the primary active site in $Fe_2NiO_4/FeNiS_2$ for facilitating the OER and ORR in alkaline systems. Finally, Zn–air battery assembled with the $Fe_2NiO_4/FeNiS_2$ nanosheets demonstrated a high-power density of 144.22 mW cm^{-2} and achieved superior cycling performance over 1500 cycles (40 min per cycle) at 2.0 mA cm^{-2}. Furthermore, introducing other sulfides or selenides into NiFe catalysts can further modulate their electronic structure, optimizing ORR/OER activities. Park et al. facilitated the intrinsic activity of NiFe-based compounds by decorating ReS_2 onto NiFe-layered double hydroxide (NiFe-LDH) nanosheets, leveraging the strong coupling effect and vertical alignment at the hetero-interface.[220] The ReS_2/NiFe-LDH hetero-nanosheets were shown to possess multiple active sites, primarily at the edges and surfaces of NiFe-LDH for OER and ORR, respectively. Oxygen vacancies on electrocatalysts can boost the ORR/OER kinetics by reducing resistance, increasing electron transfer rate, and enhancing electrochemically active sites. Thereafter, Jiang et al. designed DBD-NiFe/$NiSe_2$@NCNT with a hetero-interface rich in oxygen vacancies utilizing atmospheric pressure dielectric barrier discharge plasma, achieving superior bifunctional catalytic activity with a low OER overpotential of 292 mV at 10 mA cm^{-2}, high ORR activity with half-wave potential of 0.811 V, and exceptional stability for Zn–air battery with over 1000 cycles at 10 mA cm^{-2}.[221]

Generally, constructing heterostructures on electrocatalysts is a favorable direction to promote their intrinsic activity, because the catalytic reaction usually takes place on the interface. More importantly, the heterostructure with different active phases produced strong electronic interaction that could regulate the electron structure, finally affecting the mass and charge transfer behaviors, and adjusting the chemical adsorption energy for oxygen-based electrochemical intermediates.[222] Thereby, to accelerate the electron transfer rate, increase the electronic conductivity, as well as alleviate the self-aggregation of the NiFe-based compound, a composite structure that combines NiFe-based compounds with the high ORR activity-based second phase to form a heterostructure can be adopted.[223–228] Crucially, it is highly desirable to understand the reaction mechanism and precisely control electron regulation on the interfacial structure. Leveraging the benefits of controllable dual-interface engineering for the strategic design of advanced functional catalysts, our group developed a composite catalyst by depositing the Ni_3FeN nanoparticles onto the surface of MnO, resulting in two well-designed interfaces (Figure 8k,l). As illustrated in Figure 8m, the heterostructure catalyst with 15% Ni_3FeN loading was identified as the optimal configuration for ORR and OER catalysis. This approach, involving the decoration of Ni_3FeN on MnO with a precisely engineered interface, effectively mitigates agglomeration and modulates the electronic structure of MnO on the CNT surface (Figure 8n).[229] Consequently, this catalyst achieved outstanding rate performance up to 40 mA cm^{-2} and demonstrated stable cycling performance over 200 h at 40 mA cm^{-2} in Zn–air batteries. These innovative strategies, which integrate NiFe-based complexes with multi-metal composites, have led to the achievement of cost-effective bifunctional composite electrocatalysts with high activity and stability. However, further investigation is required to fully understand the underlying reaction mechanisms and explore additional catalytic types in the future. In addition, the semiconductor matrix, such as TiO_2, acting as the substrate for the NiFe-based catalysts, can open the pathway of the NiFe catalysts to the photo-assisted Zn–air systems. Rudra et al. demonstrate that transitional metal doping (Ni, Fe) and heteroatom co-doping on TiO_2 significantly enhance its bifunctional catalytic and photonic properties for Zn–air batteries,

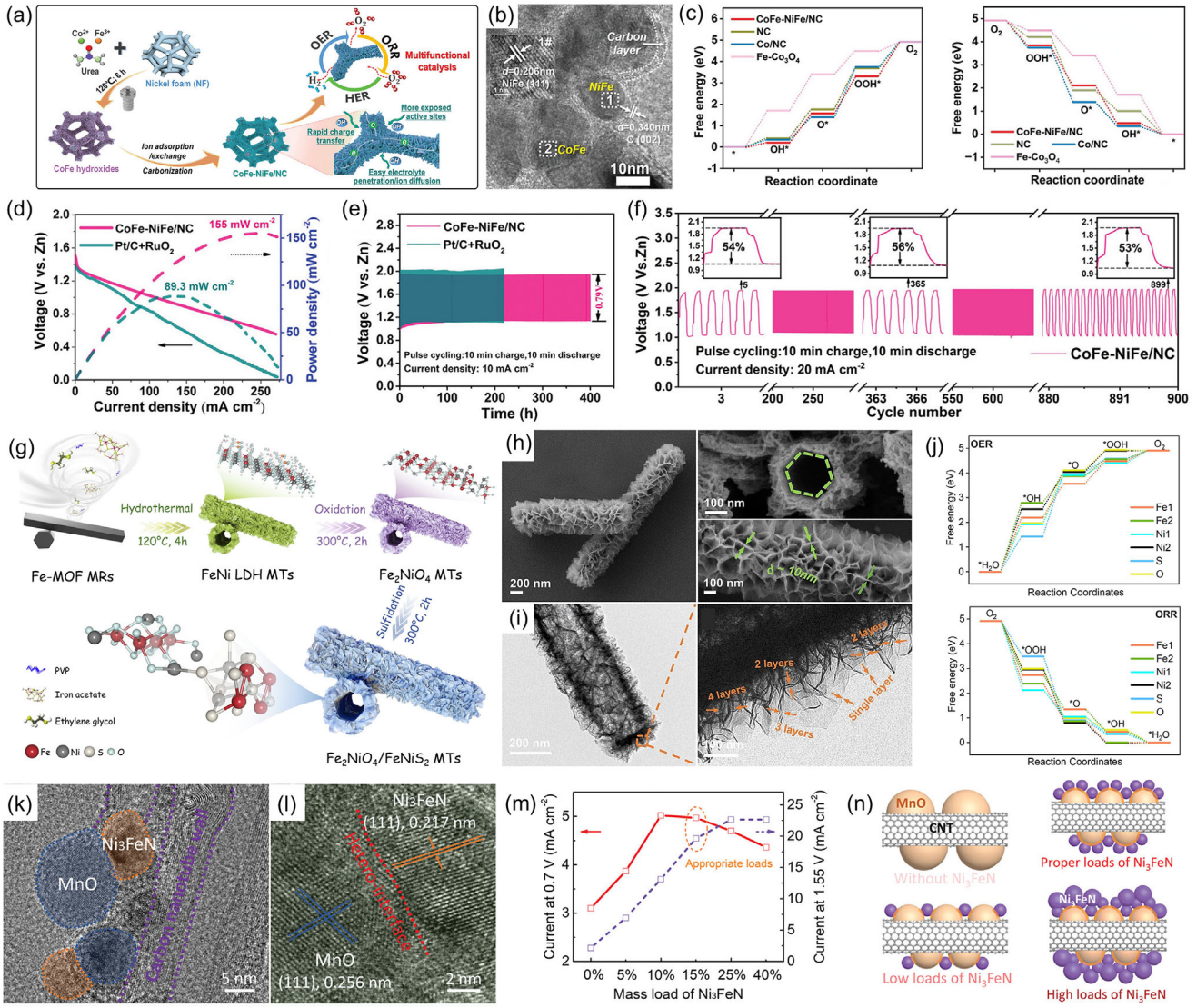

Figure 8. a) The synthesis illustration of a biphasic alloy-based monolithic catalyst with multifunctional catalysis. b) TEM images of CoFe-NiFe/NC. c) The free energy diagram of CoFe-NiFe/NC to evaluate the OER and ORR activities. The Zn–air battery performance using CoFe-NiFe/NC: d) polarization curve, galvanostatic cyclic performance at e) 10 mA cm^{-2} and f) 20 mA cm^{-2}. Reproduced with permission.[218] Copyright 2024, Wiley-VCH. g) The preparation illustration of Fe_2NiO_4/$FeNiS_2$ MTs catalysts. h) SEM and i) TEM images for Fe_2NiO_4/$FeNiS_2$ MTs catalysts. j) The calculated free energy at different sites on Fe_2NiO_4/$FeNiS_2$ towards OER and ORR. Reproduced with permission.[219] Copyright 2024, Elsevier. k) TEM and l) HRTEM images for Ni_3FeN/MnO-CNT catalysts. m) The ORR and OER activity at 0.7 and 1.55 V vs RHE for Ni_3FeN/MnO-CNT with different mass loads of Ni_3FeN. n) Schematic illustration of Ni_3FeN/MnO-CNT. Reproduced with permission.[229] Copyright 2022, Wiley-VCH.

addressing critical limitations of conventional carbon-based supports. While carbon supports suffer from oxidative corrosion at high potentials (>1.5 V vs RHE) and weak metal-support interactions, TiO_2 provides robust chemical stability and strong metal-support bonding.[230]

In addition to regulating NiFe compounds at the micro-scale, enhancing the mass transfer behavior of oxygen and electrolytes at the macro-scale is also essential to optimizing the charge-discharge cyclic performance in Zn–air batteries. The regulation of mass transfer behavior involves the construction of air electrodes.[231–233] Our group previously used chemical vapor deposition to grow a uniform Co-NCNT array on the surface of carbon cloth fibers. We found that this ordered structure can reduce the transport path of oxygen and electrolytes, greatly enhancing the charge-discharge cyclic durability for Zn–air batteries even at high current density.[234] Generally, preparing air cathode with NiFe-based catalysts uniformly loaded on the three-dimensional self-supporting current collector for Zn–air batteries includes many advantages: i) Decorating NiFe nanoparticles on the current collector with unique three-dimension networks could provide the large specific surface area to express abundant transport channel for allowing fast charge and mass transfer; ii) The flexible air cathode avoid utilizing polymer binders, which reduces the intrinsic resistance value for charge transfer and

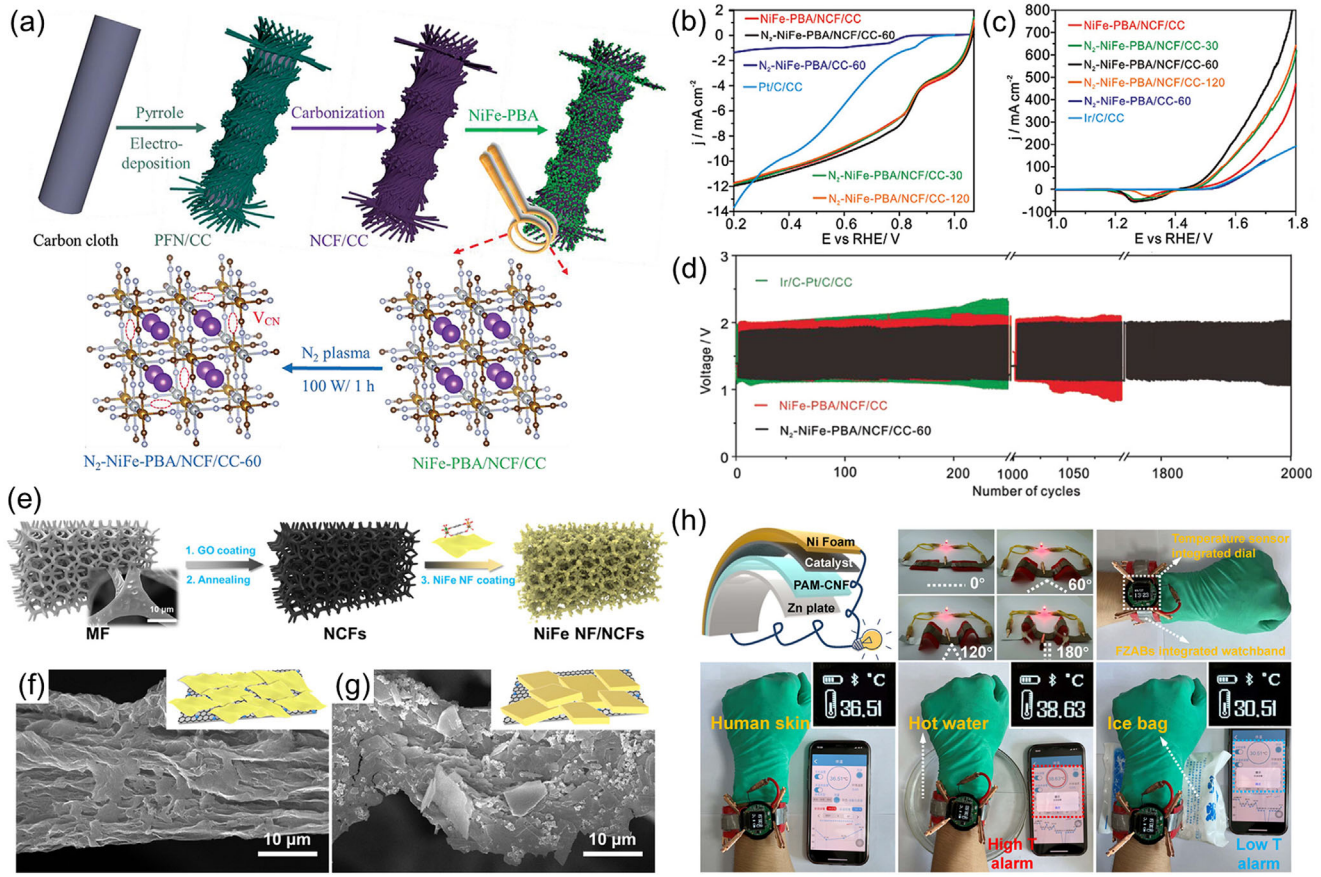

Figure 9. a) Schematic illustration of the preparation, LSV curves for b) ORR and c) OER activity, d) the Zn–air battery performance with N_2-NiFe-PBA/NCF/CC-60 catalysts and its comparison. Reproduced under the terms of 4.0 International License.[239] Copyright 2022, The Authors, published by Wiley-VCH. e) Scheme of the process of NiFe NF/NCFs; f,g) SEM and corresponding schematic preparation illustrations of NiFe NF/NCFs; h) The flexible Zn–air battery behavior using flexible NiFe NF/NCFs electrode. Reproduced under the terms of 4.0 International License.[240] Copyright 2022, The Authors, published by Wiley-VCH.

facilities more active sites exposure.[235,236,237] For instance, Zhang et al. reported NiFe-LDH/carbon nanofibers as air electrode catalysts in Zn–air batteries, in which the designed flexible air cathode delivered exceptional OER kinetics in alkaline conditions, especially as a result of the large surface area, abundant active sites exposure, and short electron transfer pathway.[238] The surface of carbon fiber is generally smooth, and NiFe-based catalyst is prone to further aggregation on its surface, which can seriously damage the number of catalytic active sites. Pre-treating flexible carbon substrates, such as acid etching, electrodeposition, plasma treatment, etc., to introduce defect sites is crucial for the uniform growth of NiFe-based catalysts. For instance, Jiang et al. pre-electrodeposited pyrrole onto carbon cloth fibers, then carbonized the coated pyrrole to form rich N sites on carbon cloth. The obtained flexible NCF/CC electrode can be applied as a self-supporting substrate to support NiFe-PBA catalysts (**Figure 9a**). To optimize oxygen catalytic activity, N_2 plasma technology was applied to create CN vacancy (V_{CN}) in NiFe-PBA for regulating the electron structure and modifying the local coordination environment of NiFe active sites.[239] Consequently, the fabricated air cathode (N_2-NiFe-PBA/NCF/CC-60) demonstrated remarkable ORR activity with a positive potential of 0.89 V at 5 mA cm^{-2} (Figure 9b), exceptional OER activity with a low overpotential of 270 mV at 50 mA cm^{-2} (Figure 9c), and impressive stability over 2000 cycles in Zn–air battery (Figure 9d). Notably, the flexible Zn–air battery equipped with this air cathode exhibited a low overpotential gap of 0.52 V at 1 mA cm^{-2}. Conventional flexible substrates, such as carbon cloth and carbon paper, are not directly suitable for loading NiFe-based catalysts, complicating the preparation process of air electrodes. Utilization of flexible carbon substrates with rich heteroatoms can compensate for this deficiency. Cao et al. applied carbonated commercial melamine foam as support to load NiFe-based metal-organic framework nanoflakes (NiFe NF/NCFs) to prepare a flexible air cathode (Figure 9e-g). The synthesized NiFe NF anchored on the NCFs surface with 3D porous structure, finally achieved high ORR/OER activities and long lifespan in Zn–air battery.[240] Besides, a flexible Zn–air battery has been successfully assembled and integrated into a watchband to drive a smartwatch with a temperature sensor, as shown in Figure 9h. This work opens an insight into the pursuit of unique energy storage devices for flexible electronics. The development of self-supporting supports provides favorable assistance for building the three-phase interface for NiFe-based catalysts, which provides the

possibility for the widespread application using rechargeable Zn–air batteries.

The integration of NiFe-based electrocatalysts with advanced support materials has emerged as a critical strategy to enhance their performance in Zn–air batteries. Combining NiFe compound nanoparticles on the N-doped carbon supports could achieve high ORR and OER activity with long stability, in which the N-doped carbon or the interfacial metal-N bond acts as ORR active sites while NiFe compounds mainly devote OER active sites, finally promoting the Zn–air battery performance. However, NiFe compounds tend to overgrow to form large particles on N-doped carbon supports through the conventional synthesis strategies, causing the reduction of the number of active Ni/Fe-NC sites. In addition, carbon materials are prone to electrochemical decomposition to form carbonates at high oxidation voltages, leading to the destruction of active sites. Therefore, developing functionalized non-carbon-based supports to uniformly load NiFe compounds for constructing highly efficient ORR/OER catalysts is worth focusing on in the future. In addition, the flexible support combined with the NiFe-based catalysts exhibits better ORR/OER activity under high current density and delivers a desirable choice to develop the flexible Zn–air batteries, owing to the enhanced electronic transfer and mechanical stability. However, the amount and distribution of NiFe-based nanoparticles on the flexible matrix need further exploration through simple and environmentally friendly strategies. More importantly, the interface contacts need to be enhanced through covalent bonding strategies to prevent delamination.

5.4. Embedding Effect

The biggest challenge faced by NiFe-based catalysts is the poor stability caused by Fe segregation during the OER process, followed by poor ORR activity. Therefore, it is necessary to encapsulate NiFe compounds with catalysts that have better ORR activity to construct bifunctional oxygen catalysts.[241] More importantly, embedding NiFe-based compounds with the second phase exhibited many advantages: i) The second phase on the outer surface of NiFe compounds can inhibit the aggregation and growth of NiFe compound nanoparticles during synthesis and reaction processes. ii) The shell of NiFe compounds can avoid direct contact with alkaline electrolytes, thereby suppressing the segregation of Fe ions. iii) The outer catalysts, such as N-doped carbon, could regulate the electron structure of NiFe compounds via the formation of interfacial bonds to adjust the adsorption free energy for oxygen-related reaction intermediates. iv) The outer catalyst with ORR activity, such as heteroatom-doped carbon, can compensate for the deficiency of single OER activity in NiFe compounds to construct suitable bifunctional catalysts. v) The outer surface catalyst skeleton can accelerate the electron and charge transfer rate on NiFe-based catalysts because of the special large specific surface area. Therefore, designing suitable supports with unique three-dimensional porous structures for embedding NiFe-based catalysts is reasonable for constructing bifunctional oxygen catalysts. Based on this, our group previously embedded CoS_x into N-doped three-dimensional porous carbon, which achieved extremely excellent bifunctional ORR and OER catalytic activity with ΔE = 0.74 V and demonstrated sustainable stability in rechargeable Zn–air batteries.[47] Embedding NiFe-based catalysts into heteroatom-doped carbon skeletons is currently the most widely reported strategy. NiFe compound catalysts endowed a small difference for the free energy between reaction intermediates, such as HOO* and HO*, remarkably promoting the OER activity. However, the high free energy difference between reaction intermediates, such as HOO^* and O_2, caused poor ORR activity.[242,243] Fortunately, metal-nitrogen-carbon materials, especially the Co–N–C, have claimed high ORR activity, benefiting from that the electron-rich N could regulate the electron states of adjacent carbon atoms to enhance the chemical chemisorption ability of oxygen and to be beneficial for the break of O═O double bonds.[244,245,246] Therefore, efficiently compositing NiFe-based compounds with ORR-active components of the Co–N–C to pursue bifunctional catalysts to lower the charge/discharge overpotential gap in Zn–air batteries.[247] As reported, the high-temperature pyrolysis could be applied to create the metal–N–C structure, in which the organic compositions containing N elements would be carbonized and synchronously doped N atoms into the carbon matrix to construct C–N species (such as graphitic C–N and pyrrolic C–N species) as ORR active sites.[248] Particularly, constructing asymmetric Co/NiFe Janus structure inside N-doped carbon provides a possible approach to designing composite catalysts with excellent bifunctional electrocatalytic activity.

Besides acting as the carbon support to boost the NiFe-based catalyst performance, the 1D CNT could also be applied to encapsulate NiFe-based nanoparticles to prevent the metal nanoparticles from aggregating and enhance the conductivity. For instance, Zhang et al. embedded the FeCoNi nanoalloy into mesoporous CNTs (FeCoNi-CNTs) to form the multi-metallic electrocatalyst (**Figure 10a**). In the carbon matrix, multiple metal modes, including metallic species (Fe, Co, and Ni), M-N, M-O, and FeCoNi alloy, coexist and are uniformly dispersed (Figure 10b,c). Consequently, the FeCoNi-CNTs achieved a high power density of approximately 210.5 mW cm^{-2} and an excellent specific capacity of 815.5 mAh g_{Zn}^{-1} in Zn–air batteries.[249] Generally, N-doped carbon with various N types (pyridinic-N, pyrrolic-N, and graphitic-N) claims different ORR/OER activities. Thereafter, Ma et al. encapsulated unique $FeNi_3$ alloys into N-doped nanotubes using in-situ catalytic assembly technique with ligand assistance, resulting in a distinct hollow tubular structure with bamboo-like joints (Figure 10d).[250] The chelated metal complex effectively prevented NiFe-based nanoparticle aggregation, and NiFe alloys were used for in-situ catalysis to form the nanotube structure. The DFT results illustrated that the pyridinic-N in N-doped carbon, combined with NiFe-based nanoparticles, adjusts the electronic state of carbon atoms for optimizing the desorption of OOH* intermediate, leading to high OER (overpotentials of 0.291 V at 10 mA cm^{-2}) and ORR (half-wave potentials of 0.782 V) activities, as well as long-term stability of 280 h for Zn–air batteries. Component adjustment and structural engineering claims as an effective strategy to enhance the activity and durability of NiFe-based catalytic materials. Waterhouse et al. employed a two-step pyrolysis method to create the ternary FeCoNi alloy nanoparticles embedded in a hierarchical nitrogen-rich carbon matrix (FeCoNi@HNC), as seen in Figure 10e. Interestingly, the FeCoNi alloy nanoparticles are homogeneously distributed and

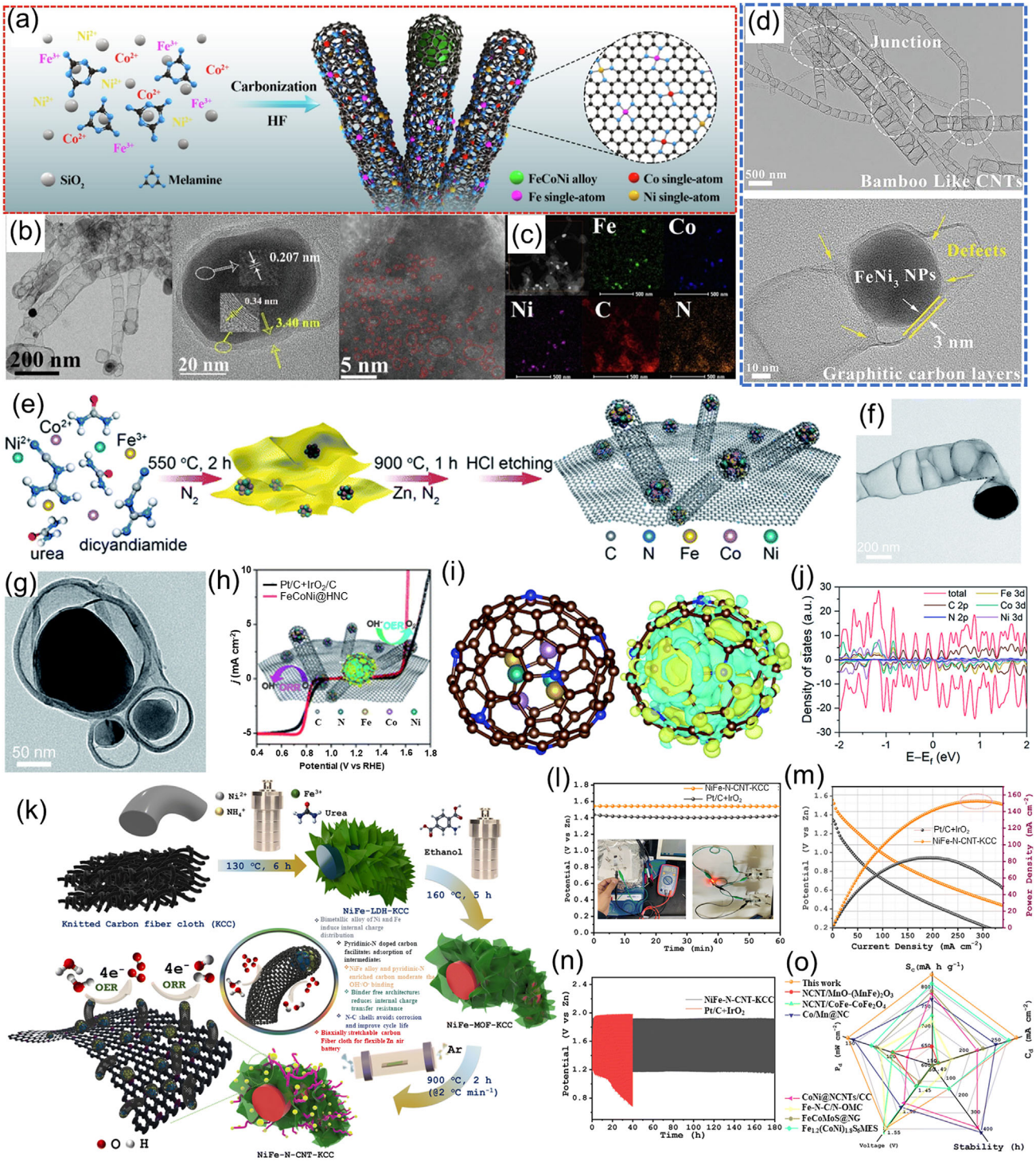

Figure 10. a) The schematic diagram, b) TEM/HRTEM images, and c) corresponding EDS mapping of the FeCoNi-CNTs. Reproduced with permission.[249] Copyright 2022, Elsevier. d) HRTEM images of $FeNi_3$@NC. Reproduced with permission.[250] Copyright 2023, Elsevier. e) The schematic diagram, f,g) TEM images, and h) ORR/OER activities, as well as i) difference charge density and j) DOS for $Fe_2Co_2Ni_2$@$C_{74}N_8$. Reproduced with permission.[251] Copyright 2021, Royal Society of Chemistry. k) Fabrication illustration of NiFe–N-CNT-KCC; l) Open circuit voltage, m) discharge polarization curve, n) cycling performance, and o) performance comparison of Zn–air battery using NiFe–N-CNT-KCC catalysts. Reproduced with permission.[141] Copyright 2024, Royal Society of Chemistry.

embedded in the hierarchical conductive network with a high surface area (Figure 10f,g). Through rational design, FeCoNi@HNC demonstrated superior ORR (half-wave potentials of 0.805 V) and OER (overpotentials of 0.391 V at 10 mA cm^{-2}) activities, achieving a peak power density of 109 mW cm^{-2} and a long lifespan over 200 cycles in Zn–air batteries (Figure 10h). More importantly, DFT calculations illustrated that the unique structure facilitates electron transfer from the alloy core to N-rich carbon shells (Figure 10i,j), optimizing the adsorption/desorption of ORR/OER intermediates.[251] Moreover, heteroatom-doped carbon enhances reaction kinetics and boosts the Zn–air battery performance through the chemisorption of O-containing intermediates and O_2 molecules on electron-deficient carbon atoms. In this case, Yoo et al. confined the NiFe-alloy nanoparticles within a pyridinic N-enriched sp^2 carbon skeleton to pursue the bifunctional ORR and OER activities (Figure 10k), where graphitic-N accelerated the charge transfer rate and pyridinic-N optimized O_2 adsorption ability. Finally, the Zn–air battery assembled with the NiFe–N-CNT-KCC delivered stable voltage, high power density, and long cyclic stability (Figure 10l-o).[141] In addition, constructing a unique core-shell structure between the NiFe-based nanoparticle and CNTs, such as converting the polydopamine (PDA) into N-doped carbon layer on NiFe-based nanoparticles or embedding NiFe alloy NPs in 3D NCNTs microspheres by pyrolyzing the nickel-iron-alkoxide and melamine, can protect the catalyst framework from accumulating during the carbonization procedure and enhance the reaction kinetics and durability.[188,197]

Benefiting from the advantages of the self-assembly of organic ligands, tunable pore structures, metal ion/cluster, abundant active sites exposure, varied d-band, and intrinsic synergistic effect, bimetallic NiFe-based MOF materials are widely selected as self-sacrificing templates accompanying preparation strategies of high-temperature annealing, phosphating, and sulfidation to obtain the functional carbon matrix encased NiFe compound nanoparticles.[252,253,254] Interestingly, NiFe-based MOF-derived carbon materials claim many advantages to combine the merits of all the pristine substances for designing unique NiFe-based MOF nanostructures with special morphologies (hollow structures and 1D/2D/3D structures) that can increase the exposure of active sites.[255,256] Recent research has revealed that the MOF (metal-organic framework)-derived hybrid catalyst containing metal nanoparticles and N-doped carbon frameworks exhibits high conductivity and sufficient porosity, which are all desirable properties for electron and mass transfer. Therefore, it is a promising strategy to embed NiFe-based compounds into MOF-derived carbon materials to construct bifunctional electrocatalysts.[257,258] As an example, Zheng et al. embedded the Ni_3Fe alloy into nitrogen-doped carbon (Ni_3Fe NCNTs-800), with the method of pyrolysis Ni-MOF and ferrocene hybridized while assisted by melamine, as shown in **Figure 11a**, in which combining the MOF precursor with melamine could effectively alleviate metal particle aggregation. As a result, the Ni_3Fe NCNTs-800 exhibited outstanding ORR and OER activities, achieving a potential gap of approximately 0.72 V, along with an ultra-high peak power density of 211 mW cm^{-2} and a long lifespan exceeding 1350 cycles in Zn–air batteries. Moreover, the theoretical calculation in Figure 11b has indicated that the strong synergistic coupling between bimetal Ni_3Fe alloys and N-doped carbon is crucial in reducing the reaction barrier for ORR/OER.[259] Carbon quantum dots (CQDs) within 10 nm sizes have been selected as electron acceptors and substantially improve the electron transfer efficiency to boost oxygen redox kinetics. Thus, combining CQDs with NiFe-based MOF catalysts paves a practicable avenue for promoting the Zn–air battery performance. Zou et al. employed a bifunctional Ni-Fe-S/NCQDs catalyst by integrating open-nanocage M1M2-sulfides with small-sized NCQDs, as shown in Figure 11c. This process involved forming the hollow structure with multiple holes through the ammonia selective etching of NiFe-PBA at room temperature. The resulting Ni-Fe-S/3NCQDs demonstrated excellent bifunctional catalytic performance, with a half-wave potential of 0.85 V ($E_{1/2}$, ORR) and an overpotential of 0.295 V at 10 mA cm^{-2} (OER), as shown in Figure 11d. The presence of S atoms, which have a strong affinity for O-species, imparts low adsorption energies for oxygen intermediates to the Ni–Fe–S species, thereby enhancing charge activation and ORR/OER activity (Figure 11e). Additionally, the unique hollow nanostructure facilitates easy penetration of electrolytes and improves access to NiOOH/FeOOH reaction sites.[260]

The effective catalytic performance of NiFe-based nanoparticles can be influenced by the number of active sites, which are determined by the electronic states and morphology of the catalysts. The distinctive pore structures and morphologies of NiFe-based nanoparticles, characterized by abundant porosity and large surface areas, particularly in core-shell configurations, can increase edge sites and enhance mass and charge transfer during ORR/OER processes.[261,262,263] Constructing a core-shell structure with a carbon shell and NiFe-based nanoparticle core can alter the electronic interactions between carbon and metal particles, while also impeding the active metal nanoparticles from electrolyte corrosion and preventing metal leaching in the process of oxidation.[132,264] Zhang et al. developed the carbon-coated FeNi alloy nanospheres with core-shell structure (FeNi@C) using a one-step process involving physical vapor evaporation and DC arc plasma technology, followed by nitrogen treatment, as illustrated in Figure 11f. In detail, the FeNi core is embedded within multiple graphene layers (Figure 11g), exhibiting clear bending and breaking phenomena, with a very thin carbon shell (<3 nm). The synergistic interaction between the N-doped carbon shell and bimetallic FeNi core is responsible for the bifunctional ORR (nearly $4e^-$ reaction process) and OER (overpotential is 326 mV at 10 mA cm^{-2}) activities, successfully enabling all-solid-state Zn–air batteries operation (Figure 11h).[265] The well-defined core-shell nanostructures preserve the intrinsic activity of the NiFe-based nanoparticles while maximizing the exposure of active sites, thereby enhancing ORR/OER bifunctional catalytic performance. Xue et al. synthesized a novel core-shell NiFe@N-graphite electrocatalyst via a one-step sintering process, as shown in Figure 11i, the highly uniform FeNi nanoparticles embedded into thin N-GR nanosheets with a unique core-shell nanostructure. The Zn–air battery assembled with NiFe@N-graphite demonstrated excellent cycling stability over 40 h and successfully powered an LED (Figure 11j,k).[207] In addition, Chen et al. encapsulated the Fe_xNi alloy within a graphitic shell, partially exposing the FeO_y thin-layered surface through the electronic modulation strategy to design bifunctional oxygen electrocatalysts with a sophisticated triphasic interfacial

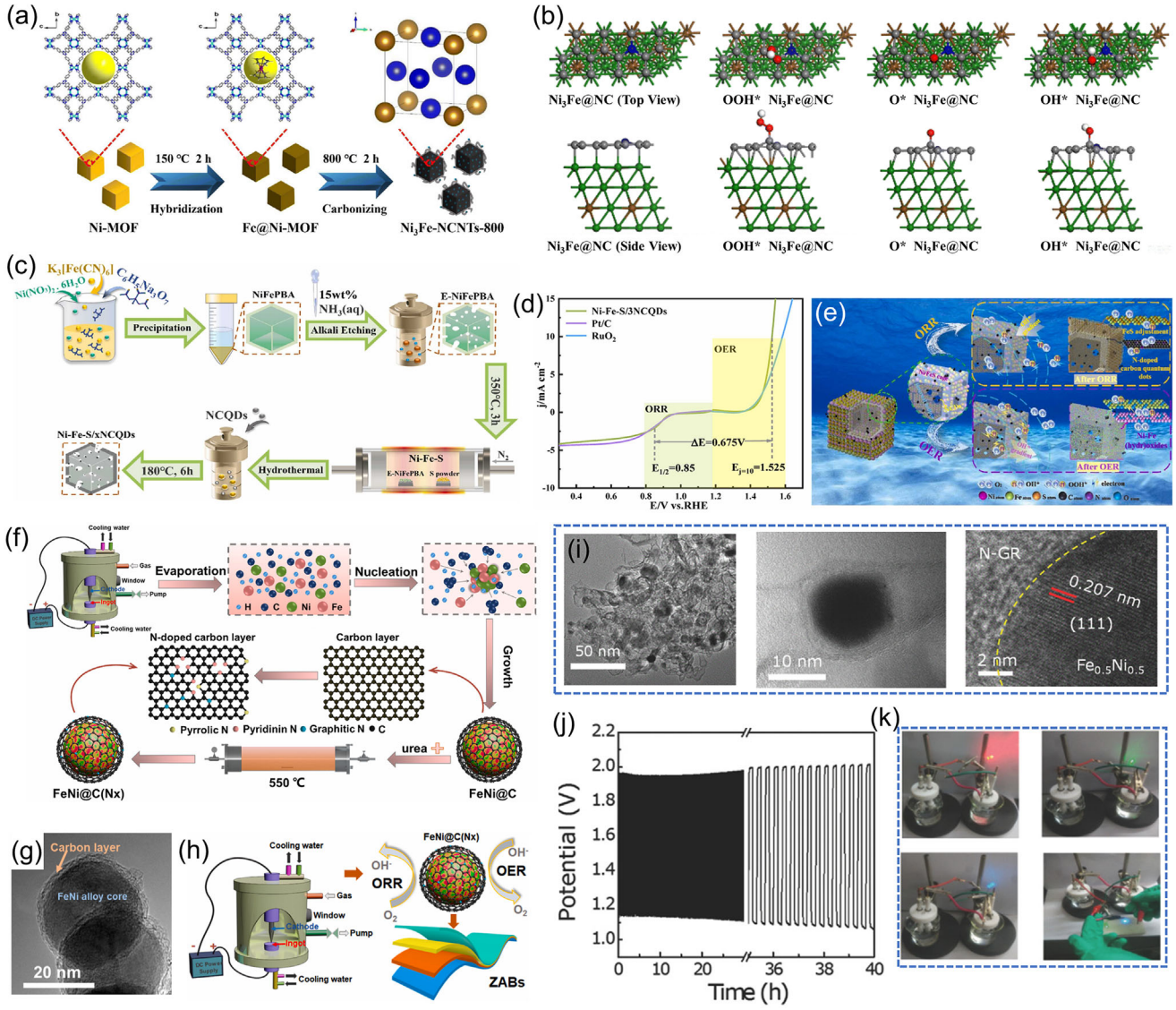

Figure 11. a) The preparation schematic diagram and b) the oxygen intermediates (OOH*, O*, and OH*) mechanism illustration adsorbed on the Ni_3Fe@NC site for the Ni_3Fe-NCNTs-800. Reproduced with permission.[259] Copyright 2023, Royal Society of Chemistry. c) The synthesis route, d) ORR and OER polarization curves, and e) ORR and OER reaction mechanisms for Ni-Fe-S/3NCQDs. Reproduced with permission.[260] Copyright 2023, Elsevier. f) The synthesis process illustration, g) HRTEM images, and h) the mechanism illustration for FeNi@C(N_{15}) catalysts. Reproduced with permission.[265] Copyright 2023, Elsevier. i) TEM images of $Fe_{0.5}Ni_{0.5}$@N-GR catalysts, j) Zn–air battery cyclic performance, and k) two Zn–air batteries using $Fe_{0.5}Ni_{0.5}$@N-GR catalysts for powdering the LED. Reproduced with permission.[207] Copyright 2018, Wiley-VCH.

structure, optimizing site density, electronic conductivity, and interfacial electronic interaction.[266] XANES analysis revealed that the tunable Fe_xNi-FeO_y-NC tri-phase interfacial configuration, facilitated by Ni incorporation, adjusted the oxidation state of Fe, and the electronic state of the in-situ generated iron oxide. Consequently, the Fe_xNi-FeO_y-NC exhibited a low OER overpotential of 308 mV at 10 mA cm^{-2} and ultra-high ORR half-wave potential of 0.890 V in alkaline electrolyte, with long durability in Zn–air battery and negligible activity decay after 500 cycles, indicating rapid charge transfer and a highly synergistic effect at the heterointerface. Transition-metal-oxides can also serve as shell material for encasing the NiFe-based nanoparticles to form the core-shell structure, enhancing the ORR performance of NiFe oxides.[267] For instance, Jiang et al. decorated the porous amorphous MnO_x layer with the ultrafine NiFeO nanoparticles (NPs), which reduces the adsorption and affinity energy of oxygen species on MnO_x shell, thereby significantly improving the reaction kinetics of the ORR.[268] As a result, the NiFeO@MnO_x demonstrated a low ORR/OER potential gap of 0.792 V between the ORR potential at −3 mA cm^{-2} and OER potential at 5 mA cm^{-2}. In the future, incorporating more metal oxides with high ORR activity as shells for NiFe-based nanoparticles could further protect against corrosion and Fe^{3+} ion leaching during the OER process, while tuning the electronic structure at the interface.

Based on the above discussion, the pristine NiFe-based compound exhibited high OER activity, however, it is not a wise

choice for direct application in Zn–air batteries, owing to the limited OER stability and poor ORR activity caused by low electron conductivity, sacrificed active sites, as well as high adsorption/desorption energy for intermediate species. In this part, many reports have proven that embedding the second phase with the NiFe-based compound with unique structures could enhance the ORR activity and boost the Zn–air battery performance by regulating the electronic structure environment and accelerating the charge and mass transfer rate based on the external conductive skeleton. Embedding strategy represents a paradigm shift in NiFe-based catalyst design, offering a holistic solution to reconcile activity, stability, and scalability. Of course, seamlessly coupling nanoscale confinement with macroscale electrode architectures, pioneering low-temperature embedding methods for industrial adoption, and merging materials science with computational modeling to predict optimal matrix-catalyst combinations are all challenges for the embedding strategy for NiFe-based materials. Therefore, reasonably selecting shell materials with high conductivity and oxidation resistance for NiFe-based compounds is still urgent for designing Zn–air batteries with superior performance even under high current density. By addressing these challenges, embedded NiFe catalysts could evolve into multifunctional nanoreactors that not only drive OER/ORR but also regulate electrolyte chemistry, propelling Zn–air batteries toward commercial viability.

5.5. Multi-Component Construction

Harnessing the synergistic influence between multiple active sites for enhancing desorption/adsorption of the oxygen-based electrocatalytic intermediate species during the ORR and OER process is crucial for boosting the ORR activity and enlarging the durability of the OER for NiFe-based catalysts. Furthermore, the multi-component construction with reinforced electronic effects of the multicomponent NiFe compounds could helpfully promote the electronic state along with a specific coordination environment at active sites, finally optimizing the affinities of the intermediates on the catalyst surface.[28,269] Optimizing the intrinsic activity and reaction kinetics of NiFe-based electrocatalysts is crucial, and this can be achieved by integrating multiple active moieties. For instance, Mousavi et al. adopted a distinctive layer-by-layer (LbL) assembled Fe/Co/Ni MOF using the 2-amino-1,4-benzenedicarboxylic acid linkers bridging (**Figure 12a,b**). The architecture-tailored multi-thin-film electrodes exhibited high crystallinity, chemical stability, hierarchical porosity, rapid mass and charge transfer, and simply accessible active sites. The synergistic interaction among the three metals (Fe, Co, Ni) enhances electronic occupancy and tunes the electronic structure/state, constructing abundant electrochemically active sites (Figure 12c). Consequently, the designed catalysts claimed super-high electrocatalytic performance, with a low OER overpotential of 254 mV at 10 mA cm^{-2} and a high ORR half-wave potential of 0.75 V vs. RHE. The Fe−Co−Ni MOF-based Zn−air battery exhibited remarkable cycling stability over 700 cycles, surpassing commercial noble metal benchmarks.[270] The concept of constructing active materials on two opposing faces or sides, first proposed by P.G. de Gennes in 1991 as the "Janus" structure.[271] This unique structure is advantageous for designing ORR/OER functional catalysts with distinct ORR and OER active sites, as it allows for the incorporation of coupled components that provide bifunctional properties and a tunable electronic structure through interfacial atoms. Ma et al. applied this concept by placing Ni and Fe single atoms on GHS (graphene hollow nanospheres), both in their inner and outer walls, to create bifunctional catalysts with abundant active sites through a step-by-step self-assembly method (Figure 12d). This design balances the competition between both the ORR and OER rate-limiting steps by separating Fe-N_4 and Ni-N_4 active sites (Figure 12e). Zn–air batteries using Ni-N_4/GHSs/Fe-N_4 catalysts exhibited a superior specific capacity of 777.6 mAh g_{Zn}^{-1} and a long lifespan exceeding 200 hours.[272] These works focus on adjusting the local electronic structure for Ni and Fe active sites, intending to optimize the adsorption energy of oxygen intermediates. Directly coupling NiFe compounds with ORR active components is also a common strategy for constructing bifunctional electrocatalysts. Metal/N-doped carbon claims the best-performing ORR catalyst besides Pt/C. Therefore, Huang et al. combined OER-functional NiFe-based catalysts with ORR-functional Fe–N–C catalysts for pursuing a remarkable record-low ΔE of 0.56 V, significantly outperforming the benchmarked Pt/C-Ir/C composite catalysts (Figure 12f-g). In addition, the overpotential exhibited by this dual-functional component direct composite strategy is significantly lower than all reported dual-functional electrocatalysts so far (Figure 12h), which confirms the progressiveness of this strategy. More interestingly, the ampere-hour-scale Zn–air batteries assembled with the bifunctional catalyst could operate even under a high current of 1 A. This work breaks the ORR/OER activity record through a facile preparation method and expands the possibility of developing practical Zn–air batteries.[273] In addition to heteroatom-doped carbon materials, Pt group-based noble metal catalysts also exhibit good ORR activity and are usually combined with NiFe-based compounds. For instance, Ni_3FeN-supported Fe_3Pt catalysts.[274] and Pd nanoparticles-$FeNi_3C_x$ composite catalysts.[275] deliver extraordinarily excellent cycling performance and low charge/discharge polarization potential gap in Zn–air batteries.

Apart from considering the electronic structure of NiFe-based catalysts, the integrated air cathode with the mixed gas/liquid/solid triple-phase interface needs the ability of feasible liquid electrolyte penetration, fast oxygen diffusion, and high electronic conductivity. Based on this consideration, Xu et al. constructed the air cathode with hydrophilic and hydrophobic layers to accelerate oxygen bubbles and hydroxide ions diffusion in electrolytes (OH^-) and enhance the active sites, thus achieving overall performance effectively in Zn–air batteries. The designed Ru_{SA}-NiFe LDH decorated air cathode can modify the three-phase interface during charge/discharge processes through the additional hydrophilic layer on top while compared with the conventional air cathode equipped with a single hydrophobic layer (**Figure 13a**). Moreover, the Ru_{SA}-NiFe LDH-based air cathode has also shown the potential in large-scale preparation through the roll-to-roll technology (Figure 13b), which enables an effective chameleon-like strategy to enhance Zn–air battery performance through the design of bifunctional catalyst and the construction of air cathodes. As a result, the Zn–air batteries with the engineered cathode exhibited an impressive charge/discharge capacity (100 mAh cm^{-2} per cycle) and an ultra-long cycle life of

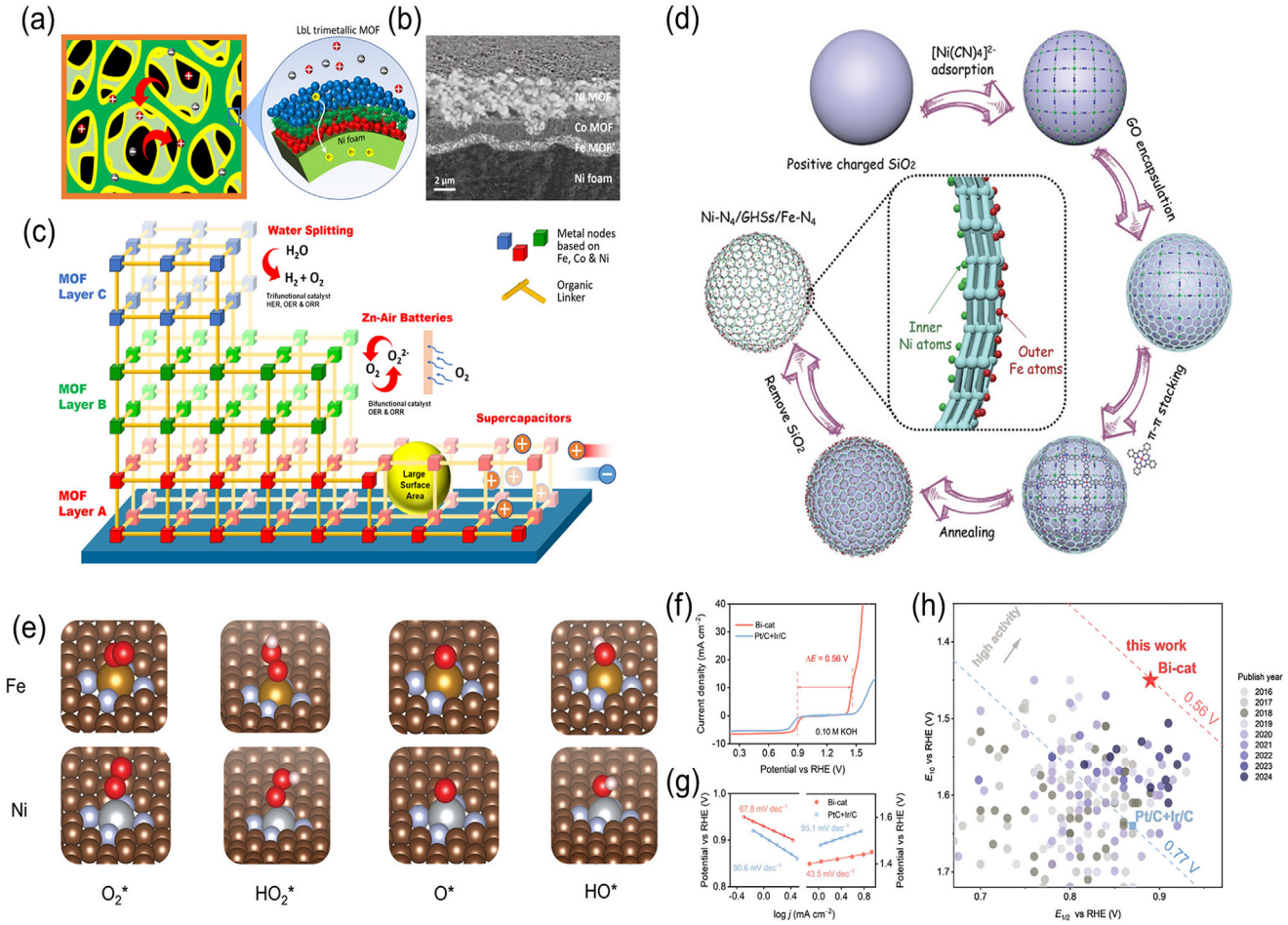

Figure 12. a) The schematic diagram, b) SEM images, c) the possible reaction mechanism scheme for the designed trilayer Fe–Co–Ni MOF. Reproduced with permission.[270] Copyright 2022, American Chemical Society. d) The schematic diagram of the preparation and e) DFT-optimized adsorption configurations of reaction adsorbates for the Ni-N_4/GHSs/Fe-N_4 catalyst. Reproduced with permission.[272] Copyright 2020, Wiley-VCH. f) The ORR and OER polarization curves corresponded with g) the Tafel slope plots for the prepared Bi-cat. h) Comparison diagram for bifunctional electrocatalytic activity among the designed catalyst with other reported catalysts. Reproduced with permission.[273] Copyright 2024, Wiley-VCH.

2400 h, surpassing most reported Zn–air batteries.[276] To address the limitations of traditional air cathode structures and improve the triple-phase interface for NiFe-based catalysts, Liu et al. introduced an innovative "air-breathing" strategy. This approach significantly enhances the triple-interface and promotes mass transfer by modifying the NiFe LDH-based self-supported air cathode with aerophilic perfluorochemical compounds (PFC) and amphiphilic ionomers. As illustrated in Figure 13c, this special air cathode increased oxygen solubility in the liquid electrolyte and enhanced the area of triple-phase boundaries to facilitate oxygen evolution.[277] In addition, the functional modifier on the self-support electrode accelerates the mass and charge transfer processes, including water, gas, ion transport, and electron transfer, because of the existence of $-SO_3^-$ (hydrophilic) and $-CF_2$ (hydrophobic) groups. Therefore, the designed Zn–air battery exhibited long durability of over 1000 h and a low discharge/charge potential gap of around 0.64 V, providing a new pathway for rationally designing the functional air cathode with NiFe-based catalysts for Zn–air batteries.

Despite introducing ionomers that could construct efficient three-phase interfaces for NiFe-based catalysts, the electron transfer between multi-component catalysts is hindered by ionomers.[278–280] Incorporating multicomponent catalysts into a self-supported air cathode can promote the utilization of catalytic features, improve electrolyte accessibility, and facilitate the desorption of oxygen bubbles.[281,282] Furthermore, designing NiFe-based catalysts with high activity and well-engineered interfaces is crucial for accelerating ORR/OER kinetics across gas, solid, and liquid phases in the Zn–air system. It has been reported that transition metals with empty "d" orbitals are expected to exhibit strong binding forces, promoting the growth of NiFe-based compounds, such as the Cu nanowire constructed more active sites for uniformly distributing the NiFe-LDH catalysts through electrochemical deposition technology while the surface NiFe-LDH impeded the further corrosion of Cu nanowires (Figure 13d), finally achieving a stable cycling performance in Zn–air battery (Figure 13e). The optimized three-dimensional structure derives an increased number of active sites, thus promoting the

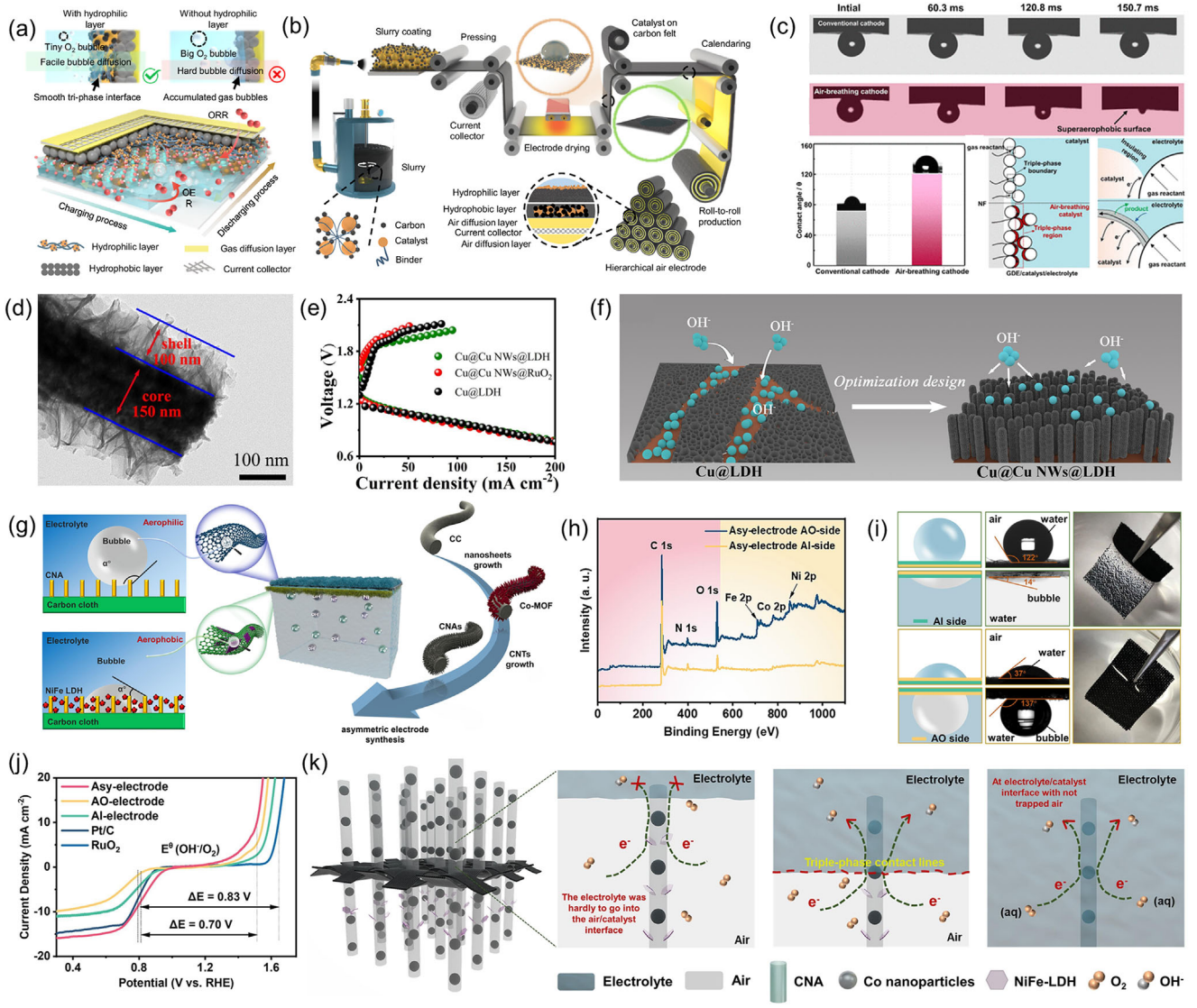

Figure 13. a) Schematic representation of oxygen bubble desorption from the engineered air cathode. b) Large-scale production of Zn–air batteries utilizing an engineered air cathode. Reproduced under the terms of 4.0 International License.[276] Copyright 2024, The Authors, published by Springer Nature. c) Modeled distribution of oxygen reactants along the conventional cathode surface, accompanied by digital photos for oxygen bubbles and a schematic showing the impact of PFSA–PFC nano-emulsion modifications on the triple-phase boundaries. Reproduced with permission.[277] Copyright 2022, American Chemical Society. d) High-resolution TEM images, e) discharge/charge profiles, and f) optimization mechanism of Cu@Cu NWs@LDH electrocatalysts. Reproduced with permission.[283] Copyright 2022, Elsevier. g) Schematic of the fabrication processes, h) XPS spectra, and i) differing wetting properties of the two sides of the asymmetric air cathode. j) Overall LSV curves for ORR and OER of the asymmetric cathode, along with comparative data. k) Reaction mechanism of the prepared catalysts at the gas–liquid–solid interface. Reproduced with permission.[284] Copyright 2024, Elsevier.

penetration of electrolytes into the catalytic layer (Figure 13f).[283] More interestingly, if the electrolyte forms the Wenzel-Cassie coexistent state on the air cathode surface, the solid catalyst surface can achieve partial wetting by both the electrolyte and atmospheric oxygen, thereby establishing a triple-phase interface. The ORR and OER processes necessitate distinct hydrophilic and hydrophobic characteristics in the catalyst. Typically, OER requires the catalyst to be hydrophilic to facilitate the accessibility of electrolytes, while ORR requires the catalyst to exhibit appropriate hydrophobicity to facilitate the diffusion of oxygen. NiFe-based compounds typically exhibit good hydrophilicity and OER activity, while heteroatom-doped carbon materials exhibit good hydrophobicity and ORR activity. Therefore, combining hydrophilic NiFe-based catalysts with hydrophobic heteroatom-doped carbon materials to construct different functional zones in the air cathode is beneficial for mass transfer behavior during charge-discharge processes. Based on this consideration, An et al. designed a special asymmetric air cathode with carbon nanotube arrays encapsulating Co nanoparticles (CNAs) on the aerophilic side for promoting the ORR kinetics and NiFe-LDH/CNAs on the aerophobic side to boost the OER kinetics (Figure 13g,h). The two sides of the asymmetric air cathode have different

wetting abilities (Figure 13i). Thereafter, the ORR and OER activity of the special asymmetric air cathode claims significantly enhanced (Figure 13j), because the adsorption and desorption of O_2 and OH^- on the asy-electrode surface have been effectively balanced, and the transport rate of gas, electrolyte reactants, and products have been promoted, as displayed in Figure 13k. Consequently, the aqueous Zn–air battery encased with the asymmetric air cathode has acquired an ultra-high power density of 236.26 mW cm^{-2}, a high open circuit voltage, and a long-term cycling stability of over 1920 cycles at 10 mA cm^{-2}.[284] Therefore, combining the NiFe-based compounds with a special structure design could promote the durability of the aerophilic/hydrophilic interface due to the independent separation of charge and discharge reactions. Accurately optimizing and coupling hydrophobic and hydrophilic layers in the catalytic layer are crucial for improving charge and discharge performance.

Based on the above discussion, introducing multiple components into oxygen electrocatalysts can fully utilize the advantages of each component, thus achieving a "synergistic effect". However, there is still no unified design criterion for accurately adjusting the interfacial interaction between NiFe-based catalysts and other phases to regulate ORR and OER activity. Introducing independent functional zones in the air electrode to promote discharge and charge reactions, respectively, is highly attractive for designing high-performance rechargeable zinc air batteries. A key challenge that needs to be resolved is how to accurately match the roles between different functional zones to improve charging and discharging performance simultaneously. After coupling the best ORR catalyst with NiFe-based catalysts into the air cathode, there is hope that the energy efficiency of rechargeable Zn–air batteries will be improved by over 70%.

6. Summary and Outlook

NiFe-based electrocatalysts show excellent OER activities owing to a suitable 3d orbital electronic structure. Different NiFe electrocatalysts, such as NiFe LDH, NiFe oxides, NiFe composites, NiFe MOFs, and NiFe alloys, have been synthesized and optimized to boost the catalytic activity and stability. However, most NiFe-based electrocatalysts exhibited unsatisfactory ORR activity due to poor oxygen adsorption capacity. Plenty of strategies have been developed to successfully apply NiFe-based electrocatalysts into rechargeable Zn–air batteries to boost the bifunctional activity and durability. Doping heteroatom species into NiFe-based electrocatalysts is useful to enhance the catalytic activity via promoting the electro-oxidation reconstruction. Moreover, the anion ions like N, S, P, and B can regulate the d-bond center of the metal center to regulate the adsorption ability of the reaction intermediates. Heteroatom-doped carbon materials, with high electron conductivity and valid surface area, are also selected as effective support for enhancing the ORR and OER activity of NiFe-based catalysts. In particular, the NiFe compound/N-doped carbon composite shows excellent bifunctional ORR and OER activities owing to the electron interaction function between NiFe compounds and N-doped carbon to facilitate charge and electron transfer rate. In addition, regulating the electronic structure and intrinsic conductivity of the NiFe-based catalysts with other active metal elements can also enhance the ORR/OER kinetics. Significant progress has been made in the energy density, energy efficiency, and cycle life of Zn–air batteries based on NiFe-based electrocatalysts. The rapid advancement of NiFe-based electrocatalysts for Zn–air batteries has unveiled both unprecedented opportunities and critical gaps. There still exist some challenges in **Scheme 3** to applying NiFe-based electrocatalysts in rechargeable Zn–air batteries:

i. Large-Scale Synthesis: Although the prices of Ni and Fe are relatively cost-effective, the complex synthesis steps make the cost of the NiFe-based catalyst does not meet practical requirements in rechargeable Zn–air batteries. To prepare NiFe-based catalysts, the preparation strategy, such as co-precipitation method, hydrothermal/solvothermal synthesis, electrodeposition, sol–gel method, spray pyrolysis, chemical vapor deposition, microwave-assisted synthesis, template-assisted synthesis, and mechanical alloying, are all required cumbersome procedure, additional solvent, precursor, and the special instruments, finally causing high cost and environmental pollution. To pursue the commercial application requirement of the Zn–air battery, the clean, simple, and low-cost preparation procedure for NiFe-based electrocatalysts needs further exploration.
ii. Energy Efficiency Bottleneck: The state-of-the-art NiFe-based bifunctional electrocatalytic materials exhibit the ORR/OER overpotential of around 0.7 V in the alkaline media while limiting the round-trip efficiencies below 70% in the rechargeable Zn–air battery. The unsatisfactory energy efficiency is hardly broken owing to the high ORR/OER overpotential gap, which is still a critical issue for commercial applications. Based on this consideration, combining the redox mediator for OER and ORR is a promising direction to break the bottleneck of the Zn–air batteries, considering that the soluble additive can change the ORR and OER route with a reduced energy barrier. In addition, constructing a suitable three-phase interface for NiFe-based electrocatalysts in Zn–air batteries can also reduce the charge-discharge voltage gap and achieve high round-trip efficiency.
iii. Dynamic Reaction Mechanism: Currently, OER and ORR mechanisms for the NiFe-based electrocatalysts have been explored through advanced in situ characterization. In general, the in-situ characterization for exploring the reaction mechanism is commonly conducted in the low-concentration KOH electrolyte. The *in-situ* characterization result could demonstrate the reaction mechanism of the catalyst by detecting reaction intermediates. However, the in situ characterization does not consider the oxygen redox chemistry of electrocatalysts under high-concentration salt electrolyte with zinc salt addictive during the dynamic discharge/charge process, which results in unclear dynamic reaction kinetics of NiFe-based electrocatalysts in practical Zn–air batteries. Therefore, the dynamic reaction mechanism of NiFe-based electrocatalysts needs to be explored during the charge/discharge process and further to guide the design direction.
iv. Iron Segregation: During the charging process, iron ions in NiFe-based catalysts react with OH^- to form FeOOH, leading to the formation of a phase interface between FeOOH and the substrate NiFe-based material. The dynamic dissolution and re-deposition process accelerates the separation of iron ions and the formation of the FeOOH phase, thus leading to

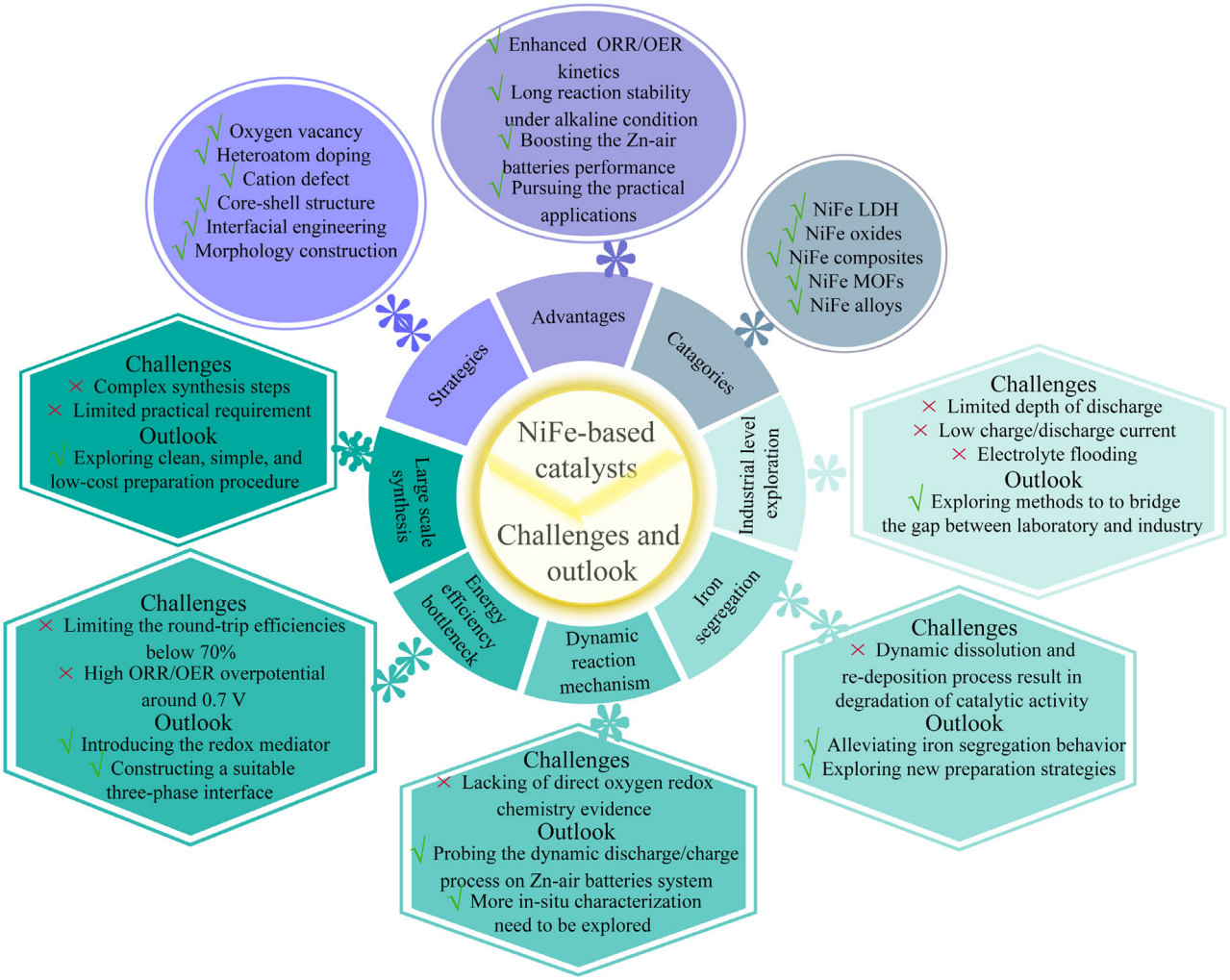

Scheme 3. Summary, challenge, and outlook of NiFe-based electrocatalysts in rechargeable Zn–air batteries.

the degradation of catalytic activity. Although surface modification strategies can alleviate iron segregation behavior, avoiding contact between iron ions and alkaline electrolytes during the electrochemical reconstruction process is difficult, especially in high-concentration alkaline electrolytes. Therefore, more effective strategies need to be developed to address the degradation of catalytic activity caused by iron segregation.

v. Industrial-Level Exploration: In the laboratory stage, Zn–air batteries are usually fabricated with metallic zinc plates and homemade configurations to evaluate their performance. Due to the use of the metallic zinc anode, the current depth of discharge (DOD) is usually less than 10%, leading to relatively low energy density based on the mass of the whole battery. In addition, the actual charge/discharge current (Current density <20 mA cm^{-2}) is also relatively low owing to the low active area of the cathode (Active area <4 cm^2) currently used in the laboratory, which still has a significant gap compared to practical applications (Industrial current 1 A, cycling stability >1000 cycles, DOD >50%). More importantly, the electrolyte flooding in the cathode and zinc dendrites in the anode can easily lead to poor cycle life of the battery at high current densities and high DOD. Therefore, to bridge the gap between laboratory and industry, more work is needed to explore practical industrial-grade Zn–air batteries. NiFe-based catalysts represent a promising class of bifunctional catalysts. Future studies should prioritize testing under industrial-level conditions—including high current densities, deep discharge depths, and energy density assessments at the full-cell level—alongside techno-economic analyses to accelerate their commercialization.

Overall, NiFe-based electrocatalysts have achieved great success in Zn–air batteries with long lifespan and low charge/discharge overpotential. However, there is still a large gap in achieving the practical application of NiFe-based electrocatalysts in rechargeable Zn–air batteries. To meet the commercial application requirement, the design and optimization of NiFe-based electrocatalysts need to be further explored, mainly focusing on the cost, activity, stability, energy efficiency, industrial requirement, and reaction mechanism. Transition from lab-scale "performance-first" strategies to green chemistry principles is

the essential direction to match well with the economically and environmentally friendly features. Adopting bio-derived ligands and recycling spent catalysts are both future exploration trends. Combining with the hot topic, the machine learning techniques can be adopted to predict optimal NiFe compositions, morphologies, and defect configurations, including experimental parameters (e.g., Ni/Fe ratios, anion types) linked to performance metrics (overpotential, cycle life). We believe that this review can provide some in-depth insights into the practical application of NiFe-based electrocatalysts in rechargeable Zn–air batteries.

Acknowledgements

L.A. thanks a grant from the Research Grants Council of the Hong Kong Special Administrative Region, China (Project No. 15308024), a grant from the Research Grants Council of the Hong Kong Special Administrative Region, China (N_PolyU559/21), a grant from the Research Institute for Smart Energy (CDB2), a grant from the Research Institute for Advanced Manufacturing (CDJQ), and a grant from Research Centre for Carbon-Strategic Catalysis (CE2X) at The Hong Kong Polytechnic University. Q.L. thanks the National Natural Science Foundation of China (52402268) and Natural Science Foundation of Jiangsu Province of China (BK20230426). X.Z. thanks the PolyU Distinguished Postdoctoral Fellowship Schemes (YWEE).

Open access publishing facilitated by Curtin University, as part of the Wiley - Curtin University agreement via the Council of Australian University Librarians.

Conflict of Interest

The authors declare no conflict of interest.

Keywords

bifunctional electrocatalysts, design strategies, NiFe-based catalysts, rechargeable Zn–air batteries

Received: March 17, 2025
Revised: May 8, 2025
Published online: May 24, 2025

[1] Y. X. Li, S. B. Song, H. Kim, K. Nomoto, H. Kim, X. Y. Sun, S. Hori, K. Suzuki, N. Matsui, M. Hirayama, T. Mizoguchi, T. Saito, T. Kamiyama, R. Kanno, *Science* **2023**, *381*, 50.
[2] H. P. Xie, Z. Y. Zhao, T. Liu, Y. F. Wu, C. Lan, W. C. A. Jiang, L. Y. Zhu, Y. P. Wang, D. S. Yang, Z. P. Shao, *Nature* **2022**, *612*, 673.
[3] Y. Zhang, B. Chen, D. Q. Guan, M. G. Xu, R. Ran, M. Ni, W. Zhou, R. O'Hayre, Z. P. Shao, *Nature* **2021**, *591*, 246.
[4] W. X. Wu, L. P. Xu, Q. Lu, J. P. Sun, Z. Y. Xu, C. S. Song, J. C. Yu, Y. Wang, *Adv. Mater.* **2024**, *37*, 2312894.
[5] Q. Lu, J. Liu, X. Zou, B. Huang, W. Wu, J. Yin, Z. Liu, Y. Wang, *Angew Chem. Int. Ed.* **2025**, 202503733.
[6] W. Sun, F. Wang, B. Zhang, M. Y. Zhang, V. Küpers, X. Ji, C. Theile, P. Bieker, K. Xu, C. S. Wang, M. Winter, *Science* **2021**, *371*, 46.
[7] X. H. Zou, M. C. Tang, Q. Lu, Y. Wang, Z. P. Shao, L. An, *Energy Environ. Sci.* **2024**, *17*, 386.
[8] H. Geng, X. Zou, Y. Min, Y. Bu, Q. Lu, *Adv. Funct. Mater.* **2025**, 2500657.
[9] X. H. Zou, Q. Lu, L. Z. Wu, K. E. Zhang, M. C. Tang, H. J. Xie, X. Zhang, Z. P. Shao, *Angew. Chem., Int. Ed.* **2025**, *64*, 202416235.
[10] Q. Lu, X. H. Zou, Y. F. Bu, Z. P. Shao, *Energy Storage Mater.* **2023**, *55*, 166.
[11] Q. Lu, X. H. Zou, Y. F. Bu, Y. Wang, Z. P. Shao, *Energy Storage Mater.* **2024**, *68*, 103341.
[12] J. Wu, X. Gao, G. M. Liu, X. Y. Qiu, Q. Xia, X. Z. Wang, W. X. Zhu, T. W. He, Y. J. Zhou, K. Feng, J. X. Wang, H. Huang, Y. Liu, M. H. Shao, Z. H. Kang, X. Zhang, *J. Am. Chem. Soc.* **2024**, *146*, 20323.
[13] J. Dai, Z. H. Shen, Y. Chen, M. R. Li, V. K. Peterson, J. Y. Tang, X. X. Wang, Y. Li, D. Q. Guan, C. Zhou, H. N. Sun, Z. W. Hu, W. H. Huang, C. W. Pao, C. T. Chen, Y. L. Zhu, W. Zhou, Z. P. Shao, *J. Am. Chem. Soc.* **2024**, *146*, 33663.
[14] X. H. Zou, Q. Lu, J. Wu, K. E. Zhang, M. C. Tang, B. X. Wu, S. X. She, X. Zhang, Z. P. Shao, L. An, *Adv. Funct. Mater.* **2024**, *34*, 2401134.
[15] M. C. Luo, Z. L. Zhao, Y. L. Zhang, Y. J. Sun, Y. Xing, F. Lv, Y. Yang, X. Zhang, S. Hwang, Y. N. Qin, J. Y. Ma, F. Lin, D. Su, G. Lu, S. J. Guo, *Nature* **2019**, *574*, 81.
[16] M. D. Zhang, Q. B. Dai, H. G. Zheng, M. D. Chen, L. M. Dai, *Adv. Mater.* **2018**, *30*, 1705431.
[17] Y. Xie, Y. Feng, S. Zhu, Y. Yu, H. Bao, Q. Liu, F. Luo, Z. Yang, *Adv. Mater.* **2024**, *37*, 2414801.
[18] Y. Li, J. Xu, F. Lan, Y. Wang, H. Jiang, X. Wu, Y. Huang, R. Li, Q. Jiang, D. Gao, P. Zhu, S. Zhao, Y. Zhao, F. Wang, L. Zhang, L. Zhang, R. Zhang, *Angew. Chem., Int. Ed.* **2024**, *64*, 202420481.
[19] J. Zhao, J. J. Zhang, Z. Y. Li, X. H. Bu, *Small* **2020**, *16*, 2003916.
[20] H. M. Sun, Z. H. Yan, F. M. Liu, W. C. Xu, F. Y. Cheng, J. Chen, *Adv. Mater.* **2020**, *32*, 1806326.
[21] X. Liu, J. S. Meng, J. X. Zhu, M. Huang, B. Wen, R. T. Guo, L. Q. Mai, *Adv. Mater.* **2021**, *33*, 2007344.
[22] Y. S. Zhou, Z. T. Wang, M. H. Cui, H. Y. Wu, Y. J. Liu, Q. R. Ou, X. L. Tian, S. Y. Zhang, *Adv. Funct. Mater.* **2024**, *34*, 2410618.
[23] S. Iqbal, B. Safdar, I. Hussain, K. Zhang, C. Chatzichristodoulou, *Adv. Energy Mater.* **2023**, *13*, 2203913.
[24] S. Gong, Y. Meng, Z. Jin, H.-Y. Hsu, M. Du, F. Liu, *ACS Catal.* **2024**, *14*, 14399.
[25] W. J. Liu, H. Jiang, H. Q. Yu, *Chem. Rev.* **2015**, *115*, 12251.
[26] J. Wang, J. Kim, S. Choi, H. Wang, J. Lim, *Small Methods* **2020**, *4*, 2000621.
[27] Y. Jia, L. Zhang, G. Gao, H. Chen, B. Wang, J. Zhou, M. T. Soo, M. Hong, X. Yan, G. Qian, J. Zou, A. Du, X. Yao, *Adv. Mater.* **2017**, *29*, 1700017.
[28] W.-X. Hong, W.-H. Wang, Y.-H. Chang, H. Pourzolfaghar, I. H. Tseng, Y.-Y. Li, *Nano Energy* **2024**, *121*, 109236.
[29] D. Tang, J. Liu, X. Wu, R. Liu, X. Han, Y. Han, H. Huang, Y. Liu, Z. Kang, *ACS Appl. Mater. Interfaces* **2014**, *6*, 7918.
[30] L. Zong, P. Li, F. Lu, C. Wang, K. Fan, Z. Li, L. Wang, *Adv. Funct. Mater.* **2023**, *33*, 2301013.
[31] L. Peng, N. Yang, Y. Yang, Q. Wang, X. Xie, D. Sun-Waterhouse, L. Shang, T. Zhang, G. I. N. Waterhouse, *Angew.Chem. Int. Ed.* **2021**, *60*, 24612.
[32] B. Zhao, Y. Wang, Z. Wang, Y. Hu, J. Zhang, X. Bai, *Chem. Eng. J.* **2024**, *487*, 150437.
[33] B. Zhang, Z. Wu, W. Shao, Y. Gao, W. Wang, T. Ma, L. Ma, S. Li, C. Cheng, C. Zhao, *Angew. Chem., Int. Ed.* **2022**, *61*, 202115331.
[34] Z. He, J. Zhang, Z. Gong, H. Lei, D. Zhou, N. Zhang, W. Mai, S. Zhao, Y. Chen, *Nat. Commun.* **2022**, *13*, 2191.
[35] J. Zhou, J. Cheng, B. Wang, H. Peng, J. Lu, *Energy Environ. Sci.* **2020**, *13*, 1933.
[36] Q. Lu, X. Zou, Y. Bu, L. An, Y. Wang, Z. Shao, *Next Energy* **2023**, *1*, 100025.
[37] M. Tang, Q. Liu, X. Zou, B. Zhang, L. An, *Adv. Mater.* **2025**, 2501361.
[38] A. Li, Z. Xu, X. Zhang, M. Wu, *J. Energy Chem.* **2025**, *106*, 688.
[39] A. Li, X. Zhang, Z. Xu, M. Wu, *Chem. Eng. J.* **2024**, *494*, 153240.
[40] D. Liu, H. Ge, M. Song, Y. Jiang, X. Gong, T. You, L. Fu, Z. Fu, Y. Zhang, *Adv. Mater.* **2024**, *37*, 2417161.

[41] M. Tang, Q. Liu, Z. Yu, X. Zou, X. Huo, B. Zhang, L. An, *Small* **2024**, *20*, 2403457.
[42] R. Huang, J. Zhang, W. Wang, X. Wu, X. Liao, T. Lu, Y. Li, J. Chen, S. Chen, Y. Qiao, Q. Zhao, H. Wang, *Energy Environ. Sci.* **2024**, *17*, 3179.
[43] M. Tang, Q. Liu, X. Zou, Z. Yu, K. Zhang, B. Zhang, L. An, *Energy Storage Mater.* **2025**, *74*, 103896.
[44] F. Mansfeld, S. Gilman, *J. Electrochem. Soc.* **1970**, *117*, 1328.
[45] X. Fan, Y. Xie, Y. Jiao, P. Wu, *ACS Nano* **2024**, *18*, 35705.
[46] M. Du, B. Chu, Q. Wang, C. Li, Y. Lu, Z. Zhang, X. Xiao, C. Q. Xu, M. Gu, J. Li, H. Pang, Q. Xu, *Adv. Mater.* **2024**, *36*, 2412978.
[47] Q. Lu, J. Yu, X. Zou, K. Liao, P. Tan, W. Zhou, M. Ni, Z. Shao, *Adv. Funct. Mater.* **2019**, *29*, 1904481.
[48] G. Nazir, A. Rehman, J. H. Lee, C. H. Kim, J. Gautam, K. Heo, S. Hussain, M. Ikram, A. A. AlObaid, S. Y. Lee, S. J. Park, *Nano-Micro Lett.* **2024**, *16*, 138.
[49] Y. He, Z. Zhao, Y. Cui, W. Shang, Y. Chen, P. Tan, *Energy Storage Mater.* **2023**, *57*, 360.
[50] L. Li, X. Tang, B. Wu, B. Huang, K. Yuan, Y. Chen, *Adv. Mater.* **2024**, *36*, 2308326.
[51] J. Wu, B. Liu, X. Fan, J. Ding, X. Han, Y. Deng, W. Hu, C. Zhong, *Carbon Energy* **2020**, *2*, 370.
[52] F. Cheng, J. Chen, *Chem. Soc. Rev.* **2012**, *41*, 2172.
[53] F. Calle-Vallejo, J. I. Martinez, J. Rossmeisl, *Phys. Chem. Chem. Phys.* **2011**, *13*, 15639.
[54] W. Zhang, J. Zhang, N. Wang, K. Zhu, C. Yang, Y. Ai, F. Wang, Y. Tian, Y. Ma, Y. Ma, X. Zhang, L. Duan, D. Chao, F. Wang, D. Zhao, W. Li, *Nat. Sustain.* **2024**, *7*, 463.
[55] K. Zeng, X. Zheng, C. Li, J. Yan, J. H. Tian, C. Jin, P. Strasser, R. Yang, *Adv. Funct. Mater.* **2020**, *30*, 2000503.
[56] B. Wei, Z. Fu, D. Legut, T. C. Germann, S. Du, H. Zhang, J. S. Francisco, R. Zhang, *Adv. Mater.* **2021**, *33*, 2102595.
[57] H. Kim, K. Lee, S. I. Woo, Y. Jung, *Phys. Chem. Chem. Phys.* **2011**, *13*, 17505.
[58] A. Kulkarni, S. Siahrostami, A. Patel, J. K. Norskov, *Chem. Rev.* **2018**, *118*, 2302.
[59] Z. Duan, G. Wang, *Phys. Chem. Chem. Phys.* **2011**, *13*, 20178.
[60] S. Wu, Z. Liang, T. Wang, X. Liu, S. Huang, *Inorg. Chem. Front.* **2025**, *12*, 848.
[61] X. Ge, A. Sumboja, D. Wuu, T. An, B. Li, F. W. T. Goh, T. S. A. Hor, Y. Zong, Z. Liu, *ACS Catal.* **2015**, *5*, 4643.
[62] S. Yang, X. Liu, S. Li, W. Yuan, L. Yang, T. Wang, H. Zheng, R. Cao, W. Zhang, *Chem. Soc. Rev.* **2024**, *53*, 5593.
[63] C. Wang, P. Zhai, M. Xia, Y. Wu, B. Zhang, Z. Li, L. Ran, J. Gao, X. Zhang, Z. Fan, L. Sun, J. Hou, *Angew. Chem., Int. Ed.* **2021**, *60*, 27126.
[64] C. Wang, P. Zhai, M. Xia, W. Liu, J. Gao, L. Sun, J. Hou, *Adv. Mater.* **2023**, *35*, 2209307.
[65] S. Xu, S. Feng, Y. Yu, D. Xue, M. Liu, C. Wang, K. Zhao, B. Xu, J. N. Zhang, *Nat. Commun.* **2024**, *15*, 1720.
[66] H. Jiao, C. Wang, H. Tian, Z.-Y. Zhang, Y. Zhao, P. Na, Y. Yamauchi, Z.-L. Wang, *Chem. Eng. J.* **2024**, *498*, 155063.
[67] W. Song, C. Xia, S. Zaman, S. Chen, C. Xiao, *Small* **2024**, *20*, 2406075.
[68] Q. Lin, G. Nan, D. Fu, L. Xie, *Phys. Chem. Chem. Phys.* **2025**, *27*, 4926.
[69] K. Fan, L. Zong, J. Liu, C. H. Chuang, M. Dong, Y. Zou, Y. Xu, H. Q. Fu, L. Zhang, L. Wang, M. Zhou, T. Zhan, P. Liu, H. Zhao, *Adv. Energy Mater.* **2024**, *14*, 2400052.
[70] D. Wu, L. Hu, X. Liu, T. Liu, X. Zhu, Q. Luo, H. Zhang, L. Cao, J. Yang, Z. Jiang, T. Yao, *Nat. Commun.* **2025**, *16*, 726.
[71] N. Zhang, X. Feng, D. Rao, X. Deng, L. Cai, B. Qiu, R. Long, Y. Xiong, Y. Lu, Y. Chai, *Nat. Commun.* **2020**, *11*, 4066.
[72] J. Jia, J. Zhang, K. Guo, L. Zhang, G. Du, H. You, J. Huang, M. Tu, H. Li, Y. Peng, W. Dou, C. Xu, *J. Energy Chem.* **2025**, *100*, 77.
[73] X. Yu, W. Zhang, L. Ma, J. Tang, W. Lu, J. Li, J. Zhang, X. Xu, *Green Chem.* **2025**, *27*, 731.
[74] J. Jiang, C. Xi, Y. Zhao, Y. Zhu, K. Hu, Y. Wang, S. Wang, Z. Zhang, S. Han, *ACS Catal.* **2025**, *15*, 2561.
[75] Z. Wang, T. Qiu, R. Jian, Y. Zhang, J. Feng, L. Gong, S. Yin, L. Li, Y. Zhu, S. Chen, J. Deng, *ChemSusChem* **2025**, *18*, 202401091.
[76] M. Qi, M. Qin, H. Wang, B. Lin, J. Chen, X. Shi, X. Du, S. Mao, J. Zhao, H. Zhang, L. Xi, Y. Wang, *Appl. Catal. B-Environ. Energy* **2024**, *356*, 124259.
[77] Y. Li, Y. Wu, M. Yuan, H. Hao, Z. Lv, L. Xu, B. Wei, *Appl. Catal. B-Environ.* **2022**, *318*, 121825.
[78] Y. Wu, Y. Li, Z. Xie, Y. Wang, Y. Wang, B. Wei, *Chem. Eng. J.* **2024**, *488*, 151086.
[79] J. Jiang, X. Guo, Y. Xin, Y. Wu, B. Tang, L. Xia, D. Zhang, Z. Cheng, P. Yu, *Chem. Eng. J.* **2024**, *479*, 147552.
[80] X. Luo, H. Zhao, X. Tan, S. Lin, K. Yu, X. Mu, Z. Tao, P. Ji, S. Mu, *Nat. Commun.* **2024**, *15*, 8293.
[81] X. Bi, Y. Jiang, R. Chen, Y. Du, Y. Zheng, R. Yang, R. Wang, J. Wang, X. Wang, Z. Chen, *Adv. Energy Mater.* **2023**, *14*, 2302388.
[82] J. Ryu, D. W. Lee, *J. Mater. Chem. A* **2024**, *12*, 10012.
[83] L. Fei, H. Sun, X. Xu, Y. Li, R. Ran, W. Zhou, Z. Shao, *Chem. Eng. J.* **2023**, *471*, 144660.
[84] Q. Wang, S. Kaushik, X. Xiao, Q. Xu, *Chem. Soc. Rev.* **2023**, *52*, 6139.
[85] L. Yan, J. Chen, C. Yang, J. Ning, Y. Hu, *Small Sci.* **2023**, *4*, 2300094.
[86] J. G. Fan, J. M. Pan, H. Wang, S. Liu, Y. Zhan, X. Yan, *Adv. Funct. Mater.* **2024**, *35*, 2417580.
[87] L. Li, J. Xu, Q. Zhu, X. Meng, H. Xu, M. Han, *Dalton Trans.* **2024**, *53*, 1915.
[88] A. Hanan, M. N. Lakhan, F. Bibi, A. Khan, I. A. Soomro, A. Hussain, U. Aftab, *Chem. Eng. J.* **2024**, *482*, 148776.
[89] R. Gao, D. Yan, *Adv. Energy Mater.* **2019**, *10*, 1900954.
[90] Y. Xiong, P. He, *J. Mater. Sci.* **2023**, *58*, 2041.
[91] J. Wang, F. Ciucci, *Small* **2017**, *13*, 1604103.
[92] S. Ci, S. Mao, Y. Hou, S. Cui, H. Kim, R. Ren, Z. Wen, J. Chen, *J. Mater. Chem. A* **2015**, *3*, 7986.
[93] G. Nie, Z. Zhang, T. Wang, C. Wang, Z. Kou, *ACS Appl. Mater. Interfaces* **2021**, *13*, 37961.
[94] Y. Zhang, Y.-y. Zhang, C.-e. Li, X.-h. Yan, S. Hu, R.-b. Yin, Y.-f. Wei, K.-z. Gao, H.-l. Gao, *Coord. Chem. Rev.* **2024**, *519*, 216103.
[95] S. Chen, J. Duan, P. Bian, Y. Tang, R. Zheng, S. Z. Qiao, *Adv. Energy Mater.* **2015**, *5*, 1500936.
[96] F. Ning, M. Shao, S. Xu, Y. Fu, R. Zhang, M. Wei, D. G. Evans, X. Duan, *Energy Environ. Sci.* **2016**, *9*, 2633.
[97] Y. Tian, G. Wang, F. Li, D. G. Evans, *Mater. Lett.* **2007**, *61*, 1662.
[98] M. Mehdi, B. S. An, H. Kim, S. Lee, C. Lee, M. Seo, M. W. Noh, W. C. Cho, C. H. Kim, C. H. Choi, B. H. Kim, M. Kim, H. S. Cho, *Adv. Energy Mater.* **2023**, *13*, 2204403.
[99] W. Ma, R. Z. Ma, C. X. Wang, J. B. Liang, X. H. Liu, K. C. Zhou, T. Sasaki, *ACS Nano* **2015**, *9*, 1977.
[100] Z. Li, M. Shao, H. An, Z. Wang, S. Xu, M. Wei, D. G. Evans, X. Duan, *Chem. Sci.* **2015**, *6*, 6624.
[101] Y. Dong, P. Zhang, Y. Kou, Z. Yang, Y. Li, X. Sun, *Catal. Lett.* **2015**, *145*, 1541.
[102] T. Zhan, Y. Zhang, X. Liu, S. Lu, W. Hou, *J. Power Sources* **2016**, *333*, 53.
[103] S. She, Y. Zhu, X. Wu, Z. Hu, A. Shelke, W. F. Pong, Y. Chen, Y. Song, M. Liang, C. T. Chen, H. Wang, W. Zhou, Z. Shao, *Adv. Funct. Mater.* **2021**, *32*, 2111091.
[104] A. C. Gandhi, H.-H. Chiu, K.-T. Wu, C.-L. Cheng, S. Y. Wu, *Appl. Surface Sci.* **2021**, *536*, 147856.
[105] K. Manjunatha, H.-H. Chiu, M.-K. Ho, T.-E. Hsu, A. Bajorek, S. Y. Wu, M. Gupta, A. A. Al-Kahtani, M. Ubaidullah, S. O. Manjunatha, N. Basavegowda, J. AngadiV, *J. Solid State Chem.* **2024**, *333*, 124619.
[106] O. N. Avci, L. Sementa, A. Fortunelli, *ACS Catal.* **2022**, *12*, 9058.

[107] G. Chen, Y. Zhu, H. M. Chen, Z. Hu, S. F. Hung, N. Ma, J. Dai, H. J. Lin, C. T. Chen, W. Zhou, Z. Shao, *Adv. Mater.* **2019**, *31*, 1900883.
[108] R. P. Forslund, W. G. Hardin, X. Rong, A. M. Abakumov, D. Filimonov, C. T. Alexander, J. T. Mefford, H. Iyer, A. M. Kolpak, K. P. Johnston, K. J. Stevenson, *Nat. Commun.* **2018**, *9*, 3150.
[109] A. Zhang, Y. Liang, H. Zhang, Z. Geng, J. Zeng, *Chem. Soc. Rev.* **2021**, *50*, 9817.
[110] K. Zhang, J. Li, J. Zhang, S. Wang, X. Liu, T. Zou, H. Yang, X. Han, Y. Han, *Chem. Eng. Sci.* **2025**, *309*, 121461.
[111] K. Zhang, T. Zou, J. Zhang, S. Wang, X. Liu, H. Yang, J. Li, X. Han, Y. Han, *Chem. Eng. J.* **2025**, *511*, 162097.
[112] X. Zhang, Y. Zhao, X. Jia, Y. Zhao, L. Shang, Q. Wang, G. I. N. Waterhouse, L. Z. Wu, C. H. Tung, T. Zhang, *Adv. Energy Mater.* **2018**, *8*, 1702780.
[113] J. Zhou, C. Huang, Q. Zhou, Y. Xie, L. Yang, L. Yu, Y. Yu, *Inorg. Chem.* **2022**, *61*, 9318.
[114] M. Wang, L. Zhang, J. Pan, M. Huang, H. Zhu, *Nano Res.* **2021**, *14*, 4740.
[115] Y. Huang, L.-W. Jiang, X.-L. Liu, T. Tan, H. Liu, J.-J. Wang, *Appl. Catal. B-Environ.* **2021**, *299*, 120678.
[116] Y. Bai, Y. Wu, X. Zhou, Y. Ye, K. Nie, J. Wang, M. Xie, Z. Zhang, Z. Liu, T. Cheng, C. Gao, *Nat. Commun.* **2022**, *13*, 6094.
[117] F. Hu, S. Zhu, S. Chen, Y. Li, L. Ma, T. Wu, Y. Zhang, C. Wang, C. Liu, X. Yang, L. Song, X. Yang, Y. Xiong, *Adv. Mater.* **2017**, *29*, 1606570.
[118] Y. Zhang, W. Zhang, X. Zhang, J. Li, G. Liu, *J. Energy Chem.* **2025**, *101*, 676.
[119] H. F. Wang, L. Chen, H. Pang, S. Kaskel, Q. Xu, *Chem. Soc. Rev.* **2020**, *49*, 1414.
[120] Y. Wang, B. Liu, X. Shen, H. Arandiyan, T. Zhao, Y. Li, M. Garbrecht, Z. Su, L. Han, A. Tricoli, C. Zhao, *Adv. Energy Mater.* **2021**, *11*, 2003759.
[121] Y. Li, W. Ma, H. Yang, Q. Tian, Q. Xu, B. Han, *Chem. Commun.* **2022**, *58*, 6833.
[122] C. Wang, H. Yang, Y. Zhang, Q. Wang, *Angew. Chem., Int. Ed.* **2019**, *58*, 6099.
[123] Y. Niu, X. Teng, S. Gong, Z. Chen, *J. Mater. Chem. A* **2020**, *8*, 13725.
[124] Z. Gong, R. Liu, H. Gong, G. Ye, J. Liu, J. Dong, J. Liao, M. Yan, J. Liu, K. Huang, L. Xing, J. Liang, Y. He, H. Fei, *ACS Catal.* **2021**, *11*, 12284.
[125] C. Pu, D. Deng, H. Li, L. Xu, *Acta Phys. Chim. Sin.* **2024**, *40*, 2304021.
[126] Y. Zhuo, D. Liu, L. Qiao, S. Chen, J. Lu, W. Fai IP, H. Pan, Z. Wang, *Adv. Energy Mater.* **2023**, *13*, 2301921.
[127] L. Gong, H. Yang, A. I. Douka, Y. Yan, B. Y. Xia, *Adv. Sustainable Syst.* **2020**, *5*, 2000136.
[128] M. Cai, Q. Zhu, X. Wang, Z. Shao, L. Yao, H. Zeng, X. Wu, J. Chen, K. Huang, S. Feng, *Adv. Mater.* **2023**, *35*, 2209338.
[129] H. Meng, B. Wu, D. Zhang, X. Zhu, S. Luo, Y. You, K. Chen, J. Long, J. Zhu, L. Liu, S. Xi, T. Petit, D. Wang, X.-M. Zhang, Z. J. Xu, L. Mai, *Energy Environ. Sci.* **2024**, *17*, 704.
[130] M. Wang, J. Xie, Z. Lu, J. Wang, X. Yin, Y. Cao, *Adv. Funct. Mater.* **2025**, 2423767.
[131] K. Song, B. Yang, X. Zou, W. Zhang, W. Zheng, *Energy Environ. Sci.* **2024**, *17*, 27.
[132] X. Wang, W. Pi, S. Hu, H. Bao, N. Yao, W. Luo, *Nano-Micro Lett.* **2024**, *17*, 11.
[133] B. Wang, J. Chen, L. Luo, G. Huang, Q. Shi, Q. Wei, M. Shang, Q. Liu, *Adv. Funct. Mater.* **2025**, 2505763.
[134] Z. Q. Liu, X. Liang, F. X. Ma, Y. X. Xiong, G. Zhang, G. Chen, L. Zhen, C. Y. Xu, *Adv. Energy Mater.* **2023**, *13*, 2203609.
[135] Y. Zhao, D. P. Adiyeri Saseendran, C. Huang, C. A. Triana, W. R. Marks, H. Chen, H. Zhao, G. R. Patzke, *Chem. Rev.* **2023**, *123*, 6257.
[136] H. Zhang, L. Chen, F. Dong, Z. Lu, E. Lv, X. Dong, H. Li, Z. Yuan, X. Peng, S. Yang, J. Qiu, Z. Guo, Z. Wen, *Energy Environ. Sci.* **2024**, *17*, 6435.
[137] F. Wu, F. Tian, M. Li, S. Geng, L. Qiu, L. He, L. Li, Z. Chen, Y. Yu, W. Yang, Y. Hou, *Angew. Chem., Int. Ed.* **2025**, *64*, 202413250.
[138] Z. Zhang, H. Zhao, S. Xi, X. Zhao, X. Chi, H. Bin Yang, Z. Chen, X. Yu, Y. G. Wang, B. Liu, P. Chen, *Nat. Commun.* **2025**, *16*, 1301.
[139] K. Zhu, X. Zhu, W. Yang, *Angew. Chem., Int. Ed.* **2019**, *58*, 1252.
[140] S. C. Karthikeyan, S. Sidra, S. Ramakrishnan, D. H. Kim, P. J. J. Sagayaraj, K. Sekar, D. J. Yoo, *Appl. Catal. B-Environ. Energy* **2024**, *355*, 124196.
[141] M. B. Poudel, S. Vijayapradeep, K. Sekar, J. S. Kim, D. J. Yoo, *J. Mater. Chem. A* **2024**, *12*, 10185.
[142] S. Hong, K. Ham, J. Hwang, S. Kang, M. H. Seo, Y. W. Choi, B. Han, J. Lee, K. Cho, *Adv. Funct. Mater.* **2022**, *33*, 2209543.
[143] P. M. Bacirhonde, D. Shrestha, K. Kang, E. M. Hia, N. Komalla, N. Y. Dzade, M. Buldu-Akturk, M. P. Browne, M. B. Poudel, D. J. Yoo, E. S. Jeong, A. Y. Mohamed, B. G. Han, D. Y. Cho, M. T. Curnan, G. H. Gu, J. W. Han, C. H. Park, *Adv. Energy Mater.* **2025**, 2404479.
[144] M. B. Poudel, M. P. Balanay, P. C. Lohani, K. Sekar, D. J. Yoo, *Adv. Energy Mater.* **2024**, *14*, 2400347.
[145] C. Xuan, K. Xia, W. Lei, W. Xia, W. Xiao, L. Chen, H. L. Xin, D. Wang, *Electrochim. Acta* **2018**, *291*, 64.
[146] H. Wang, X. Zhao, Y. Luo, Y. Wang, G. Liu, J. Li, *J. Electrochem. Soc.* **2023**, *170*, 076501.
[147] Y. Li, H. Guo, J. Zhao, Y. Zhang, L. Zhao, R. Song, *Chem. Eng. J.* **2023**, *464*, 142604.
[148] X. Yang, L. C. Elrod, T. Le, V. S. Vega, H. Naumann, Y. Rezenom, J. H. Reibenspies, M. B. Hall, M. Y. Darensbourg, *J. Am. Chem. Soc.* **2019**, *141*, 15338.
[149] B. Q. Li, S. Y. Zhang, C. Tang, X. Cui, Q. Zhang, *Small* **2017**, *13*, 1700610.
[150] L. Wang, L. Lin, H. Zhang, J. Yu, L. Chen, *Mater. Lett.* **2024**, *365*, 136429.
[151] C. Lai, M. Gong, Y. Zhou, J. Fang, L. Huang, Z. Deng, X. Liu, T. Zhao, R. Lin, K. Wang, K. Jiang, H. Xin, D. Wang, *Appl. Catal. B-Environ.* **2020**, *274*, 119086.
[152] H. Liao, T. Luo, P. Tan, K. Chen, L. Lu, Y. Liu, M. Liu, J. Pan, *Adv. Funct. Mater.* **2021**, *31*, 2102772.
[153] B. Wang, C. Tang, H. F. Wang, B. Q. Li, X. Cui, Q. Zhang, *Small Methods* **2018**, *2*, 1800055.
[154] Y. P. Deng, Y. Jiang, R. Liang, N. Chen, W. Chen, Z. W. Yin, G. King, D. Su, X. Wang, Z. Chen, *J. Am. Chem. Soc.* **2023**, *145*, 20248.
[155] J. Li, J. Song, B.-Y. Huang, G. Liang, W. Liang, G. Huang, Y. Qi Jin, H. Zhang, F. Xie, J. Chen, N. Wang, Y. Jin, X.-B. Li, H. Meng, *J. Catal.* **2020**, *389*, 375.
[156] G. Fu, Z. Cui, Y. Chen, L. Xu, Y. Tang, J. B. Goodenough, *Nano Energy* **2017**, *39*, 77.
[157] C. Feng, M. B. Faheem, J. Fu, Y. Xiao, C. Li, Y. Li, *ACS Catal.* **2020**, *10*, 4019.
[158] B. Singh, T. Ansari, *ACS Appl. Nano Mater.* **2024**, *7*, 15754.
[159] Y. J. Wu, J. Yang, T. X. Tu, W. Q. Li, P. F. Zhang, Y. Zhou, J. F. Li, J. T. Li, S. G. Sun, *Angew. Chem., Int. Ed.* **2021**, *60*, 26829.
[160] S. Luo, C. Dai, Y. Ye, Q. Wu, J. Wang, X. Li, S. Xi, Z. J. Xu, *Angew. Chem., Int. Ed.* **2024**, *63*, 202402184.
[161] J. Nie, J. Shi, T. Huang, M. Y. Xie, Z. Y. Ouyang, M. H. Xian, G. F. Huang, H. Wan, W. Hu, W. Q. Huang, *Adv. Funct. Mater.* **2024**, *34*, 2314172.
[162] F. Shi, L. Xiao, Z. Zhou, X. Zhao, Y. Liu, J. Mao, J. Qin, Y. Deng, J. Yang, *Adv. Funct. Mater.* **2025**, 2501070.
[163] K. Chen, S. Kim, R. Rajendiran, K. Prabakar, G. Li, Z. Shi, C. Jeong, J. Kang, O. L. Li, *J. Colloid. Interface Sci.* **2021**, *582*, 977.
[164] S. Liu, Y. Shi, F. Tang, P. Wei, W. Huang, J. Wu, S. Zhao, J. Zhu, C. Shi, L. Hu, *J. Alloys Compd.* **2024**, *987*, 174248.
[165] F. N. I. Sari, Y. C. Lai, Y. J. Huang, X. Y. Wei, H. Pourzolfaghar, Y. H. Chang, M. Ghufron, Y. Y. Li, Y. H. Su, O. Clemens, J. M. Ting, *Adv. Funct. Mater.* **2024**, *34*, 2310181.

[166] Z. Wang, J. You, Y. Zhao, R. Yao, G. Liu, J. Lu, S. Zhao, *J. Environ. Chem. Eng.* **2023**, *11*, 109080.
[167] Z. Jin, J. Lyu, Y.-L. Zhao, H. Li, X. Lin, G. Xie, X. Liu, J.-J. Kai, H.-J. Qiu, *ACS Mater. Lett.* **2020**, *2*, 1698.
[168] D. H. Wu, M. Ul Haq, L. Zhang, J. J. Feng, F. Yang, A. J. Wang, *J. Colloid. Interface Sci.* **2024**, *662*, 149.
[169] Y. Yao, Z. Li, Y. Dou, T. Jiang, J. Zou, S. Y. Lim, P. Norby, E. Stamate, J. O. Jensen, W. Zhang, *Dalton. Trans.* **2023**, *52*, 4142.
[170] Z. Jin, X. Zhou, Y. Hu, X. Tang, K. Hu, K. M. Reddy, X. Lin, H. J. Qiu, *Chem. Sci.* **2022**, *13*, 12056.
[171] G. Fang, J. Gao, J. Lv, H. Jia, H. Li, W. Liu, G. Xie, Z. Chen, Y. Huang, Q. Yuan, X. Liu, X. Lin, S. Sun, H.-J. Qiu, *Appl. Catal. B-Environ.* **2020**, *268*, 118431.
[172] T. Yu, Y. Zhang, Y. Hu, K. Hu, X. Lin, G. Xie, X. Liu, K. M. Reddy, Y. Ito, H.-J. Qiu, *ACS Mater. Lett.* **2021**, *4*, 181.
[173] Z. Jin, J. Lyu, K. Hu, Z. Chen, G. Xie, X. Liu, X. Lin, H. J. Qiu, *Small* **2022**, *18*, 2107207.
[174] Y. Han, J. Wang, Y. Liu, T. Li, T. Wang, X. Li, X. Ye, G. Li, J. Li, W. Hu, Y. Deng, *Carbon Neutral.* **2024**, *3*, 172.
[175] B. Guo, R. Ma, Z. Li, S. Guo, J. Luo, M. Yang, Q. Liu, T. Thomas, J. Wang, *Nano-Micro Lett.* **2020**, *12*, 20.
[176] D. Zhou, Y. Jia, H. Yang, W. Xu, K. Sun, J. Zhang, S. Wang, Y. Kuang, B. Liu, X. Sun, *J. Mater. Chem. A* **2018**, *6*, 21162.
[177] Y.-j. Wu, J.-z. Zheng, X. Zhou, T.-x. Tu, Y. Liu, P.-f. Zhang, L. Tan, S. Zhao, *Inorg. Chem. Front.* **2023**, *10*, 2444.
[178] L. Qiu, Q. Wang, P. Yan, X.-Y. Yu, *J. Mater. Chem. A* **2022**, *10*, 21251.
[179] W. Li, Y. Wu, M. Chen, P. Dai, T. Jiang, S. Zhou, *J. Alloys Compd.* **2022**, *925*, 166658.
[180] H. Sun, M. Zhao, C. Ma, W. Chen, Y. Yang, Y. Han, *Nano Res.* **2022**, *16*, 4980.
[181] Y. Liu, J. Ma, T. K. A. Hoang, L. Yang, Z. Chen, *Nanoscale* **2023**, *15*, 1172.
[182] Y. Wang, Y. Gao, L. Ma, Y. Xue, Z. H. Liu, H. Cui, N. Zhang, R. Jiang, *ACS Appl. Mater. Interfaces* **2023**, *15*, 16732.
[183] M. Zhang, J. Zhang, S. Ran, L. Qiu, W. Sun, Y. Yu, J. Chen, Z. Zhu, *Nano Res.* **2020**, *14*, 1175.
[184] H. Jia, X. Meng, Y. Lin, D. Wang, G. Li, G. Zhang, *Phys. Chem. Chem. Phys.* **2023**, *25*, 28841.
[185] D. Bin, B. Yang, C. Li, Y. Liu, X. Zhang, Y. Wang, Y. Xia, *ACS Appl. Mater. Interfaces* **2018**, *10*, 26178.
[186] Y. Chen, J. Peng, W. Duan, G. He, Z. Tang, *ChemCatChem* **2019**, *11*, 5994.
[187] X. Chen, D. Chen, G. Li, P. Sha, J. Yu, L. Yu, L. Dong, *Electrochim. Acta* **2022**, *428*, 140938.
[188] Q. Wang, G.-C. Xu, D.-J. Liu, H. Ding, L. Zhang, *Int. J. Hydrogen Energy* **2023**, *48*, 12712.
[189] Y. Qian, T. An, E. Sarnello, Z. Liu, T. Li, D. Zhao, *ACS Appl. Energy Mater.* **2019**, *2*, 1784.
[190] J. Zhu, M. Xiao, Y. Zhang, Z. Jin, Z. Peng, C. Liu, S. Chen, J. Ge, W. Xing, *ACS Catal.* **2016**, *6*, 6335.
[191] D. Chen, X. Chen, Z. Cui, G. Li, B. Han, Q. Zhang, J. Sui, H. Dong, J. Yu, L. Yu, L. Dong, *Chem. Eng. J.* **2020**, *399*, 125718.
[192] J.-N. Liu, C.-X. Zhao, J. Wang, X.-Q. Fang, C.-X. Bi, B.-Q. Li, Q. Zhang, *Joule* **2024**, *8*, 1804.
[193] C. Allard, L. Alvarez, J. L. Bantignies, N. Bendiab, S. Cambre, S. Campidelli, J. A. Fagan, E. Flahaut, B. Flavel, F. Fossard, E. Gaufres, S. Heeg, J. S. Lauret, A. Loiseau, J. B. Marceau, R. Martel, L. Marty, T. Pichler, C. Voisin, S. Reich, A. Setaro, L. Shi, W. Wenseleers, *Chem. Soc. Rev.* **2024**, *53*, 8457.
[194] C. Zhao, Y. Jin, Z. Yu, S. Li, F. Meng, Y. Yuan, Y. Cheng, W. Du, *Mater. Chem. Phys.* **2023**, *295*, 127168.
[195] J. H. Hong, G. D. Park, Y. C. Kang, *Inter. J. Energy Res.* **2021**, *46*, 5215.
[196] C. Sun, Y.-J. Zhao, X.-Y. Yuan, J.-B. Li, H.-B. Jin, *Rare Met.* **2022**, *41*, 2616.
[197] M. Jiang, Z. Tan, M. Cao, *Int. J. Hydrogen Energy* **2021**, *46*, 15507.
[198] H. Lei, Z. Wang, F. Yang, X. Huang, J. Liu, Y. Liang, J. Xie, M. S. Javed, X. Lu, S. Tan, W. Mai, *Nano Energy* **2020**, *68*, 104293.
[199] Q. Lu, X. Zou, C. Wang, K. Liao, P. Tan, R. Ran, W. Zhou, M. Ni, Z. Shao, *Energy Storage Mater.* **2021**, *39*, 11.
[200] O. Ambriz-Peláez, J. Béjar, C. M. Ramos-Castillo, M. Guerra-Balcázar, L. Álvarez-Contreras, N. Arjona, *Appl. Surf. Sci.* **2022**, *601*, 154253.
[201] L. Yan, Z. Xu, X. Liu, S. Mahmood, J. Shen, J. Ning, S. Li, Y. Zhong, Y. Hu, *Chem. Eng. J.* **2022**, *446*, 137049.
[202] D. Song, H. Guo, K. Huang, H. Zhang, J. Chen, L. Wang, C. Lian, Y. Wang, *Mater. Today* **2022**, *54*, 42.
[203] X. Guo, X. Zheng, X. Hu, Q. Zhao, L. Li, P. Yu, C. Jing, Y. Zhang, G. Huang, B. Jiang, C. Xu, F. Pan, *Nano Energy* **2021**, *84*, 105932.
[204] W. Zeng, C. Wei, K. Zeng, X. Cao, M. H. Rümmeli, R. Yang, *ChemElectroChem* **2020**, *8*, 524.
[205] Y. Ma, W. Chen, Z. Jiang, X. Tian, X. WangGuo, G. Chen, Z.-J. Jiang, *J. Mater. Chem. A* **2022**, *10*, 12616.
[206] X. Han, N. Li, J. S. Baik, P. Xiong, Y. Kang, Q. Dou, Q. Liu, J. Y. Lee, C. S. Kim, H. S. Park, *Adv. Funct. Mater.* **2023**, *33*, 2212233.
[207] P. Liu, D. Gao, W. Xiao, L. Ma, K. Sun, P. Xi, D. Xue, J. Wang, *Adv. Funct. Mater.* **2018**, *28*, 1706928.
[208] K. Khan, X. Yan, Q. Yu, S.-H. Bae, J. J. White, J. Liu, T. Liu, C. Sun, J. Kim, H.-M. Cheng, Y. Wang, B. Liu, K. Amine, X. Pan, Z. Luo, *Nano Energy* **2021**, *90*, 106488.
[209] X. Zou, Q. Lu, M. Tang, J. Wu, K. Zhang, W. Li, Y. Hu, X. Xu, X. Zhang, Z. Shao, L. An, *Nano-Micro Lett.* **2025**, *17*, 6.
[210] G.-L. Li, S. Cao, Z.-F. Lu, X. Wang, Y. Yan, C. Hao, *Appl. Surf. Sci.* **2022**, *591*, 153142.
[211] G. Lee, W. Yang, J. Kim, *J. Alloys Compd.* **2024**, *970*, 172484.
[212] R. Majee, Q. A. Islam, S. Bhattacharyya, *ACS Appl. Mater. Interfaces* **2019**, *11*, 35853.
[213] I. Jeong, Y. Shim, S. Oh, J. M. Yuk, K. M. Roh, C. W. Lee, K. T. Lee, *Adv. Energy Mater.* **2024**, *14*, 2402342.
[214] T. Lan, H. Du, Y. Li, K. Qu, J. Zhao, X. Zhang, Y. Dong, Y. Zhang, X. Zhang, D. Zhang, *Jo. Alloys. Compd.* **2023**, *943*, 169144.
[215] X. Guo, X. Zhang, Y. Wu, Y. Xin, D. Li, Y. Zhang, P. Yu, *Dalton. Trans.* **2023**, *52*, 4315.
[216] Z. Hu, S. Dong, Q. He, Z. Chen, D. Yuan, *Inorg. Chem.* **2023**, *62*, 7471.
[217] L. Wan, Z. Zhao, X. Chen, P.-F. Liu, P. Wang, Z. Xu, Y. Lin, B. Wang, *ACS Sustainable Chem. Eng.* **2020**, *8*, 11079.
[218] X. Yang, H. Mao, Z. Zhou, K. Li, C. Li, Q. Ye, B. Liu, Y. Fang, X. Cai, *Adv. Funct. Mater.* **2024**, *34*, 2402933.
[219] X. Li, D. C. Nguyen, K. Dong, S. Prabhakaran, D. T. Tran, D. H. Kim, N. H. Kim, J. H. Le, *Chem. Eng. J.* **2024**, *489*, 151210.
[220] X. Han, N. Li, Y. B. Kang, Q. Dou, P. Xiong, Q. Liu, J. Y. Lee, L. Dai, H. S. Park, *ACS Energy Lett.* **2021**, *6*, 2460.
[221] T. Hu, Z. Jiang, Z. Fu, Z.-J. Jiang, *J. Mater. Chem. A* **2022**, *10*, 8739.
[222] T.-E. Ko, S. Hosseini, C.-M. Tseng, J.-E. Tsai, W.-H. Wang, Y.-Y. Li, *J. Taiwan Inst. Chem. Eng.* **2022**, *136*, 104397.
[223] X. Guo, X. Hu, D. Wu, C. Jing, W. Liu, Z. Ren, Q. Zhao, X. Jiang, C. Xu, Y. Zhang, N. Hu, *ACS Appl. Mater. Interfaces* **2019**, *11*, 21506.
[224] Y. Zhou, J. Si, H. Wang, X. Li, S. Zhang, C. Deng, *Energy Fuels* **2023**, *37*, 9619.
[225] X. Hu, T. Huang, Y. Tang, G. Fu, J. M. Lee, *ACS Appl. Mater. Interfaces* **2019**, *11*, 4028.
[226] Z. Fu, S. Liu, Z. Mai, Z. Tang, D. D. Qin, Y. Tian, X. Wang, *Chem. Asian J.* **2020**, *15*, 3568.
[227] X. Bao, K. Xie, Z. Zhang, Z. Liu, H. Zhou, F. Luo, D. Zhou, H.-E. Wang, *Ionics* **2022**, *28*, 1273.
[228] G. Zhang, X. Liu, L. Wang, G. Xing, C. Tian, H. Fu, *ACS Nano* **2022**, *16*, 17139.

[229] Q. Lu, X. Zou, Y. Bu, K. Liao, W. Zhou, Z. Shao, *Small* **2022**, *18*, 2105604.
[230] M. I. Hossain, F. K. Tareq, S. Rudra, *Electrochem. Commun.* **2025**, *176*, 107942.
[231] S. Zeng, G. Duan, R. Yu, Q. Qin, S. He, S. Jiang, H. Yang, X. Han, J. Han, B. Y. Xia, *Prog. Mater. Sci.* **2025**, *147*, 101356.
[232] X. Han, N. Li, P. Xiong, Y. Kang, Q. Dou, Q. Liu, W. Li, J. Y. Lee, H. S. Park, *Compos. Part B-Eng.* **2022**, *234*, 109670.
[233] K. Zhang, H. Yang, X. Han, S. Wang, X. Liu, T. Zou, J. Li, J. Zhang, H. Zhang, Y. Han, *Ind. Eng. Chem. Res.* **2024**, *63*, 22403.
[234] Q. Lu, X. Zou, K. Liao, R. Ran, W. Zhou, M. Ni, Z. Shao, *Carbon Energy* **2020**, *2*, 461.
[235] C. Lai, J. Fang, X. Liu, M. Gong, T. Zhao, T. Shen, K. Wang, K. Jiang, D. Wang, *Appl. Catal. B-Environ.* **2021**, *285*, 119856.
[236] Z. Song, Z. Li, Y. Liu, L. Chen, J. Zhang, Z. Zheng, *CrystEngComm* **2022**, *24*, 6980.
[237] W. Wang, Y. Liu, J. Li, J. Luo, L. Fu, S. Chen, *J. Mater. Chem. A* **2018**, *6*, 14299.
[238] J. Li, Y. Qin, Z. Bai, S. Li, L. Li, B. Ouyang, E. Kan, W. Zhang, *Appl. Surf. Sci.* **2024**, *648*, 159080.
[239] C. Lai, H. Li, Y. Sheng, M. Zhou, W. Wang, M. Gong, K. Wang, K. Jiang, *Adv. Sci.* **2022**, *9*, 2105925.
[240] D. Zheng, W. Liu, X. Dai, J. Feng, X. Xu, R. Yin, W. Que, W. Shi, F. Wu, H. Wu, X. Cao, *Adv. Energy Sustainability Res.* **2022**, *3*, 2200014.
[241] K. Guo, L. Bao, Z. Yu, X. Lu, *Chem. Soc. Rev.* **2024**, *53*, 11100.
[242] X. Cui, P. Ren, D. Deng, J. Deng, X. Bao, *Energy Environ. Sci.* **2016**, *9*, 123.
[243] Y. Wang, G. Zhang, M. Ma, Y. Ma, J. Huang, C. Chen, Y. Zhang, X. Sun, Z. Yan, *Sci. China Mater.* **2020**, *63*, 1182.
[244] G. Zhang, X. Liu, L. Wang, F. Sun, Y. Yang, C. Tian, P. Yu, Q. Pan, H. Fu, *ACS Sustainable Chem. Eng.* **2019**, *7*, 19104.
[245] X. Dong, Z. Yao, Y. Li, J. Wang, Q. Zhong, *ChemistrySelect* **2023**, *8*, 202203929.
[246] X. Chen, D. Chen, G. Li, C. Gong, Y. Chen, Q. Zhang, J. Sui, H. Dong, J. Yu, L. Yu, L. Dong, *J. Alloys Compd.* **2021**, *873*, 159833.
[247] X. Chen, J. Pu, X. Hu, Y. Yao, Y. Dou, J. Jiang, W. Zhang, *Small* **2022**, *18*, 2200578.
[248] Y. Lei, Y. Xiang, C. Xu, R. Jin, L. Sun, H. Chen, M. Yang, Y. Si, C. Chen, C. Guo, *J. Alloys Compd.* **2024**, *980*, 173590.
[249] H. Fang, H. Bian, B. Hu, J. Liu, S. Li, M. Wang, L. He, Z. Zhang, *Appl. Surf. Sci.* **2022**, *604*, 154590.
[250] X. Xie, H. Peng, K. Sun, X. Lei, R. Zhu, Z. Zhang, G. Ma, Z. Lei, *Chem. Eng. J.* **2023**, *452*, 139253.
[251] J. Liu, Z. Luo, X. Zhang, H. Zheng, L. Peng, D. Qian, C. Jia, D. Sun-Waterhouse, G. I. N. Waterhouse, *J. Mater. Chem. A* **2021**, *9*, 27701.
[252] Y. He, Z. Yin, Z. Wang, H. Wang, W. Xiong, B. Song, H. Qin, P. Xu, G. Zeng, *J. Mater. Chem. A* **2022**, *10*, 9788.
[253] J. Liu, D. Zhu, Y. Zheng, A. Vasileff, S.-Z. Qiao, *ACS Catal.* **2018**, *8*, 6707.
[254] W. Liu, C. Ni, M. Gao, X. Zhao, W. Zhang, R. Li, K. Zhou, *ACS Nano* **2023**, *17*, 24564.
[255] K. Yue, J. Liu, C. Xia, K. Zhan, P. Wang, X. Wang, Y. Yan, B. Y. Xia, *Mater. Chem. Front.* **2021**, *5*, 7191.
[256] W. Meng, R. Pang, M. Li, L. Han, X. Kong, D. Zhang, S. Zhang, Y. Zhang, Y. Shang, A. Cao, *Small* **2024**, 2310469.
[257] L. Liu, Z. Hu, M. Wang, J. Ma, Z. Chen, X. Ning, D. Yuan, *J. Alloys Compd.* **2022**, *925*, 166665.
[258] F. Chang, H. Du, P. Su, Y. Sun, R. Ye, Q. Tian, G. Zhang, H. Li, J. Liu, *Small Struct.* **2023**, *5*, 2300111.
[259] Q. Yan, X. Duan, Y. Liu, F. Ge, H. Zheng, *J. Mater. Chem. A* **2023**, *11*, 1430.
[260] R. Wang, J. Liu, J. Xie, Z. Cai, Y. Yu, Z. Zhang, X. Meng, C. Wang, X. Xu, J. Zou, *Appl. Catal. B-Environ.* **2023**, *324*, 122230.
[261] E. Jang, J. Cho, J. Kim, J. Kim, *Appl. Surf. Sci.* **2024**, *663*, 160201.
[262] F. Liao, X. Zhao, G. Yang, Q. Cheng, L. Mao, L. Chen, *J. Alloys Compd.* **2021**, *872*, 159649.
[263] S. Sultan, J. N. Tiwari, A. N. Singh, S. Zhumagali, M. Ha, C. W. Myung, P. Thangavel, K. S. Kim, *Adv. Energy Mater.* **2019**, *9*, 1900624.
[264] R. Feng, L. Chen, L. Huang, H. Wu, Y. Ge, J. Xu, M. Zeng, W. Li, *New J. Chem.* **2025**, *49*, 132.
[265] W. Miao, X. Cao, M. Qin, E. Lv, H. Yu, X. Zhang, X. Dong, *Compos. Part B-Eng.* **2023**, *260*, 110769.
[266] J. Zhu, M. Xiao, G. Li, S. Li, J. Zhang, G. Liu, L. Ma, T. Wu, J. Lu, A. Yu, D. Su, H. Jin, S. Wang, Z. Chen, *Adv. Energy Mater.* **2019**, *10*, 1903003.
[267] M.-I. Jamesh, D. Hu, J. Wang, F. Naz, J. Feng, L. Yu, Z. Cai, J. C. Colmenares, D.-J. Lee, P. K. Chu, H.-Y. Hsu, *J. Mater. Chem. A* **2024**, *12*, 11771.
[268] Y. Cheng, S. Dou, J. P. Veder, S. Wang, M. Saunders, S. P. Jiang, *ACS Appl. Mater. Interfaces* **2017**, *9*, 8121.
[269] P. Akbarian, M. Kheirmand, *J. Electrochem. Soc.* **2024**, *171*, 020514.
[270] F. Shahbazi Farahani, M. S. Rahmanifar, A. Noori, M. F. El-Kady, N. Hassani, M. Neek-Amal, R. B. Kaner, M. F. Mousavi, *J. Am. Chem. Soc.* **2022**, *144*, 3411.
[271] P. G. de Gennes, S. Matter, *Angew. Chemie. Int. Ed.* **2003**, *31*, 842.
[272] J. Chen, H. Li, C. Fan, Q. Meng, Y. Tang, X. Qiu, G. Fu, T. Ma, *Adv. Mater.* **2020**, *32*, 2003134.
[273] J. Wang, X. Q. Fang, J. N. Liu, Y. W. Song, M. Zhao, B. Q. Li, J. Q. Huang, *Adv. Funct. Mater.* **2024**, *35*, 2413562.
[274] Z. Cui, G. Fu, Y. Li, J. B. Goodenough, *Angew. Chem., Int. Ed.* **2017**, *56*, 9901.
[275] T. Li, Y. Chen, Z. Tang, Z. Liu, C. Wang, *Electrochim. Acta* **2019**, *307*, 403.
[276] X. Zhong, X. Xiao, Q. Li, M. Zhang, Z. Li, L. Gao, B. Chen, Z. Zheng, Q. Fu, X. Wang, G. Zhou, B. Xu, *Nat. Commun.* **2024**, *15*, 9616.
[277] L. Wan, Z. Xu, Q. Cao, Y. Liao, B. Wang, K. Liu, *Nano Lett.* **2022**, *22*, 4535.
[278] X. Han, N. Li, P. Xiong, M. G. Jung, Y. Kang, Q. Dou, Q. Liu, J. Y. Lee, H. S. Park, *InfoMat* **2021**, *3*, 1134.
[279] Q. Shi, H. Guo, D. Ou, L. Gao, S. Ye, Q. Liu, W. Yang, F. Hu, Z. Liang, *J. Energy Storage* **2023**, *72*, 108073.
[280] Z. Zhang, D. Zhou, L. Zhou, H. Yu, B. Huang, *Ionics* **2017**, *24*, 1709.
[281] L. Wu, Z. Pan, S. Yuan, X. Shi, Y. Liu, F. Liu, X. Yan, L. An, *Chem. Eng. J.* **2024**, *488*, 151000.
[282] K. Zhang, Y. Xu, F. Liu, Q. Wang, X. Zou, M. Tang, M. K. H. Leung, Z. Ao, X. Zhao, X. Zhang, L. An, *Adv. Sci.* **2024**, *12*, 2410763.
[283] X. Cai, T. Jiang, M. Wu, *Appl. Surf. Sci.* **2022**, *577*, 151911.
[284] S. Li, H. Zhang, L. Wu, H. Zhao, L. Tao, L. Li, C. Sun, D. Ju, B. An, *Chem. Eng. J.* **2024**, *482*, 148868.

Xiaohong Zou received her Ph.D. at Nanjing Tech University in 2022. Now she is a post-doctor at the Hong Kong Polytechnic University (PolyU). Her main research interests are energy storage and conversion devices, especially Li–O_2 batteries, Zn–air batteries, and solid-state batteries.

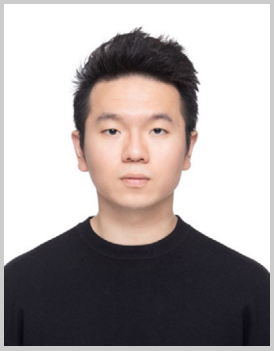

Mingcong Tang received his B.S. degree (2020) from the University of California, San Diego, and M.S. degree (2022) from the University of Michigan, Ann Arbor. He is currently pursuing his Ph.D. degree at the Hong Kong Polytechnic University under the supervision of Dr. Liang An. His current research is focusing on aqueous Zinc metal-based batteries.

Qian Lu received his Ph.D. at Nanjing Tech University in 2021, and worked as a research assistant at Hong Kong Polytechnic University in 2018. Now he is an associate professor at Nanjing University of Information Science and Technology and a post-doctor at the Chinese University of Hong Kong. His main research interests are metal–air batteries, lithium–sulfur batteries, and water electrolysis.

Kouer Zhang received her B.S. degree (2022) from Xi'an Jiaotong University. She is currently pursuing her Ph.D. degree at the Hong Kong Polytechnic University under the supervision of Dr. Liang An. Her current research is focusing on electrocatalysis and energy conversion and storage.

Lizhen Wu received his B.S. degree (2018) from Dalian Maritime University, and M.S. degree (2021) from Tianjin University. He is currently pursuing his Ph.D. degree at the Hong Kong Polytechnic University under the supervision of Dr. Liang An. His current research is focusing on water electrolyzers.

Zongping Shao is currently a John Curtin Distinguished Professor of Curtin University, Australia. He obtained his Ph.D. degree from the Dalian Institute of Chemical Physics, Chinese Academy of Sciences, in 2000. He worked as a visiting scholar at the Institute Researches Sur La Catalyse, CNRS, France, and a research associate at the California Institute of Technology, USA, from February 2000 till June 2005. He joined Nanjing Tech University in July 2005. His current research interests include fuel cells, rechargeable batteries, solar cells, oxygen-permeable membranes, and environmental treatment.

Liang An received his B.S. degree from Harbin Institute of Technology in 2008 and Ph.D. degree from The Hong Kong University of Science and Technology in 2012. He is currently an Associate Professor of Mechanical Engineering at The Hong Kong Polytechnic University. His research interests include advanced energy conversion and storage technologies, such as fuel cells and batteries.